DEVELOPMENT OF N-NITROSAMINE SENSOR BASED ON GRAPHENE SCREEN-PRINTED ELECTRODE MODIFIED WITH PALLADIUM NANOPARTICLES COATED WITH MOLECULARLY IMPRINTED POLYMER

KANPITCHA SOMNET

A THESIS SUBMITTED IN PARTIAL FULFILLMENT OF THE REQUIREMENTS FOR THE DEGREE OF MASTER OF SCIENCE
MAJOR IN CHEMISTRY
FACULTY OF SCIENCE
UBON RATCHATHANI UNIVERSITY
ACADEMIC YEAR 2021

ACKNOWLEDGEMENT

I would like to thank my advisor Assoc. Prof. Dr. Maliwan Amatatongchai and my co-advisor Dr. Chanpen Karuwan for her constant advice, guidance, insight, and for sharing her extensive chemistry knowledge. I wish to thank Asst. Prof. Dr. Nathawut Choengchan, Assoc. Prof. Dr. Purim Jarujamrus and Assoc. Prof. Dr. Sanoe Chairam for comments and suggestions.

I would like to thank the Thailand Graduate Institute of Science and Technology-(TGIST) grant from National Science and Technology Development Agency (NSTDA) for financial support and Ubon Ratchathani University for partially support. My gratitude is extended to Department of Chemistry, Faculty of Science, Ubon Ratchathani University for providing all laboratory facilities.

Above all, my deepest gratitude is given to my beloved parents for their eternal love and care throughout my life.

Kanpitcha Somnet
Researcher

บทคัดย่อ

เรื่อง	:	การพัฒนาเอ็นไนโตรซามีนเซนเซอร์ชนิดใหม่โดยใช้ขั้วไฟฟ้ากราฟีนแบบพิมพ์สกรีนดัดแปรด้วยอนุภาคพาลาเดียมนาโนที่เคลือบด้วยพอลิเมอร์ที่มีรอยพิมพ์ประทับโมเลกุล
ผู้วิจัย	:	กานพิชชา สมเนตร
ชื่อปริญญา	:	วิทยาศาสตร์มหาบัณฑิต
สาขาวิชา	:	เคมี
อาจารย์ที่ปรึกษา	:	รองศาสตราจารย์ ดร.มะลิวรรณ อมตธงไชย
อาจารย์ที่ปรึกษาร่วม	:	ดร. จันทร์เพ็ญ ครุวรรณ์
คำสำคัญ	:	พร้อมใช้งาน, เอ็น-ไนโตรซามีน, พอลิเมอร์ที่มีรอยพิมพ์ประทับโมเลกุล, คอร์-เชลล์ไมโครสเฟียร์, การควบคุมคุณภาพอาหาร

งานวิทยานิพนธ์นี้ได้สร้างเซนเซอร์โวลแทมเมตริกขนาดกะทัดรัดสำหรับการตรวจวัดสาร เอ็น-ไนโตรโซไดฟีนิลลามีน (NDPhA) ที่มีความไวและความจำเพาะเจะจงโดยใช้ขั้วไฟฟ้ากราฟีนแบบพิมพ์สกรีนดัดแปรด้วยอนุภาคพาลาเดียมนาโนที่เคลือบด้วยพอลิเมอร์ที่มีรอยพิมพ์ประทับโมเลกุล (PdNPs@MIP/SPGrE) นอกจากนี้ยังมีการนำเสนอแนวทางใหม่สำหรับการพิมพ์ 3 มิติของ NDPhA บนพื้นผิวของอนุภาคพาลาเดียมนาโน PdNPs ถูกสังเคราะห์ขึ้นครั้งแรกโดยการรีดิวซ์ด้วยโซเดียมโบโรไฮไดรด์ จากนั้นสามารถสร้างพอลิเมอร์แบบคอร์-เชลล์ได้สำเร็จโดยการเคลือบพื้นผิวของอนุภาคพาลาเดียมนาโนอย่างต่อเนื่องด้วยพอลี (ไวนิลไพร์โรลิโดน) และที่ปลายมี MIP ที่ประกอบด้วยพอลี (เอ็น-ไอโซโพริพิลอะคริลาไมด์) - โค-ไตรเมทิลอลโพรเพน ไตรเมทิลอะคริเลต

ลักษณะทางสัณฐานวิทยา โครงสร้าง และการพิสูจน์เอกลักษณ์ด้วยเทคนิคไฟฟ้าเคมีแสดงให้เห็นว่า PdNPs@MIP มีลักษณะทรงกลม มีขนาดไมโคร มีความสามารถในการเร่งปฏิกิริยาสูง และพื้นที่ผิวจำเพาะที่มีไซต์ที่มีรอยพิมพ์ประทับโมเลกุลของ NDPhA เป็นจำนวนมาก งานวิจัยนี้สร้างเซนเซอร์ที่มีรอยพิมพ์ประทับโมเลกุลของ NDPhA ขนาดกะทัดรัดโดยการเคลือบบนพื้นผิว SPGrE ด้วย PdNPs@MIP การวิเคราะห์เชิงปริมาณดำเนินการโดยการวัดด้วยเทคนิคลิเนียสวิฟ สทริปปิงโวลแทมเมตรี (LSASV) โดยใช้ศักย์ไฟฟ้าในการสะสมที่ +0.02 โวลต์ เป็นเวลา 60 วินาที ช่วงความเป็นเส้นตรงสำหรับการตรวจวัด NDPhA คือ 0.01 - 0.1 ไมโครโมลาร์ (r^2 = 0.996) และ 0.1 - 100 ไมโครโมลาร์ (r^2 = 0.992) โดยมีความไวที่สอดคล้องกันเท่ากับ 51.935 และ 0.821 (ไมโครแอมแปร์ วินาที) ไมโครโมลาร์$^{-1}$ ตามลำดับ ระบบให้ความแม่นยำที่ดีที่ %RSD 1.67% โดยมีขีดจำกัดต่ำสุดในการตรวจวัดที่ 0.0013 ไมโครโมลาร์ (3Sb, n = 3) ความถูกต้องในการตรวจวัดภายในวันเดียวกันและระหว่างวันพิจารณาจาก %bias ของสารมาตรฐานอ้างอิงรับรอง (certified reference material; CRM) คือ -0.74% และ -1.01% ตามลำดับ งานวิจัยนี้แสดงให้เห็นถึงการใช้งานที่ประสบความสำเร็จของ

เซนเซอร์ขนาดกะทัดรัดที่ประดิษฐ์ขึ้นเพื่อตรวจวัด NDPhA ในตัวอย่างเครื่องดื่มและตัวอย่างสังเคราะห์ ซึ่งเซนเซอร์ที่มีรอยพิมพ์ประทับโมเลกุลของ NDPhA ขนาดกะทัดรัดสามารถใช้เป็นแนวทางทางเลือกในการควบคุมคุณภาพอาหารได้

ABSTRACT

TITLE : DEVELOPMENT OF N-NITROSAMINE SENSOR BASED ON GRAPHENE SCREEN-PRINTED ELECTRODE MODIFIED WITH PALLADIUM NANOPARTICLES COATED WITH MOLECULARLY IMPRINTED POLYMER
AUTHOR : KANPITCHA SOMNET
DEGREE : MASTER OF SCIENCE
MAJOR : CHEMISTRY
ADVISOR : ASSOC. PROF. MALIWAN AMATATONGCHAI, Ph.D.
CO- ADVISOR : CHANPEN KARUWAN, Ph.D.
KEYWORDS : READY-TO-USE, N-NITROSAMINE, MOLECULARLY IMPRINTED POLYMER, CORE-SHELL MICROSPHERE, FOOD QUALITY CONTROL

This research involves the creation of a compact voltammetric sensor for the sensitive and selective determination of N-nitrosodiphenylamine (NDPhA) using screen-printed graphene electrodes modified with a molecularly-imprinted polymer (MIP) coating on a palladium nanoparticle core (PdNPs@MIP/SPGrE). A new approach is also proposed for the 3D printing of NDPhA on a PdNPs surface. PdNPs were first synthesized by chemical reduction using sodium borohydride. The core-shell polymer can then be successfully created by continuously coating the surface of the PdNPs with poly(vinylpyrrolidone) and terminating with an MIP consisting of poly (*N*-Isopropylacrylamide)-co-trimethylolpropane trimethyl acrylate.

Morphological, structural, and electrochemical characterization revealed that the prepared microscopic, spherical PdNPs@MIP uniformly possessed high electrocatalytic capability and a specific surface area with a large number of NDPhA MIP sites. In this study, compact NDPhA MIP sensors were created by coating the SPGrE substrate with PdNPs@MIP. The quantitative analysis was performed by linear sweep anodic stripping voltammetry (LSASV) using a deposition potential of +0.02 V for 60 s. The linearity range for the NDPhA measurement is 0.01 - 0.1 μM (r^2 = 0.996) and 0.1 – 100 μM (r^2 = 0.992), with a corresponding sensitivity range of 51.935 and 0.821 (μA s) μM^{-1}, respectively. The system provides reliable accuracy of %RSD 1.67% with a minimum

detection limit of ($3S_b$, n = 3) of 0.0013 μM. The intraday and inter-day accuracy (%bias) is determined by the certified reference material (CRM) which were -0.74% and -1.01%, respectively. This research demonstrates the successful application of a compact sensor fabricated to measure NDPhA in beverage and synthetic samples. The compact NDPhA the molecular-imprinted sensor can serve as an alternative approach to food quality control.

CONTENTS

CONTENTS (CONTINUED)

LIST OF TABLES

LIST OF FIGURES

LIST OF FIGURES (CONTINUED)

LIST OF FIGURES (CONTINUED)

FIGURE **PAGE**

LIST OF FIGURES (CONTINUED)

LIST OF APPREVIATIONS

ABBREVIATION	DEFINITION
SPGrE	Screen printed graphene electrode
NDPhA	N-nitrosodiphenylamine
NAs	N-nitrosamine
PdNPs	Palladium nanoparticles
NIPAM	N-Isopropylacrylamide
TRIM	Trimethylolpropane trimethacrylate
AIBN	2,2′-azobis(2-methylpropionitrile)
PVP	Poly(vinylpyrrolidone)
$NaBH_4$	Sodium borohydride
MIP	Molecularly imprinted polymer
WE	Working electrode
RE	Reference electrode
CE	Counter electrode
CV	Cyclic voltammetry
LSASV	Linear sweep stripping voltammetry
mg	Milligram
mL	Milliliter
μA	Microampere
μL	Microliter
DI	Deionization
mM	Millimolar
M	Molar
μM	Micromolar

CHAPTER 1
INTRODUCTION

1.1 The importance and the source of the research

N-Nitrosamines are a group of potential human carcinogens formed from nitrification or oxidation of amine precursors. Nitrosodiphenylamine (NDPhA) has been classified as one of the carcinogenic and mutagenic substances [9] and identified as one of five pollutants possibly occurring in the public water system by the United-state Environmental Protection Agency (US-EPA) [4, 10]. Because of its high toxicity and potential for contamination in water systems, it has sparked public concern about food safety and human health. The US-EPA established the maximum NDPhA content in drinking water at 7 g L^{-1} (0.035 μM) based on a lifetime cancer risk of 1 in 100,0000 [11]. As a result, rapid, sensitive, and selective detection methods for NDPhA in drinking water, beverages, and food are important for public health. Various analytical methods have been applied to NDPhA detection, including the nitrification or oxidation of amine precursors [1 , 2] . They are widespread in human life and consumer products such as processed food [3], beverages [2, 4], cosmetics [5, 6], and cigarettes [7, 8]. As a type of volatile N-nitrosamine, nitrosodiphenylamine gas chromatography [12] and liquid chromatography [13] tandem with mass-spectrometric detection and fluorimetry [11]. It is always desirable to design methods for on-site analysis and household testing kits for food management that are time-saving, cost-effective, and ready-to-use. The electrochemical method is considered a suitable complementary tool to address this demand because of its benefits of simplicity, low costs, and quick time when compared to other methods.

Previous reports presented several electrochemical methods for detecting NDPhA using different electrode materials, such as Hg [14], Au [15], and glassy carbon [16-18] as working electrodes. The analysis was based on amperometric detection of NDPhA in a flow injection system at ruthenium oxides stabilized by cyano cross-links layer modified glassy carbon electrode (GCE) [16]. Poly(diallyldimethylammonium chloride)-stabilized graphene/platinum nanoparticles (PDDA-Gr/PtNPs) [17] and

graphite polyurethane composite (GPUE) [18] modified GCEs are used in the nanomaterial-based sensors with voltammetric detections of NDPhA. However, all of these electrodes somehow have limitations, such as electrode fouling issues and a large positive potential for NDPhA oxidation (0.75-1.56 V vs Ag/AgCl). As a result, several chemicals may interfere with the measurements. To the best of knowledge, there is no record of employing screen printed electrode to create a compact NDPhA sensor. Sensors that are ready-to-use, affordable, portable, and well-suited for on-site monitoring applications require additional development. Furthermore, for practical application/commercialization, sensitivity and selectivity must be improved in order to complement the capacity to function in food samples.

Molecularly imprinted polymers (MIP) with tailored-made affinity and specificity to target analytes have been proven in a wide range of applications, including electrochemical sensors, to improve sensor performance and selectivity [19, 20]. Polymerization may be controlled by adjusting the monomer-to-template ratio, the initiation method or source the surface or place location where it happens, and so on [21, 22]. Furthermore, the polymer chains can be integrated onto a variety of surfaces to generate different architectures such as layer, core-shell, or beads. Core-shell polymerization, or polymerization of the MIP shell around the core, results in a higher surface area-to-volume ratio, more easily accessible recognition sites, improved bidding kinetics and binding capacity, and lower heterogeneities [23-26]. Palladium nanoparticles (PdNPs) are a viable alternative nano-core due to their extra ordinary catalytic, conductivity, and electro-chemical properties [27], as well as their abundance and lower cost when compared to Pt and Au nanoparticles [28, 29]. The PdNPs's good electrical properties and excellent conductivity, combined with the specific recognition site of the MIP shell, will endow sensor with powerful performance for the target analytes. As a result, NDPhA imprinting on core-shell sensing platforms provides selectivity and sensitivity, as well as accuracy for food sample analysis.

In this work, A novel NDPhA compact electrochemical sensor based on a screen-printed graphene electrode modified with palladium nanoparticles and coated with a molecularly imprinted polymer (PdNPs@MIP/SPGrE) was developed. This is the first time that an NDPhA imprinted polymer has been polymerized on the surface of PdNPs. The 3D-imprinting on the surface of PdNPs was effectively achieved by sequentially

coating the surface of PdNPs with PVP, followed by a molecularly imprinted polymer of poly(N-isopropylacrylamide)-co-trimethylolpropane trimethacrylate. A novel PdNPs@MIP is cost-effective, easy to synthesis, has a large number of NDPhA imprinted sites, and has excellent electro-catalytic activity for NDPhA oxidation. The SPGrE was easily prepared by screen-printing, and the synthesized PdNPs@MIP was dropped casting on the electrode surface to fabricated NDPhA-recognition sites imprinted sensor. The compact sensor (PdNPs@MIP/SPGrE) has high selectivity and sensitivity, is rapid to analyze, utilizes a small reagent, and is suitable for large-scale manufacturing. It is suitable for food-quality control and on-site monitoring applications.

1.2 Objectives

1.2.1 To synthesize and characterize of palladium nanoparticles coated with molecularly imprinted polymer (PdNPs@MIP) nanocomposites by using transmission electron microscopy (TEM), electrochemical impedence spectroscopy (EIS), field emission scanning electron microscope (FESEM), fourier-transform infrared spectroscopy (FT-IR), and x-ray photoelectron spectroscopy (XPS).

1.2.2 To study electrochemical behavior of NDPhA on the screen printed graphene electrode modified with PdNPs@MIP by using electrochemical techniques such as cyclic voltammetry (CV) and linear sweep voltammetry (LSV).

1.2.3 To optimize the parameters used in the detection to enhance the sensitivity and selectivity for NDPhA determination.

1.2.4 To study the analytical features of the developed MIP sensor on the quantitative analysis of NDPhA.

1.2.5 To apply the MIP sensor for NDPhA in real samples.

1.3 Expected outcomes

A highly sensitive and selective compact sensor was developed based on the PdNPs@MIP/SPGrE for determination of NDPhA in real samples.

1.4 Scope of research

In this work, a novel NDPhA sensor based on a screen-printed graphene-paste electrode, modified with palladium nanoparticles coated with a molecularly imprinted polymer (PdNPs@MIP/SPGrE), for sensitive and selective detection of NDPhA was developed. NDPhA imprinted polymer is firstly synthesized on the surface of PdNPs core. PdNPs@MIP was prepared by successively coating the surface of PdNPs with polyvinylpyrrolidone (PVP) to afford PdNPs-PVP. For the polymerization step, N isopropyl acrylamide (NIPAM) was selected as functional monomers and trimethylopropane trimethacrylate (TRIM) as a cross-linker. A compact MIP-sensor based on PdNPs coated with a MIP for NDPhA's was firstly developed for quantitative determination using an SPGrE modified with the MIP composite. The portable PdNPs@MIP sensor was constructed using a commercial mini-potentiostat and a laptop. To achieve the research objectives, the scope of the research was set as following.

1.4.1 Synthesis of the PdNPs@MIP

1.4.2 Characterization of the PdNPs@MIP nanocomposites

1.4.2.1 transmission electron microscopy (TEM)

1.4.2.2 electrochemical impedence spectroscopy (EIS)

1.4.2.3 field emission scanning electron microscope (FE-SEM)

1.4.2.4 fourier-transform infrared spectroscopy (FT-IR)

1.4.2.5 x-ray photoelectron spectroscopy (XPS)

1.4.3 Electrochemical behavior of NDPhA on the PdNPs@MIP/SPGrE

1.4.3.1 Study of NDPhA oxidation using cyclic voltammetry.

1.4.3.2 Studies of parameters that affect the sensitivity of the PdNPs@MIP/SPGrE using voltammetry, e.g., PdNPs-PVP loading, molar ratio of template: monomers, molar ratio of monomer: cross-linker, MIP loading, accumulation time, pH of supporting electrolyte.

1.4.4 Analytical features

1.4.4.1 Linearity range for determination of NDPhA

1.4.4.2 Limit of detection (LOD)

1.4.5 Interference study (glucose, fructose, citric acid, caffeine, ascorbic acid, uric acid, diphenylamine, $NaNO_3$, NaCl, and ethanol)

1.4.6 Possibility to apply in real samples (beverage samples, e.g., beer, wine, apple juice, orange juice, green tea, and etc.)

1.4.7 Reproducibility

1.4.8 Studies the stability of the developed the MIP sensor

CHAPTER 2
LITERATURE REVIEWS

2.1 Nitrosamine and N-nitrosodiphenylamine

N-nitrosamines (NAs) are a significant class of volatile human carcinogens. They are formed in foods when nitrogen oxide interacts with amines. In acidic conditions, nitrite in food, whether reduced from nitrate fertilizer or added as a preservative, is hydrogenated to hydronitrogenoxide ($H_2NO_2^+$). The resulting hydronitrogenoxide ($H_2NO_2^+$) reacts with another molecule of nitrite to form nitrogen anhydride after dehydration (Figure 2.1). N-nitrosamines are formed when nitrogen anhydride donates a nitroso group to amines in food. Secondary amine may generate stable nitrosamines, but primary amine-derived nitrosamines break down fast and tertiary amine can scarcely form nitrosamine [30].

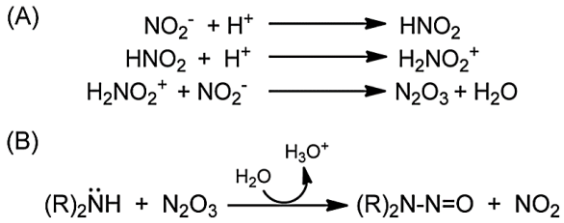

Figure 2.1 N-nitrosamine formation. (A) Formation of a nitrous anhydride from a nitrite (B) nitrosation from a nitrous anhydride and an amine [30]

NAs increase cell growth, leading in tumor formation in vivo, especially in the liver, lung, esophagus, bladder, and pancreas [10]. The International Agency for Research on Cancer (IARC) has classified a number of NAs that enhance the risk of cancer in humans. In 1987, the IARC have thought over N-nitrosodimethylamine (NDMA) and N-nitrosodiethylamine (NDEA) are probably carcinogenic to human, and N-nitrosodibutylamine (NDBA), N-nitrosopiperidine (NPIP), N-nitrosopyrrolidine (NPYR), N-nitrosomorpholine (NMOR), N-nitrosodi-n-propylamine (NDPA), and N-nitrosodiphenylamine (NDPhA) are possibly a carcinogen for human [31, 32]. NAs are

divided into two categories: volatile and nonvolatile. Nonpolar, low molecular weight volatile nitrosamine molecules are extracted from foods using distillation. NAs are linked to proteins and other materials in meat products (for example, sausage and salami), making their extraction difficult. The United States Environmental Protection Agency (US-EPA) has defined nitrosodiphenylamine (NDPhA), a form of volatile NAs, as a carcinogenic and mutagenic substance [9] and listed it as one of five pollutants possibly present in the public water system [4, 10]. Figure 2.2 displays structural representation of NDPhA. Because of its high toxicity and potential for contamination in the water system, it has raised concerns about food safety and human health. The US-EPA set the maximum NDPhA concentration in drinking water at 7 g L^{-1} (0.035 μM) based on a lifetime cancer risk of 1 in 100,000 [11].

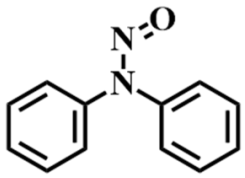

Figure 2.2 Structural representation of NDPhA

2.2 Chemical sensor

The IUPAC (International Union of Pure and Applied Chemistry) set a definition of a chemical sensor; "*A chemical sensor is a device that transforms chemical information into an analytically useful signal, ranging from the concentration of a specific sample component to total composition analysis*." This relatively broad definition excludes the fact that a sensor is often a continuously operating device and that the sensing process must be reversible, especially because intermittently operating sensors with irreversible properties are generally referred to as dosimeters [33, 34]. Figure 2.3 reports a scheme with the classification adopted by IUPAC.

Chemical sensors typically include a sensitive layer or coating and a transducer (transducer is derived from the Latin *transducere*, which means to 'transfer' or 'translate'; a device that translates energy from one domain (e.g. chemical) to another (e.g. physical) is termed a transducer). When a chemical species interacts with the coating (absorption, chemical reaction, charge transfer, etc.), the physicochemical

characteristics of the coating, such as its mass, volume, optical properties, or resistance, reversibly change (Figure 2.4).

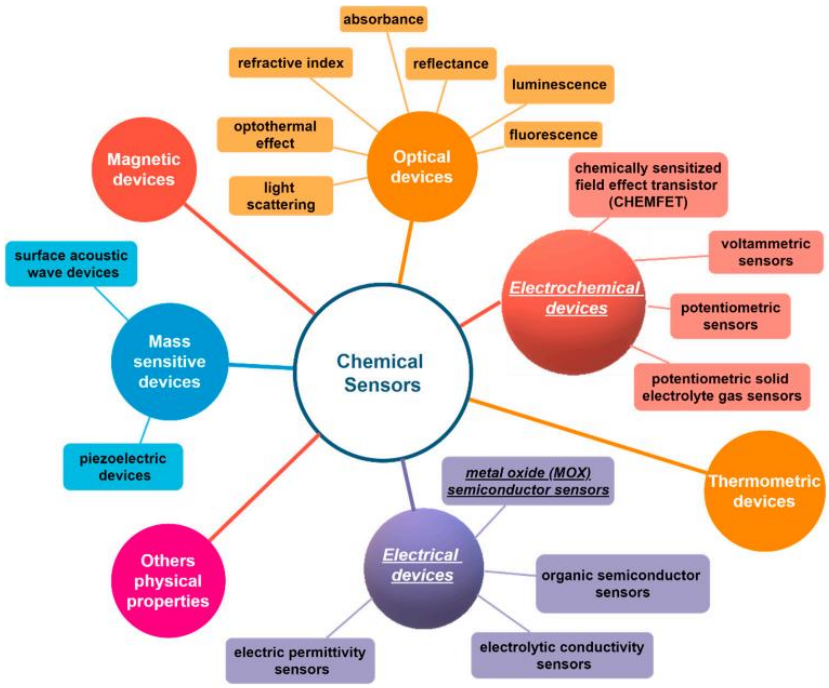

Figure 2.3 The chemical sensors classification from International Union of Pure and Applied Chemistry (IUPAC) [34]

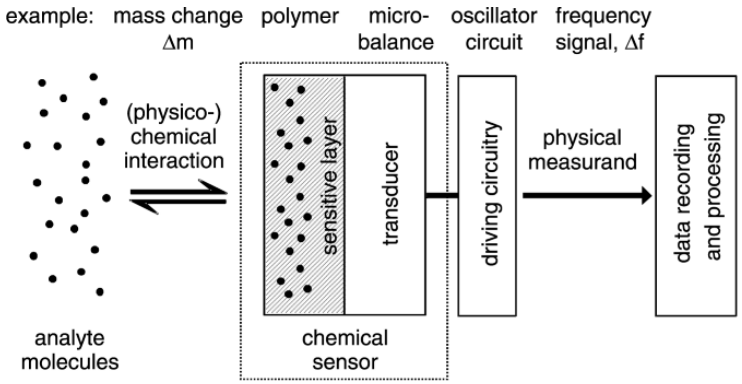

Figure 2.4 Components of chemical sensors exemplified for the mass sensitive principle [35]

These changes in the sensitive layer are detected by an appropriate transducer and converted into an electrical signal, such as a frequency, current, or voltage, which is

then read out and subjected to further data treatment and processing. The mass-sensitive concept may be defined as follows: analyte molecules are absorbed to an extent governed by intermolecular forces into a coating material (polymer). The shift in the resonance frequency of the transducer, such as a microbalance, is caused by the change in mass of the polymeric coating. This frequency shift is the electrical signal that will be employed in later data processing. A wide variety of transducers based on various physical concepts have been devised. According to Janata's suggestions, four major groups of transducers may be recognized [35-37].

(1) chemomechanical sensors (e.g. mass changes due to bulk absorption)

(2) thermal sensors (e.g. temperature changes through chemical interaction)

(3) optical sensors (e.g. changes of light intensity by absorption)

(4) electrochemical sensors (e.g. changes of potential or resistance through charge transfer)

Among the chemical sensor types, electrical and electrochemical sensors are the most simple, and thus have received the most attention and use in practical applications: either gases or substances in the liquid phase can be detected and quantified utilizing simple electrical and electrochemical transduction platforms [38].

2.3 Electrochemical Sensors

Electrochemical sensors translate information from electrochemical reactions (the reaction between an electrode and an analyte) into a useable qualitative or quantitative signal. Potentiometric, conductometric, and amperometric/voltammetric electrochemical sensors are the most common. As seen in Figure 2.5, electrochemical sensors can provide electrical outputs in digital signals for further analysis. In general, the reactions observed in these sensors are the result of chemical and electrical interactions, which are ultimately based on conductometric, amperometric, and potentiometric measurements. Electrochemical transducers are the most commonly utilized transducers in the development of novel sensors, including biosensors. They are the market leaders in terms of availability and have already demonstrated their actual benefits [39, 40].

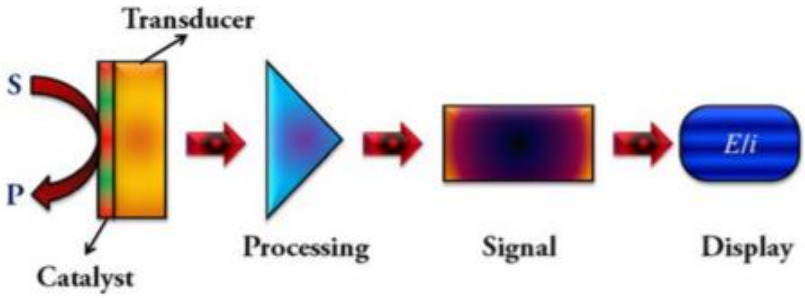

Figure 2.5 The main stages in the sensor operation [40]

Electrochemical sensor technology is an important part of modern analytical chemistry and has captured vast attention. Understanding the principles of sensors necessitates a strong understanding of several academic areas related to every aspect of science. As a result, chemists, physicists, biologists, biologists, electrical engineers, and biologists work in this multidisciplinary field. Sensors have potential uses in a variety of fields, including science, pharmaceuticals, medicine, analysis, chemistry, materials engineering, synthesis, molecular engineering, and biotechnology.

Electrochemical sensors and detectors are intriguing for detecting onsite contamination as well as meeting environmental standards. They are used to regulate the checking at various points of the measurement, which might offer useful information at various stages of the decision-making process. This is especially critical for biological samples, which are often tiny in size, and tissue harm should be minimized, especially when in vivo monitoring is necessary. The ability to automate and manufacture small sensors is extremely useful for scientific purposes. Electrochemical sensors provide several advantages over traditional analytics, which will lead to widespread usage in the near future. They are a fascinating scientific instrument because of their innate selectivity and sensitivity to electroactive analytes, and they are less time consuming, flexible, and simple to set up. They are portable and lightweight devices that are simple to use and small, leading in faster research data arrangement. The choice of suitable functional principles, design, and material for a sensing toolbox is influenced by factors such as portability, selectivity, sensitivity, the requirement for single or multivariate discovery, and any applicable field applications. The selection of fabrication techniques and resources is critical for sensor operation, and sensor performance typically depends

on these critical parameters. As a result, future advancements in device design should focus on the development of novel materials and technologies. The use of nanomaterials and porous particles in electrochemical sensing tools to improve selectivity and volatility is becoming progressively growing [40].

There are three types of electrochemical sensing: Conductimetric, Potentiometric, and Voltammetric [41].

(1) Conductimetric sensor: The concentration of charge between two electrodes can be calculated via a conductimetric measurement of solution resistance. These measures are not species-specific but are utilized in conjunction with separation techniques like high performance liquid chromatography.

(2) Potentiometric sensor: A potentiometer is used to measure the equilibrium potential of an indicator electrode against a selected reference electrode at zero current (approximated by using a high-impedance voltmeter). If a suitable electrode material can be found, ion-selective electrodes can provide good selectivity to a specific species, in many cases with minimal interference from other ions.

(3) Voltammetric sensor: A current-voltage profile is created by registering the current as a function of applied potential using a potentiostat (or potential is recorded as a function of applied current using a galvanostat). Working (indicator), auxiliary, and reference electrodes are usually necessary; the reference electrode can also serve as an auxiliary electrode if the currents are very small. More information and lower detection limits can be achieved than with potentiometric sensors, and many electroactive species can be determined in the same experiment if they respond at different applied potentials. As a result, the previous separation of components of complicated mixtures is not required in the most easily applicable situations for these types of sensors.

2.4 Voltammetric sensor

The dropping mercury electrode (DME), created by Heyrovsky in 1922 and for which he received the Nobel Prize in 1959, was the first voltammetric instrument capable of examining current-voltage profiles in a practical fashion from a sensing standpoint [42]. Dynamic processes are probed, as unliked to potentiometric sensors. This might be used to determine the number of reducible species in a solution (but unfortunately for only a few oxidizable ones owing to the oxidation of mercury itself).

The first reproducible measurements of numerous species, notably metal ions, were made by selective reduction based on their half-wave potentials, as well as investigations of the process of reduction and quantification of several organic species [43, 44]. Liquid mercury has a very wide negative potential range in aqueous solutions due to a significant overpotential for hydrogen evolution that is unmatched by any other electrode material. The cyclic operation of the dropping mercury electrode involves continual drop development at the end of a small capillary until it falls owing to gravity and another begins to form. As a result, it is a hydrodynamic electrode in the sense that there is enforced convection induced by movement (growth) of the electrode (drop) itself rather than movement of the solution. Thus, if the experimental data are treated in the correct way, pseudo-steady-state voltammograms can be constructed. The DME was a breakthrough that was used for many years, but future practical advancements were delayed since the related control and analysis instrumentation was not sufficiently sophisticated. This changed when integrated circuits became available, allowing for simple current sampling at particular areas of drop growth. It resulted in the widespread use of normal and differential pulse polarography, wherein pulses were synchronized with drops and applied at the end of drop life. Once this was accomplished, other waveforms, such as square wave polarography, could be developed; this had also been proposed in the early 1950s but had not been properly realized due to insufficiently good electronics. The hanging mercury drop electrode, which has since been largely replaced by the static mercury drop electrode, eliminated the periodic variation in current caused by drop growth, which was also one of the main benefits, especially with organic compounds, of avoiding long-term adsorption on the mercury surface.

There was clearly a need to employ other electrode materials which permit sensing in the positive potential range via oxidation and preferably offer access to both positive and negative potential ranges. The noble metals, platinum and gold, and, to a lesser extent, silver, were the first materials to be investigated for this purpose. This enabled the fabrication of solid electrodes of various shapes and sizes, but it did not address the issue of repeatability unless highly efficient and consistent stirring could be carried out. Carbon-based electrode materials have been produced, sometimes with worse electrode kinetics but with the benefit of being more cheaply available than noble metals. Other materials have followed. Bismuth, for example, has a large negative potential range that

is nearly as excellent as mercury, but without the toxicity issues. Procedures for cleaning and conditioning solid electrode surfaces have been developed to help alleviate some of the problems associated with solid surface contamination.

The problem of getting steady-state, reproducible data at solid electrodes was overcome by using forced convection, either of the electrodes or of the solution. The best example of the former is rotating disc and ring-disc electrodes and of the latter channel/tube or wall jet. In these cases, true steady-state current-voltage profiles may be recorded. The diffusion-limited current is directly proportional to the concentration (the potential can be set at this value and the current recorded as a function of concentration), and the shape of the voltammetric curve may provide some kinetic information. However, even with high convection rates, the detection limit is of the order of 10^{-4} M. This may be considerably improved by using pre-concentration techniques such as stripping voltammetry, different preconcentration timescales, and determination steps enabling lower concentrations to be measured.

Since the 1970s, pulse techniques, particularly differential pulse voltammetry and square wave voltammetry, have flourished in terms of their range of applicability at solid electrodes and are especially simple to execute with digital-based instrumentation. Because of their transient nature, they allow for a 1,000-fold decrease in the detection limit. They also enable the investigation of electrode kinetics while providing analytical information. Square wave voltammetry has the added benefit of being fast, which means that, in addition to reducing experimental time, problems associated with dissolved oxygen are reduced, which is especially useful with pre-concentration stripping voltammetric procedures that can reach down to 10^{-9} M or even lower.

Before the advent of equipment that allow the use of pulse approaches, alternating current voltammetry began to show great promise in the 1960s and 1970s. Cyclic and linear sweep voltammetry had shown themselves not able to go much below 10^{-5} M. Although the information acquired by alternative current (AC) voltammetry is similar in terms of sensitivity and detection limit to that received by pulse voltammetry, it is not widely employed due to the digital nature of modern electrochemical instruments. However, the scope of electrochemical impedance spectroscopy utilizing modest alternating voltage perturbations has expanded, with applications in sensor

characterization becoming more widespread and the development for impedimetric sensing [41].

2.5 Molecularly imprinted polymer

Since Wulff and Sarhan released one of the earliest papers on molecular imprinting in 1972 [45], molecular imprinting is one of the most prominent strategies for presenting molecular recognition sites, and it has attracted an increasing number of attempts to prepare complementary parts of target molecules [46]. This approach is primarily based on the molecular identification reaction that occurs in the surroundings of the target molecule, which is referred to as a template. The template and functional monomers first formed the pre-complex, as shown in Figure 2.6. After the cross-linker and pre-complex interactions that retain the position of the functional groups to bind the template capable of producing molecular recognition sites, the polymerization was accomplished. After removing the template with suitable desorption agents at the conclusion of the polymerization stage, the polymeric matrix includes specialized recognition sites, allowing molecularly imprinted polymers (MIPs) to bind the template with great selectivity as compared to other competing molecules [47]. MIPs may be created using a variety of cross linkers, functional monomers, and solvents. The quality of MIPs and their binding properties are affected not only by the mixture, but also through experimental conditions such as initiator type and quantity, polymerization temperature, interaction mechanisms, and so on.

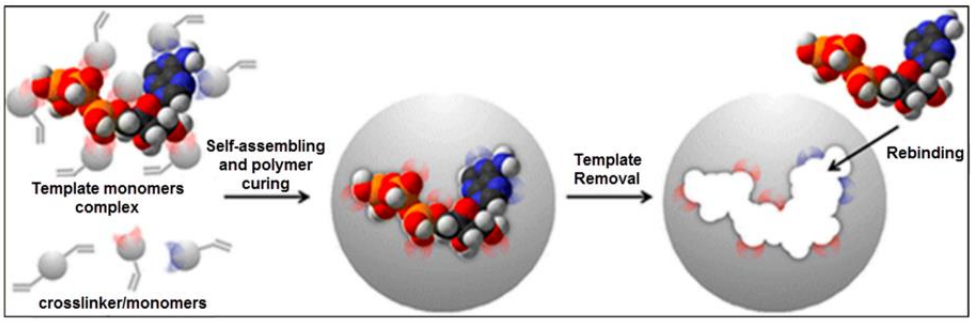

Figure 2.6 A schematic representation of the molecular imprinting method [48]

It is widely assumed that the template works as a crucial molecule and that the other compounds (cross-linkers, functional monomers, and solvents) should be chosen depending on the chemical and physical properties of the template [49]. Furthermore, by altering the monomer and cross-linker composition, the stability as binding strength of the target molecule of the imprinted polymers is adjusted [50]. Baggiani et al. presented an alternate viewpoint to the molecular imprinting process based on these findings [51]. As seen in Figure 2.7, the presence of the template in the pre-complex mixture improves the interactions that already exist in a non-imprinted polymer (NIP). As a result, if the NIP fails to attach the target molecule, the MIP exhibits a poor imprinting effect.

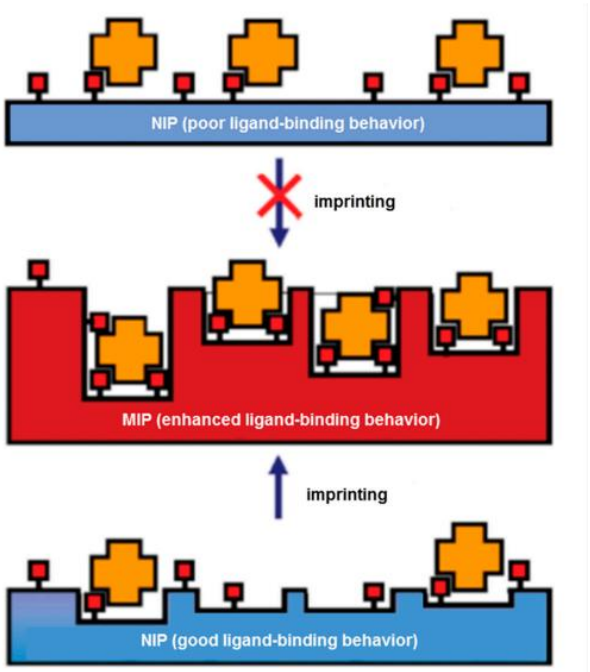

Figure 2.7 A schematic illustration of the alternative imprinting hypothesis [51]

There are four types of molecular imprinting: Covalent imprinting, Non-covalent imprinting, Metal-ion exchange imprinting, and Semi-covalent imprinting [45].

(1) Covalent imprinting: Wulff and Sarhan [52, 53] initially published the covalent imprinting approach for the imprinting of D-glyceric acid (the template) employing molecules with boronic acid and amine-based functionalities for the steric arrangement and polymerizable vinyl groups combined with divinylbenzene as a cross-

linker. The first approach reported for the design of artificial receptors was molecular imprinting by covalent forces. Because of the high stability of the template-monomer(s) complex, which arises from the strong bonds formed between them, and theoretically leads to highly specific and high-affinity MIPs, this approach is suitable when a high level of precision on the specificity of the imprinting is desired. However, what is its main benefit becomes also its major disadvantage given the difficulty to remove the template once the MIP is synthesized. This is demonstrated by the poor template recovery after polymerization, as well as the increased difficulty in rebinding/removing the template when employed as a MIP, resulting in slower kinetics. To use this method, the template molecule must have at least one functional group that may be derivatized, such as alcohols, aldehydes, ketones, amines, or carboxylic acids, which are typical examples in the literature. The template must be removed when the specific cavities have been created by chemically cleaving the bonds using the synthesized MIP. This can be achieved in a variety of methods, including acidic hydrolysis or reductive cleavage of the ester bonds using concentrated acids or bases, or by using high pressure or supercritical CO_2. Other disadvantages of this synthetic approach include (1) the template modification implies an extra step, and (2) the limited number of species that may form a covalent bond with reversible properties (the list includes carboxylic and boronic esters, ketals, disulfide bonds, acetals, and imines), which limits the species that can be used as templates and, as a result, the MIPs that can be synthesized using this strategy.

(2) Non-covalent imprinting: The nature of the prearrangement in non-covalent imprinting (with a wider range of chemical functionalities and a comparably easier synthesis procedure) became a significant milestone that opened the way for a wide range of uses and applications in a wide range of scientific areas. The Van der Waals forces, dipole-dipole, charge-dipole, cation-π, π-stacking, hydrogen bonding, or electrostatic (charge-charge) interactions, and among others are predominant for the formation of the self-assembled pre-polymerization complex in this approach. In contrast, functional monounsaturated monomers such as vinylic, acrylic, or methacrylic monomer are utilized in the synthesis of the MIP, along with a large amount of cross-linker of the same kind (vinylic, acrylic, or methacrylic). The final organic network material is generally produced via free radical polymerization (thermally or UV

induced). The main benefits of non-covalent imprinting are the infinite number of templates that may be employed, the simplicity of preparation, the faster and more efficient template removal, and, most importantly, the more favorable rebinding kinetics. However, the specificity of the binding sites is clearly compromised due to heterogeneity from the different pre-polymerization complexes formed, direct competition from the solvent, the cross-linker (which is added in high proportion to obtain a polymer with greater rigidity), or underestimation of the chaos generated by the polymerization process, which is frequently promoted by thermal-induced polymerization, the so-called free radical polymerization (FRP).

(3) Metal-ion exchange imprinting: Metal-ion exchange imprinting, similar to semi-covalent imprinting, aims to take advantage of metal ions to create ionic bonds (which are stronger than hydrogen bonds or electrostatic interactions) that facilitate the interaction between the monomer and the template molecule, while also combining the benefits of covalent and non-covalent imprinting. Metal ions, in other words, serve as an assembly pivot for the production of the pre-polymerization complex. The metal ion may create a complex with the template and monomer(s) that form coordinative bonds with metals, or it may be imprinted using ionophores. By altering the metal, its oxidation state, and/or the ligand properties, the interaction of the metal ions and the stability of the complexes generated may be controlled. The interaction of metal ions and the stability of the complexes generated may be controlled by altering the metal, its oxidation state, and/or the ligand properties. Moreover, in addition to serving as a monomer via the incorporation of the accompanying ligand (e.g., porphyrins) into the polymeric material, they can also serve as a template for the imprinting of metal ions.

(4) Semi-covalent imprinting: The semi-covalent technique approach combines the benefits of both covalent and non-covalent synthesis while counterbalancing their disadvantages. The basic idea is to create a MIP based on covalent imprinting (a pre-polymerization complex with covalent bonds), and then after the polymerization step, the covalent features involved are replaced by non-covalent functionalities, allowing the template to be rebinded using non-covalent interactions. This combined technique thus benefits from covalent imprinting's lower non-specific contacts and more precise cavities, as well as non-covalent imprinting's more favorable template rebinding process (the rebind is only affected by diffusion parameters, without counting any other kinetic

parameter than diffusion). Crowding and steric hindrance between the MIP and the template, on the other hand, may occur as a result of the change in functionalities, causing a loosening in the polymer binding capacity and hampered the imprinting. To counteract this disadvantage, a linker group (also known as a sacrificial spacer) may be utilized to connect the template and the monomer(s) that are lost after template removal. In this way, the sacrificial spacer helps to covalently bind the template and functional monomer(s) during pre-polymerization while also preventing steric effects following template removal. Carbonate ester, carbamate, urea, salicylamide, or silyl ether are some examples of sacrificial spacer groups identified in the literature. However, the inclusion of sacrificial spacers decreases the number of options for tailor-made cavities by imprinting process, adds an extra coupling phase that must be optimized, and gives a less efficient template recognition if the required attraction dipoles are not strong enough.

2.6 Screen-printed disposable electrodes

Screen-printed electrodes (SPEs) are disposable sensors that rely on screen-printing technology. They are created by printing different types of inks on various ceramic or plastic substrates. Polyester screens are often used for printing; the analyst could design different patterns of these screens based on the analytical purpose. Both the selectivity and sensitivity required for the analytical technique are mostly dictated by the composition of the different inks used for printing. Furthermore, there is a wide range of commercially available products of this type [54].

The SPEs surface may be easily adjusted to fit a variety of purposes connected to various analytes and to achieve a variety of enhancements. The composition of printing inks, which may be varied by adding a range of chemicals like as polymers, metals, complexing agents, enzymes, and so on, is one of the two key tactics that contribute to the high adaptability of SPEs. Alternately, electrodes can be changed by depositing various things on their surfaces, such as metal coatings, enzymes, polymers, and so on [55].

The primary benefits of these electrodes are their ease of use, dependability, possible mobility, and tiny instrumental setups including the reference, working, and auxiliary electrodes, as well as their important economic advantage, which is their low

cost [56]. Furthermore, the same electrode surface may be securely utilized for further examination since its disposable nature prevents electrode poisoning from repeated usage. These SPEs have also been shown to be particularly beneficial in comparison to other solid electrodes for direct and reliable examination of a variety of materials from diverse sources. The repeatability of the results following repeated usage of the SPEs is regarded as an important aspect [57].

2.7 Palladium nanoparticles (PdNPs)

Metallic nanoparticles are appealing due to their exceptional electrical, optical, and electrocatalytic properties. They are widely employed in various domains, including chemistry, electronics, catalysis, and biology, as a class of adaptable nanomaterials [58]. Palladium nanoparticles (PdNPs) in particular are intensively explored in the field of catalysis, and they are suitable alternatives for platinum nanoparticles due to their quick electron transport, large surface to volume ratio, low toxicity, virtuous electrical behavior, and plentiful availability [59,60]. The performance of PdNPs is heavily influenced by their size, shape, and aggregation state, among other factors. Pd NPs are generally fastened by appropriate support materials to make them homogeneous in size and equally disseminated, which not only successfully solves the stability problem but also improves their electrocatalytic activity [61].

2.8 Electrochemical techniques

2.8.1 Cyclic voltammetry (CV)

CV is a potentiodynamic electrochemical technique that may be used to get qualitative and quantitative information on electrochemical reactions, such as electrochemical kinetics, reaction reversibility, reaction mechanisms, electrocatalytic processes, and other characteristics. The Solartron 1287 is an example of a potentiostat, which is used in this approach. The measurement is typically carried out in a three-electrode configuration or electrochemical cell that has a working electrode, a counter electrode, and a reference electrode. In this electrochemical cell, the electrolyte is either a liquid solution or a solid membrane. The potential of the working electrode in the examined system is monitored with respect to the reference electrode during CV measurement, and the potential is scanned back and forth between defined higher and

lower limits. At the same time, the current flowing between the working and counter electrodes is measured. As seen in Figure 2.8, the potential is generally linear over time with a slope; this slope represents the scan rate of the potential.

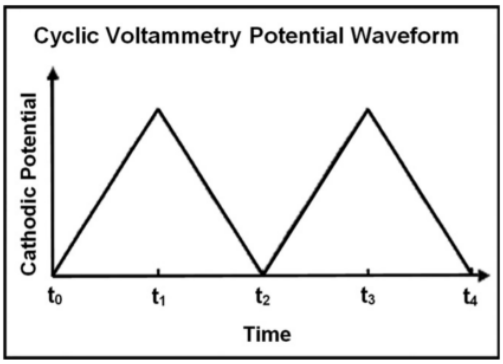

Figure 2.8 Typical CV potential waveform [62]

The current flowing through the working electrode is greatly influenced by the potential scan rate, the working electrode's state, and electrolyte composition. The cyclic voltammogram, depicted in Figure 2.9, is a plot of current vs. potential. In this figure, the CV represents a reversible oxidation–reduction reaction. The upward peak represents oxidation of the active species in the solution, whereas the descending peak suggests reduction of the species. This technique can also be used to study the surface redox reaction on the working electrode [62].

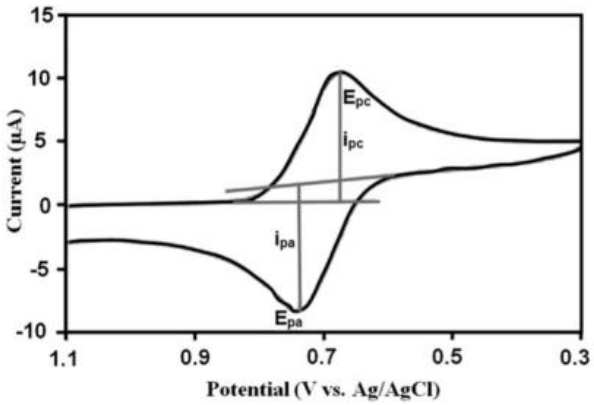

Figure 2.9 Typical cyclic voltammogram. E_{pc} and E_{pa} are the cathodic and anodic peak potentials, and i_{pc} and i_{pa} are the cathodic and anodic peak currents, respectively [62]

2.8.2 Stripping voltammetry

Stripping analysis entails concentrating the analyte into or onto the surface of the working electrode. Following the preconcentration procedure, an electrochemical measurement of the preconcentrated analyte or stripping from the electrode surface is performed using a potential scan. The preconcentration and measurement steps work together to provide an exceedingly favorable signal-to-background ratio. The inclusion of a "built in" preconcentration stage is a characterization characteristic of stripping analysis. Stripping analysis is substantially more sensitive than direct polarographic procedures due to the inclusion of a preconcentration step. Furthermore, this approach provides a broad linear range and a direct examination of analyte trace concentrations. Fast linear sweep voltammetry was the first modern variant of classical stripping to appear in 1947-1960, followed by the introduction of square wave and pulse Polarography by Barker et al [63-65].

2.9 Related Research

2.9.1 Screen-printed electrode (SPE)

In 2012, W. Kit-Anan et al. [66] developed a new paper-based electrochemical sensor as a low-cost and disposable point-of-care device for pre-screening purposes. Electrodes of this new sensor are fabricated using two printing techniques, i.e., screen-printing for base material and inkjet-printing for modifying functional material, and the performance of fabricated sensors for Ascorbic acid detection is demonstrated. The paper-based device consists of three electrodes including Polyaniline (PANI) modified Screen-Printed Carbon Electrode (SPCE) as working electrode and two bare SPCEs as reference and counter electrodes (Figure 2.10). Three SPCEs are initially screen-printed on a filter paper, and PANI is consecutively inkjet-printed on the designated working SPCE. Its electrochemical performances are systematically investigated towards Ascorbic acid using Cyclic Voltammetry (CV) with different acetate buffer pHs and numbers of printed-PANI layers. The CV results show that the optimal buffer pH and number of PANI layers are 4.0–5.0 and 5, respectively. Consequently, real-time detection of Ascorbic acid concentration is performed using Chronoamperometry technique under the optimal conditions from previous CV studies. From the results, the sensor exhibits a good sensitivity of 17.7 µA/mM and a moderately

low limit-of-detection of 30 ± 3 µM in a concentration range of 30–270 µM. According to cost versus performance, the utilization of paper-based sensor with inkjet-printed PANI modified SCPE is an alternative for low-cost and disposable point-of-care applications.

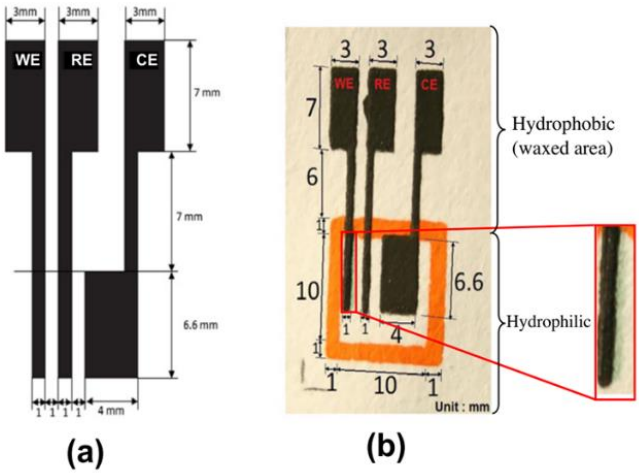

Figure 2.10 Layout of three electrodes; (a) designed device, (b) fabricated device [66]

In 2017, C. Karuwan et al. [67] proposed a new method for mass fabrication of new microfluidic device with integrated graphene-based electrochemical electrodes by screen printing technique for in-channel amperometric detection. Graphene-based working and counter electrodes were fabricated by screen printing graphene paste on a glass substrate followed by screen printing of silver/silver chloride (Ag/AgCl) reference electrode. The screen-printed substrate was then bonded to prefabricated polydimethylsoloxane (PDMS) sheet containing microchannels via oxygen plasma treatment. The developed microfluidic device was then applied for glutathione analysis in pharmaceutical products. The method offers effective and fast glutathione detection with good analytical features including a wide dynamic range (10-500 µM) and a low detection limit (3 µM). In addition, the screen-printed graphene electrode (SPGE) exhibits a good stability in microfluidic flow system and good repeatability for amperometric detection. The method has numerous advantages including low

fabrication cost, high sensitivity, high throughput and satisfactory reproducibility. Thus, it holds great promise for advanced analytical applications.

In 2019, P. Pasakon et al. [68] fabricated a screen-printed carbon paste electrode (SPCE) combined with multi walled carbon nanotubes (MCNT) and graphene (GP) in different mixing ratios. The process of printing pastes and electrodes is as follows. Graphene was prepared by electrolytic exfoliation. For this, two carbon rods were immersed in a 3% (w/w) sodium polystyrene sulfonate (PSS) solution. A potential of 8 V was then applied between them for 15 h leading to exfoliation of graphene sheets from the graphite. PSS stabilizes the dispersion and prevents restacking of graphene sheets. The graphene/PSS dispersion was filtered with filter paper and washed with ethanol and DI water several times. The collected solids were dried at 100 °C for 15 h and stored in a desiccator. Printable paste was prepared by mixing commercial carbon paste with MCNT and graphene/PSS in different quantities and dispersed homogeneously in a mortar. The pastes were screen printed onto polyvinyl chloride (PVC) sheets through a silk-screen printing mesh (mesh size 120 µm) over 2 cycles. After that, Ag/AgCl ink was printed on the PVC sheet for 2 cycles. Finally, insulating ink was printed on PVC sheet for 2 cycles. PVC sheet was baked at 60 °C for 1 h to remove any solvent. Figure 2.11, consists of three screen-printed parts, two carbon elements functioning as working electrode (WE) and counter electrode (CE) as well as an Ag/AgCl element as reference electrode (RE). The sensing area of the electrode is defined by insulating ink screen printed on the PVC sheet in the final step. The surface area of the WE is 7.68 mm^2. The as-prepared electrode was then employed to detect H2O2 and nicotinamide adenine dinucleotide (NAD^+/NADH) achieving sensitivity and LOD of 0.0027 µA $µM^{-1}$ and 7.1 µM for H_2O_2, and 0.0075 µA $µM^{-1}$ and 3.6 µM for NADH, respectively. Therefore, it was found that the addition of MCNT and graphene to commercial carbon paste for screen printable electrochemical sensor is feasible for fabrication of sensing electrodes for electrochemical detection.

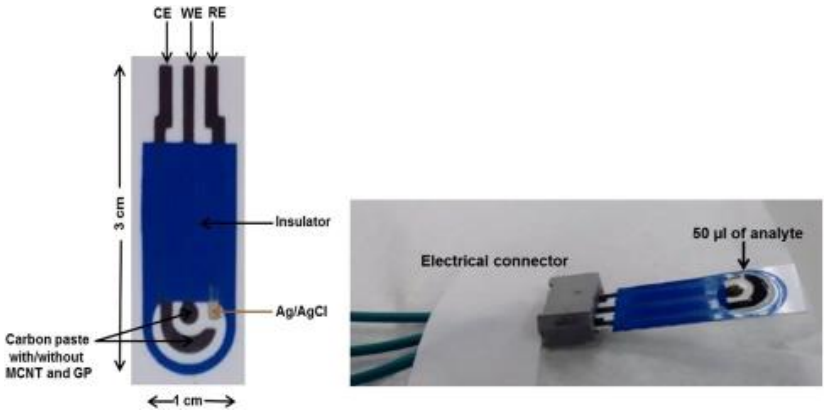

Figure 2.11 Components of fabricated electrode and electrical connectors [67]

In 2019, J. Kampeera et al. [68] presented a rapid detection platform for Vibrio parahaemolyticus by combining loop-mediated isothermal amplification (LAMP) and disposable electrochemical sensors based on screen-printed graphene electrodes (SPGEs). The LAMP reactions using primers targeting V. parahaemolyticus toxR gene were optimized at an isothermal temperature of 65 °C, providing specific detection of V. parahaemolyticus within 45 min at the detection limit of 0.3 CFU per 25 g of raw seafood. The LAMP amplicons can be effectively detected using unmodified SPGEs, redox active molecules namely Hoechst-33258 and a portable potentiostat. A simple and easy-to-use mini-potentiostat was developed for onsite detection of LAMP amplicons. The circuit was designed to be compact with low power consumption and operable with a small battery as shown in Figure 2.12 The case of portable mini-potentiostat was prototyped using a 3D printer and then manufactured using a computational numerical control (CNC) machine. The software of mini-potentiostat was developed and written using C programming. Presently, the mini-potentiostat could perform two electrochemical methods including cyclic voltammetry (CV) and chronoamperometry. The parameter settings were the same as those of a standard potentiostat but the potential range and resolution were limited to 0–1 V and 0.05 V, respectively. Therefore, the proposed system is particularly suitable as a point-of-care device for on-site detection of foodborne pathogens.

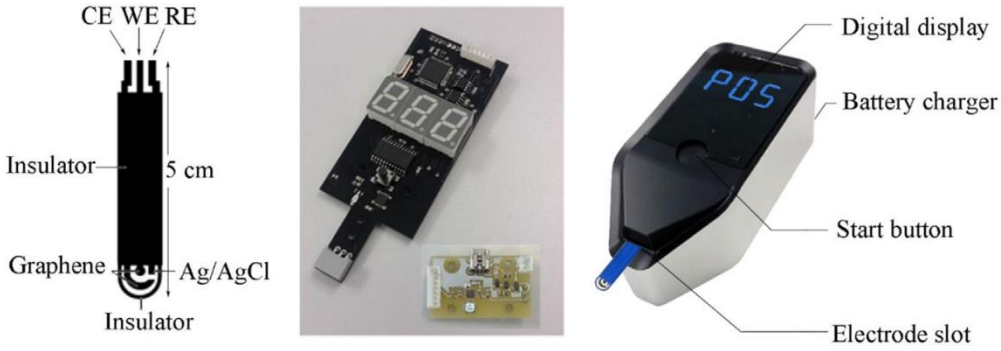

Figure 2.12 Design of screen-printed graphene electrode (SGPE) comprising counter electrode (CE), working electrode (WE) and reference electrode (RE) and photographs of printed circuit board (PCB) and housing of portable mini-potentiostat along with a SGPE [68]

2.9.2 Determination methods for N-nitrosamines (NAs)

In 2007, R. T. S. de Oliveira et al. [69] developed an electroanalytical procedure for N-nitrosamines (N-nitrosopyrrolidine, N-nitrosopiperidine, and N-nitrododiethylamine in aqueous solutions by using the electrochemical methods cyclic and square-wave voltammetry. Cyclic voltammetry was used to study the electrochemical behavior of N-nitrosamines on the boron-doped diamond electrodes. The irreversible electrooxidation peak was observed at 1.8 V (vs. Ag/AgCl) for both N-nitrosamines. Under optimized conditions, the square wave voltammetry technique was applied for determination of N-nitrosamines at frequency (f) of 250 Hz, amplitude (E_{sw}) of 50 mV and scan increment (E_s) of 2 mV in Britton-Robinson buffer solution pH 2 as electrolyte (Figure 2.13). The detection and quantification limits determined for total N-nitrosamines were 6.0 X 10^{-8} and 2.0 X 10^{-7} mol L^{-1}, respectively.

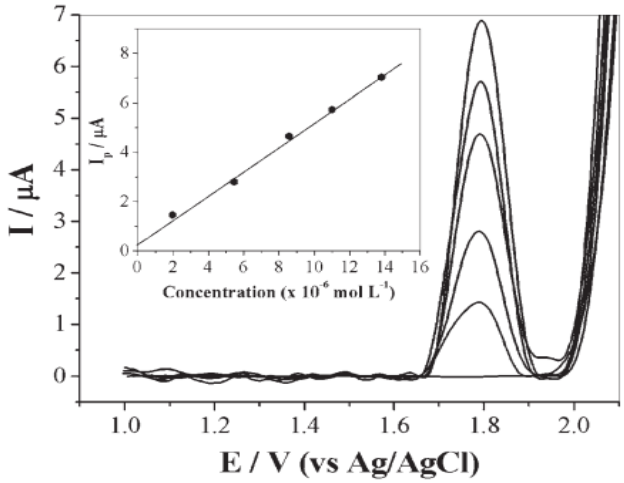

Figure 2.13 Square-wave voltammetry response of a BDD electrode for different total N-nitrosamines concentrations in B – R buffer solutions pH 2. Inset: Linear dependence of the peak current on total N-nitrosamines concentrations, f = 250 Hz, E_{sw} = 50 mV, E_s = 2 mV [69]

In 2008, H. L. Yang et al. [15] proposed a method for quantification of N-nitrosodiphenylamine at an Au electrode in the medium of room temperature ionic liquids (RTILs) [$BMIM^+$][BF_4^-] acting as an electrolyte. Due to the RTILs has good solubility of organic compounds and allows a wide performance potential window of the platinum or gold noble electrode. After the investigation of the electrocatalytic behavior of NDPhA at a gold electrode in this room temperature ionic liquid electrolyte, highly sensitive determination of NDPhA was designed. In this work, the porous gold electrodes with different active surface areas prepared using the glucose reduction method have the same effect on the electrocatalytic oxidation of NDPhA in the ionic liquid phase. Electrodes with different active surface area were achieved by changing the anodic oxidation time at 10 V from a solution of 0.1 M pH 7.4 PBS. Figure 2.14 shows porous Au electrodes of different roughness and found that the peak current for the oxidation of NDPhA with the same concentration in the RTILs increased as the roughness increases. Therefore, a sensor with high sensitivity was constructed by applying porous Au electrodes with highly electrocatalytic activity and large active surface area. The present approach on one hand broadens the application field of room

temperature ionic liquids, and on the other hand provides a sensitive analytical method for environmental detection.

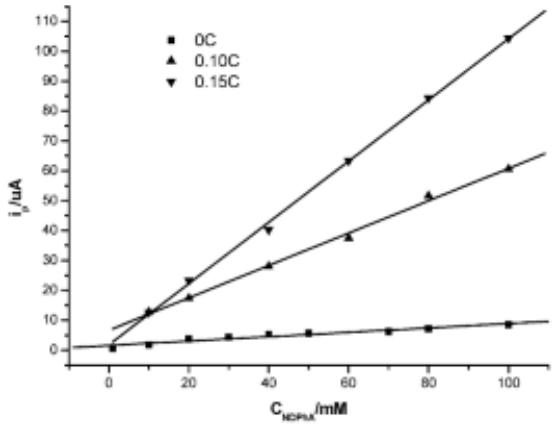

Figure 2.14 Plots of peak current vs. concentration of NDPhA showing comparison of flat Au electrode and porous Au electrode prepared by electrochemical deposition method. Each data in the plot was averaged by three measurements [15]

In 2009, K. A. Shah et al. [71] improved the determination of 4-(methylnitrosamino)-1-(3-pyridyl)-1-butanol (NNAL) in human urine by solid phase extraction on a molecularly imprinted polymer column provided by Supelco (Bellefonte, PA, USA) coupled with HPLC and -MS/MS detection. The influence of ion suppression due to sample matrix effect was evaluated and found to influence the response of NNAL. Under optimization condition, the extraction steps and chromatographic separation were modified to yield a 25-fold improvement in sensitivity and through avoidance of ionization suppression that was found with a previously published method and sample throughput has been improved. The dynamic range of the assay extends from 20 to 2500 pg/mL with a mean $r^2 > 0.998$. The lower limit of quantitation for the assay was 20 pg/mL despite the use of an inherently lower sensitivity instrument. The method was validated according to current FDA guidelines for bioanalytical method validations.

In 2016, X. Cetó et al. [72] report on the development of an impedimetric sensor towards the determination of Nnitrosodimethylamine (NDMA) in water samples. The approach presented herein is based on the usage of a molecular imprinted polymer (MIP) as the recognition element in conjunction with a glassy carbon electrode (GCE)

as the electrochemical transducer. The MIP particles were first synthesized by the precipitation polymerization method, and afterwards entrapped in an electropolymerized polypyrrole membrane. Figur 2.15 shows schematic of the MIP sensor preparation and approach for the detection of NDMA. Briefly, NDMA (0.135 mmol, template) and MAA (0.45 mmol, monomer) were first mixed in 40 mL of methanol for 1 h in ice to allow the creation of complexes between the functional monomer and the template via interfacial hydrogen bonding. However, complexation proceeds quickly to reach a new equilibrium, and thus shorter reaction times should be considered for further experiments. Subsequently, EGDMA (1.8 mmol, crosslinker) and AIVN (0.12 mmol, catalyst) were added to the mixture. The solution was mixed at room temperature for a few minutes and then sonicated for 10 min. After purging with nitrogen for 5 min, the solution was sealed and placed in a water bath at 60 ◦C for 18 h. The synthesized particles were collected by centrifugation at 10,000 rpm for 5 min. The template molecule was extracted by washing 8 times with 15 mL of ethanol. The particles were finally dried overnight at 100 ◦C. Similarly, a control NIP was also prepared following the same procedure, but in the absence of NDMA (the template molecule). The mean size distribution of the MIP and NIP particles was estimated to be ca. 820 nm and 115 nm, respectively. The developed sensor showed a selective response towards NDMA with a linear range from 10 to 230 g L^{-1} and a limit of detection of 0.85 g L^{-1}; without showing significant response towards structurally-related compounds. The MIP gave an order of magnitude higher sensitivity for NDMA detection than the non-imprinted polymer (NIP). Lastly, the developed sensor was applied to the determination of NDMA in spiked drinking and recycled water samples, obtained from conventional treatment and disinfection systems, without showing any matrix effect.

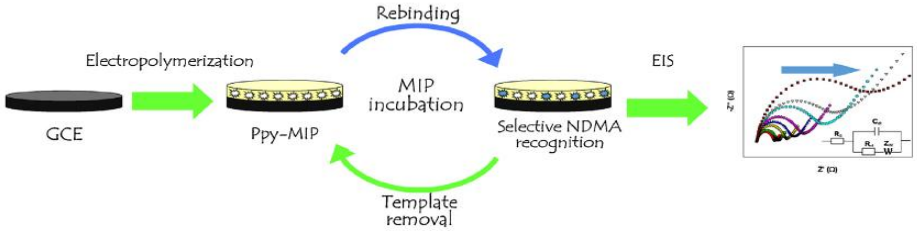

Figure 2.15 Schematic of the MIP sensor preparation and approach for the detection of NDMA [72]

In 2016, X. Zheng et al. [73] synthesized a novel hollow molecularly imprinted polymer (HMIPs) microspheres via two-stage dispersion polymerization and swelling seed polymerization technique with nicotinamide (NAM) as the template molecule. Binding experiments showed that the HMIPs possessed excellent binding properties toward N-nitroamines, including fast mass transfer rate, and efficient adsorption performance with the adsorption capacity reaching up to 1.7 mg/g, which was 3 times higher than that of hollow non-imprinted polymers (HNIPs). The fast-binding kinetics for one N-nitrosamine (4-(methylnitrosamino)-1-(3-pyridine)-1-butanone, NNK) was attributed to the hollow porous structure with the imprinted cavities on both external and internal surface of the HMIPs. Hollow porous polymers were prepared by two-step swelling polymerization. Prior to polymerization, hollow polystyrene (HPS) particles (0.4g) were dispersed in10 mL of sodium dodecylsulfonate (SDS) solution (0.2% wt), 2 mL of dibutyl phthalate (DBP), 2.5 mL of toluene, and AIBN (50 mg) were added into another 10 mL of SDS solution (0.2% wt). After ultrasonication for 15 min, the two mentioned above solutions were mixed and kept at room temperature with magnetic stirring for 24 h. In the second swelling step, NAM (0.06 g), MAA (0.26 g), 5 mL of toluene, EGDMA (3 g) and 10 mL of PVA solution (1.25% wt) were mixed under ultrasonication for 30 min. Then this emulsion was added into the first step swelling emulsion mentioned above and maintained for 24 h. Finally, the swelling emulsion was transferred into three-necked flask adding 40mL of PVA solution (1.25% wt) and purging with high purity nitrogen for 30min, the polymerization was carried out at 75°C under mechanical stirring for 10h. After polymerization, the hollow imprinted PS particles were washed with deionized water, methanol and methanol/acetic acid solution (9:1, v/v) to remove residual monomers, dispersant and template molecules. Hollow non-imprinted polymers (HNIPs) were prepared under the same conditions without NAM.

In 2018, Z. Li et al. [12] proposed synthesis method of MIPs with high specific surface area and extraction efficiency for determination of NDPhA in water samples using MIPs solid-phase extraction (SPE) coupled with gas chromatography mass spectrometry (GC-MS) detection. The MIPs were successfully prepared using the method of precipitation polymerization. Based on the chemical structure of NDPhA, N, N-Diphenylformamide (NDPhF) was chosen as the template molecule (Figure 2.16)

with a very high structural similarity to NDPhA. The template (1.8 mmol), the monomer MAA (7.2 mmol), the cross-linker EGDMA (36 mmol) and the initiator AIBN (60 mg) were dissolved in 240 mL of acetonitrile/water (3:1, v/v) in a flask. The solvent was purged with nitrogen for 20 min to remove dissolved oxygen and allow the flask filled with nitrogen. The polymerization was performed at 60 °C for 24 h in a thermostatic water bath. The polymer, obtained in the form of precipitates, was washed with methanol in a Soxhlet apparatus for 24 h to remove NDPhF and other unreacted components. The non-imprinted polymers (NIPs) were synthesized following the same procedure except that the template molecule was not added.

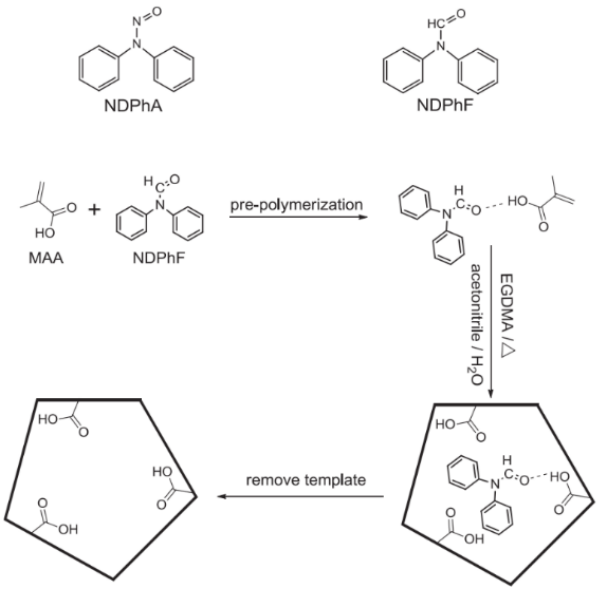

Figure 2.16 Molecular structures of N-Nitrsodiphenylamine (NDPhA) and the template molecule N, N-Diphenylformamide (NDPhF). And the schematic representation of the MIPs synthesis, suggesting its molecular structure [12]

In 2019, X. Peng et al. [17] fabricated a simple and high-performance electrochemical sensor for NDPhA detection constructed based on poly(diallyldimethylammonium chloride)-stabilized graphene/platinum nanoparticles modified GCE (PDDA-Gr/PtNPs/GCE) as an electrochemical sensing platform. The PDDA-Gr/PtNP nanocomposite is synthesized by a facile wet-chemical approach. Figure 2.17 presents the synthesis of PDDA-Gr/PtNPs and electrochemical sensing of

NDPhA. It combines the prominent properties of graphene (large surface areas and high conductivity) with the outstanding catalytic activity of Pt nanoparticles. Because of its remarkable synergistic effect, the PDDA-Gr/PtNPs/GCE shows excellent performance towards electro-oxidation of NDPhA with a significantly increased peak current and negatively shifted peak potential compared to graphene modified electrode (PDDA-Gr/GCE); it exhibits good linearity for NDPhA detection with a linear range of for NDPhA detection with a linear range of 1.0 x 10^{-7} to 5.0 x 10^{-5} mol L^{-1} and a detection limit of 3.3 x 10^{-8} mol L^{-1} (S/N = 3) under optimum conditions. Moreover, this cost-effective and convenient sensor also has good stability, repeatability and anti-interference ability and is promising for trace analysis of NAs in environmental pollutants.

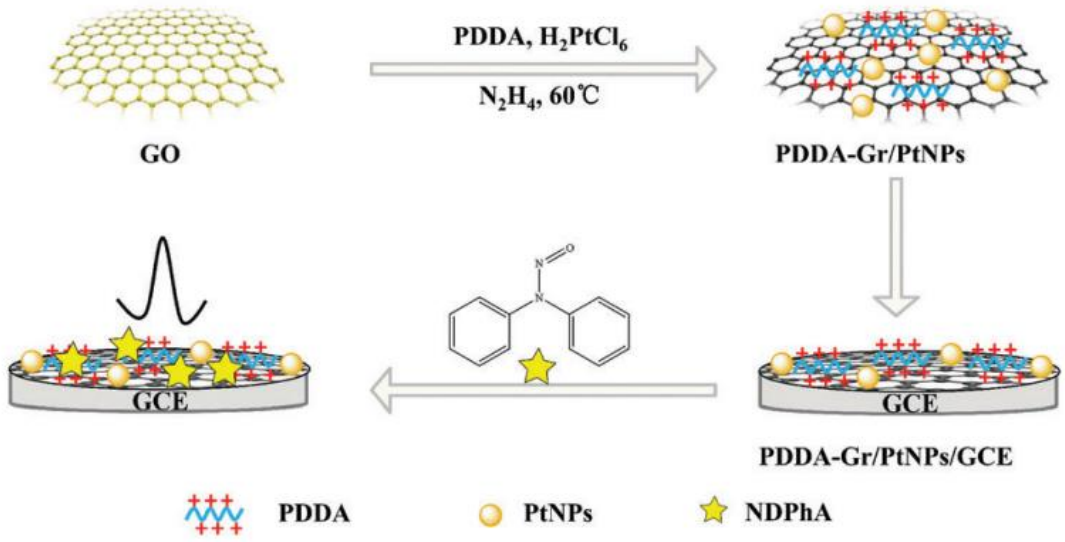

Figure 2.17 Synthesis of PDDA–Gr/PtNPs and electrochemical sensing of NDPhA [17]

In 2019 Z. Li et al. [13] developed a highly selective and sensitive method for the determination of nitrosamines, namely nitrosodiethylamine, nitrosopiperidine, nitrosodi-n-propylamine, nitrosodibutylamine, and nitrosodiphenylamine in water and beverage samples. A new molecularly imprinted polymer (MIP) was synthesized and used as sorbents in SPE for the sample preparation. Prepared samples were analyzed using high performance liquid chromatography-tandem mass spectrometry (HPLC-

MS/MS). Satisfactory recoveries were obtained at three different concentrations (5, 20, and 50 ng/L, n = 3) in the range of 93–107% with relative standard deviations of 3.1–9.8%. Limit of detection and limit of quantitation for the five NAs were in the range of 0.2–0.7 ng/L and 0.6–2.1 ng/L, respectively. Method precisions ranged from 4.9% to 10.5%. This novel method of MIP-SPE coupled with HPLC-MS/MS was successfully applied to the determination of these five NAs in different types of water and beverages samples.The MIP materials were synthesized by precipitation polymerization using MAA as the functional monomer, EGDMA as the cross-linker, AIBN as the initiator and the five compounds N,N-diethylformamide, N,N-formylpiperidine, N,N-dipropylformamide, N,N-diphenylformamide, and N,N-dibutylformamide. For the preparation of MIPs, (1) Each of the template compounds of 3 mmol individual were added into 100 mL acetonitrile/water (3:2, v/v) in a 250 mL threenecked glass flask and then 60 mmol MAA was added. The mixture solution was stored at 4 °C for 24 h for the pre-polymerization. (2) After that, 300 mmol EGDMA and 120 mg AIBN were added into the mixture solution and the solution was stirred for 5 min to dissolve the initiators. Then the mixture solution was deoxygenated by filling the flask with high purity nitrogen for 15 min. After the deoxygenation, the flask was placed in oil bath (60 °C) for 24 h for polymerization. (3) After the polymerization, the synthesized polymers were filtered and washed with the mixture of methanol: acetic acid (9:1, v/v), acetonitrile, and ultrapure water, n sequence, to remove the templates and other unreacted components. Then the synthesized MIPs were dried at 60 °C under a vacuum for use. As a control experiment, the NIPs were prepared using the same synthetic procedure of MIPs without the addition of the five templates.

In 2019 L. V.L. Martoni et al. [18] proposed the electrochemical determination of the N-nitrosodiphenylamine by comparing the voltammetric response of two non-modified carbon electrodes: a glassy carbon (GCE) and a solid graphite polyurethane composite (GPUE). The surfaces of the electrodes were characterized by atomic force microscopy. The electroactive areas of GCE and GPUE were 0.040 and 0.068 cm^2, respectively, calculated from chronocoulometry measurements using $K_4Fe(CN)_6$ as probe and the integrated form of Cottrell Equation. Cyclic voltammograms obtained for N-nitrosodiphenylamine using both electrodes indicated anodic and cathodic peaks (vs. Ag/AgCl (3.0 mol L^{-1} KCl), in agreement with the

literature. At GCE, the electrochemical reduction of the molecule is a diffusion-controlled process, whereas at GPUE some degree of adsorption was also observed. Square wave and differential pulse voltammetry were explored to optimize the best analytical performance for the quantification of the molecule. Under optimized conditions, SW voltammograms for several NDPhA concentrations in 0.10 mol L^{-1} phosphate buffer (pH 2.1) using GCE and GPUE are shown in Figure 2.18A and B respectively. The linear range (sensitivity and limit of detection) observed using GCE was between 8.02 and 46.6 µmol L^{-1} (1.09 µA L µmol^{-1} cm^{-2} and 4.54 µmol L^{-1}) and using GPUE was from 2.51 to 17.5 µmol L^{-1} (5.50 µA L µmol^{-1} cm^{-2} and 0.270 µmol L^{-1}), with the peak currents densities increasing linearly with the concentrations as shown in Figure 2.18C and D, respectively for each electrode. Considering higher sensitivity and lower detection limits values, the GPUE was selected for the quantification of Nnitrosodiphenylamine in synthetic urine samples. The developed method presented a competitive detection limit compared to other sensors reported in the literature, considering the use of a non-modified electrode, with low cost of fabrication, easiness of surface renovation, and sustainability.

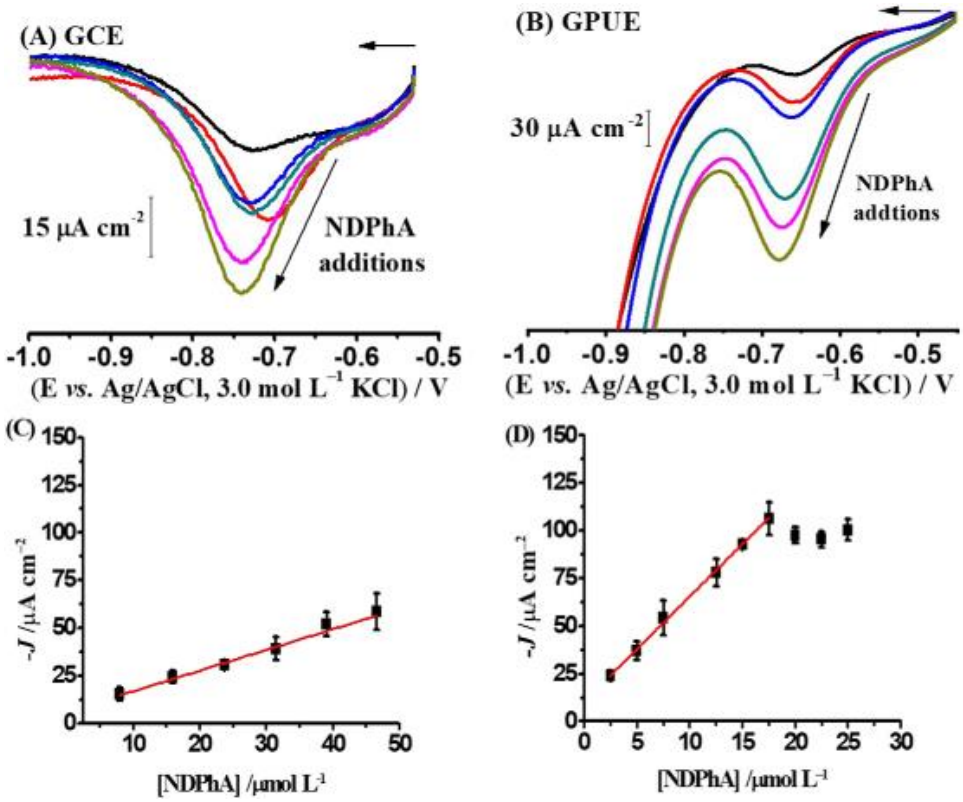

Figure 2.18 SW voltammograms obtained using GCE (A) and GPUE (B) for various concentrations of NDPhA: from 8.02 to 46.6 µmol L^{-1} and from 2.51 to 17.5 µmol L^{-1}, respectively, in 0.10 mol L^{-1} phosphate buffer (pH 2.1). Parameters of SWV: pulse amplitude 50 mV, frequency 25 Hz, potential increment 5 mV, corresponding to an effective scan rate of 50 mV s^{-1}. Graphs (C) and (D) show the respective analytical curves, n = 3 [18]

CHAPTER 3
EXPERIMENTAL

This section describes instrumentation, chemical and research methods for synthesis PdNPs@MIP and the MIP sensor fabrication.

3.1 Instrumentation

Equipment used in this work were listed in table 3.1.

Table 3.1 Instrumentation used for nanocomposites characterization and voltammetry

Instrument	Model	Company
Nanocomposite characterization		
FT-IR	spectrum II spectrometer	Perkin Elmer, USA
UV-Visible	UV-2600	Shimadzu, Japan
TEM	1230 JEOL	JEOL, Japan
SEM	JSM 7610F	JEOL, Japan
EDS	INCAx-Max20	OXFORD instruments, United Kingdom
XPS	AXIS ULTRA^{DLD}	Kratos Analytical, U.K
EIS	Autolab potentiostat PGSTAT302N	Metrohm, Switzerland
Voltammetry		
Potentiostat	EmStat3 potentiostat	PalmSens BV, The Netherlands

3.2 Reagents and Chemicals

Table 3.2 List of reagents, grade, and their suppliers

Chemical and reagent	Grade	Suppliers
Palladium chloride ($PdCl_2$)	59%	Acros Organics
Tri-sodium citrate dihydrate ($Na_3C_6H_5O_7$)	ACS	Sigma-Aldrich
Sodium borohydride ($NaBH_4$)	ACS	Sigma-Aldrich
Ethanol (CH_3CH_2OH)	ACS	Sigma-Aldrich
Methanol (CH_3OH)	ACS	Sigma-Aldrich
Poly(vinylpyrrolidone) (PVP)	average molecular mass of 10,000 $g.mol^{-1}$	Sigma-Aldrich
N-Isopropylacrylamide (NIPAM)	97%	Sigma-Aldrich
2,2′-azobis(2-methylpropionitrile) (AIBN)	98%	Sigma-Aldrich
Trimethylolpropane trimethacrylate (TRIM)	ACS	Sigma-Aldrich
Boric acid (H_3BO_3)	99.5%	Sigma-Aldrich
Phosphoric acid (H_3PO_4)	85%	Sigma-Aldrich
Acetic acid (CH_3COOH)	99.7%	Sigma-Aldrich
Nitrosodiphenylamine (NDPhA)	99.5%	Chem Service
Certified reference material of NDPhA	Analysis	Restex Corporation
Ascorbic acid ($C_6H_8O_6$)	ACS	Sigma-Aldrich
Glucose ($C_6H_{12}O_6$)	AR	Sigma-Aldrich
Fructose ($C_6H_{12}O_6$)	AR	Sigma-Aldrich
Caffeine ($C_8H_{10}N_4O_2$)	AR	Sigma-Aldrich
Uric acid ($C_5H_4N_4O_3$)	Laboratory	Acros Organics
Citric acid ($HOC(COOH)(CH_2COOH)_2$)	ACS	Sigma-Aldrich
Diphenylamine ($(C_6H_5)_2NH$)	ACS	Sigma-Aldrich
Sodium nitrate ($NaNO_3$)	AR	Sigma-Aldrich
Sodium chloride (NaCl)	AR	Sigma-Aldrich
Sodium hydroxide (NaOH)	ACS	Sigma-Aldrich

3.3 Research Methods

3.3.1 Preparation of stock solution

0.1 M NDPhA solution was prepared by dissolving 0.0990 g of NDPhA with ethanol and diluting to 5 mL in a volumetric flask.

0.04 M Boric acid (H_3BO_3) solution was prepared by dissolving 0.2473 g of H_3BO_3 with deionized water and diluting to 100 mL in a volumetric flask.

0.04 M Phosphoric acid (H_3PO_4) solution prepared by pipetting 0.28 mL of H_3PO_4 with deionized water and diluting to 100 mL in a volumetric flask.

0.04 M Acetic acid (CH_3COOH) solution prepared by pipetting 0.64 mL of CH_3COOH with deionized water and diluting to 100 mL in a volumetric flask.

0.2 M Sodium hydroxide (NaOH) solution was prepared by dissolving 0.8000 g of NaOH with deionized water and diluting to 100 mL in a volumetric flask.

0.04 M Britton–Robinson buffer (B-R buffer) pH 3.0 was prepared by mixing 100 mL of 0.04M H_3BO_3, 0.04 M H_3PO_4 and 0.04 M CH_3COOH, then the mixture was adjusted to pH 3.0 by 0.2 M NaOH.

3.3.2 Preparation of PdNPs@MIP

Palladium nanoparticles (PdNPs) were selected as cores for the imprinted surface. We adopted the method described by Ullah and his co-workers [75] to synthesize PdNPs. Firstly, we mixed an aqueous solution of trisodium citrate (0.5 mL, 0.4 M) and a solution of $PdCl_2$ (5 mL, 0.10 M) into a flask containing DI water (30 mL). The mixture was stirred continuously at 60°C for 30 min. Next, we added an aqueous solution of $NaBH_4$ (0.5 mL, 0.1 M) to the flask, and the reaction continued under constant stirring until the color turned to dark brown (~2 h), which indicated the successful synthesis of PdNPs (Scheme 3.1). Finally, the precipitate was centrifuged, washed thrice with DI water, and let dry at 80°C for 2.5 h.

Figure 3.1 illustrates the synthesis of palladium nanoparticles coated with molecularly imprinted polymers (PdNPs@MIP). PdNPs were coated with poly(vinylpyrrolidone) or PVP to create the polymerizable functional groups using a sol-gel method [77, 78]. First, PVP (0.04 g) was dissolved in ethanol (3 mL) to make a PVP solution. The solution was mechanically stirred and maintained at 50°C. Next, PdNPs (40 mg) were added to the PVP solution and vigorously stirred for 30 mins at

room temperature. Finally, the precipitate was centrifuged, washed thrice with DI water, and let dry in a desiccator to yield the PdNPs-PVP nanocomposites.

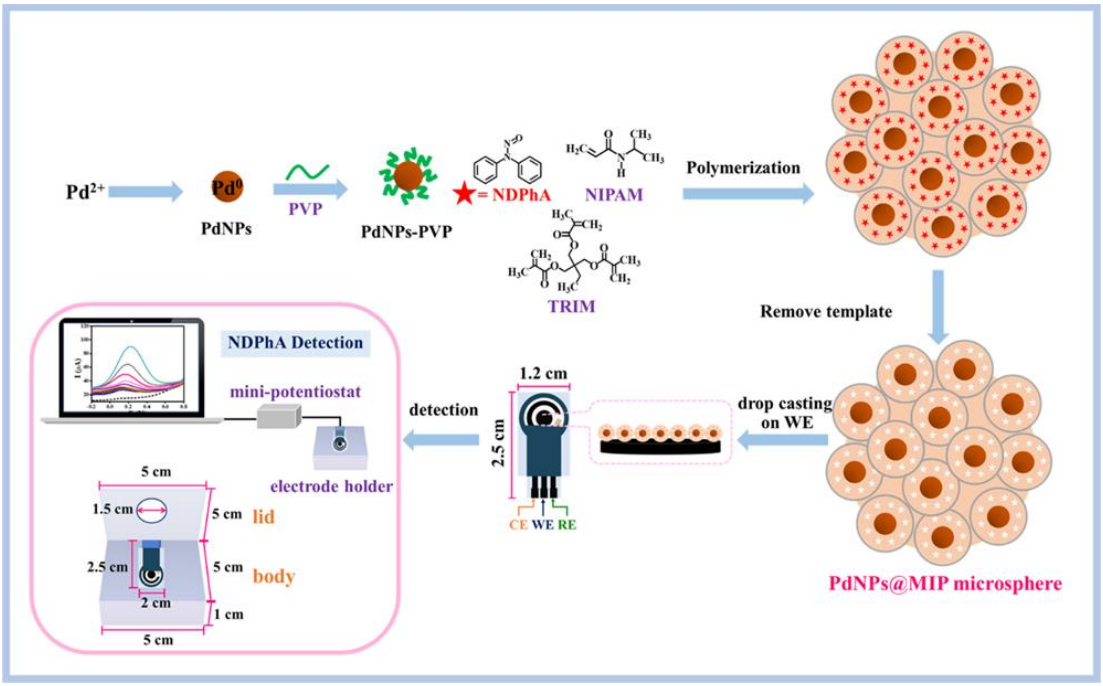

Figure 3.1 Preparation of palladium nanoparticles coated with molecularly imprinted polymers (PdNPs@MIP) and the NDPhA imprinted sensor via drop coating on the SPGrE

This work created nitrosodiphenylamine or NDPhA recognition sites on the surface of PdNPs cores via the precipitation polymerization method. Briefly, NDPhA template (0.12 mmol), NIPAM functional monomer (0.24 mmol), and PdNPs-PVP (20 mg) were mixed in 20 mL of methanol under ice bath for 1 h. This allowed the creation of complexes between the functional monomer and the template via facial hydrogen bonding. Next, TRIM cross-linker (0.9 mmol) and AIBN initiator (0.06 mmol) were added to the mixture. The solution was mixed at room temperature for a few minutes and then sonicated for 10 min. After purging with nitrogen for 5 min, the solution was sealed and placed in a water bath at 60 ◦C for 18 h. The synthesized particles were collected after centrifugation at 10,000 rpm for 5 min. The template molecule was extracted to generate recognition sites by washing eight times with ethanol (80 mL) and

dried overnight at 100 ^{0}C. Similarly, a control non-imprinted polymer (NIP) was prepared following the same procedure but without NDPhA

3.3.3 Screen printed graphene electrode (SPGrE).

Disposable electrochemical analytical devices were fabricated in-house according to our previously described protocols [23, 74]. The configuration of the devices comprised of a three-electrode cell construction (Scheme 3.1), a 4 mm-circular working electrode (graphene), a reference electrode (Ag/AgCl), and a counter electrode (graphene). The screen-printed graphene electrodes (SPGrE) were prepared using an MK-MINI screen printer (Minami, Japan). Commercial graphene ink (Serve Science Ltd, Thailand) was screen printed onto clear polyvinyl chloride (PVC) (Navanakornplastic Co. Ltd., Pathum Thani, Thailand) sheets through silk-screen printing mesh (mesh size 120 µm) for two cycles. Next, a reference area was screen-printed with Ag/AgCl ink (Gwent Electronic Materials Ltd., Pontypool, U.K.) on the PVC sheet for two cycles. Finally, A detection area with insulating ink was printed on the PVC sheet for two cycles and then baked the sheet at 60 °C for 1 h to remove any solvent. Next, A homemade electrode holder (5.0 × 5.0 × 1.0 cm) was assembled from an acrylic sheet and placed an assembled electrical connector inside the body. The center of the holder lid was drilled to make a 2.0 cm sample injection hole. The electrode holder was designed for efficient handling of sample/standard adding and for tight fixing of the SPGrE.

3.3.4 Electrochemical measurements

Electrochemical measurements were performed using a homemade reactor with an EmStat3 potentiostat (5.0 × 6.7 × 2.8 cm) (PalmSens BV, The Netherlands). Further, we used "PSTrace for windows" with multi-trace software. The measurement cell was formed by a working electrode (PdNPs@MIP/SPGrE), a reference electrode (Ag/AgCl), and a counter electrode (SPGrE). The circular modified graphene working electrode (4 mm diameter) had an active surface area of around 0.126 cm^2. Cyclic voltammograms (CV) were recorded using 0.04 M Britton–Robinson buffer (B-R buffer) electrolyte solution, at a scan rate of 50 mV s^{-1} and across a potential range of -0.3 to +0.6 V. Linear sweep anodic stripping voltammetry (LSASV) was selected for quantitative analyses. After filling the detection area with the standard or sample solution, Deposition potential of +0.02 V was applied for 60 seconds. Then, the linear

sweep scanned from -0.2 to +0.8 V at a scan rate of 50 mV s^{-1} to remove the deposited NDPhA, and the corresponding current signal was recorded

3.3.5 Fabrication of PdNPs@MIP/SPGrE

The PdNPs@MIP dispersion (2.5 µL, 5 mg mL^{-1} in dimethylformamide) was dropped onto the SPGrE surface and allowed to dry at room temperature to furnish the imprinted sensor (PdNPs@MIP/SPGrE).

3.3.6 Accuracy test and actual sample application

This work analyzed the NDPhA content in beverage samples (beer, dark wine, red wine, green tea, orange juice, and apple juice), synthetic samples, and Certified Reference Materials (CRM) to evaluate the performance of the proposed dual-imprinted sensor (PdNPs@MIP/SPGrE). Samples were filtered through a 0.25-micron cellulose membrane, diluted appropriately with B-R buffer at pH 3, and then determined via an external calibration curve. To assess the accuracy of the NDPhA imprinted sensor, Recoveries with 0.05 or 0.1 µM of spiked NDPhA added to the samples before filtration were investigated. This work determined the samples for the analyte and calculated the recoveries. NDPhA concentration results obtained from the compact sensor were compared to those obtained from a standard HPLC method [34].

The calibration mix (CRM 31032/607) of nitrosamines, with a certified concentration of NDPhA of 10,122.087 ± 94.340 µM, was evaluated by applying the developed PdNPs@MIP sensor.

3.4 Characterization of the nanoparticles

3.4.1 UV-Visible spectroscopy

UV-Visible spectra were measured in a 1 cm path length quartz cell using a double beam, spectrophotometer (UV-2600, Shimadzu, Japan) with a 10 mm quartz cell (45 × 12.5 × 12.5 mm). The samples were dissolved in ethanol. Result were presented in Section 4.1.1.

3.4.2 Infrared spectroscopy

Infrared spectroscopy is a significant technique in the functional groups identification in molecules. The study was performed by using FT-IR and recorded using a spectrum II spectrometer (Perkin Elmer, USA) with an operating range of 4000-500 cm^{-1}. Results are discussed in Section 4.1.2.

3.4.3 Scanning electron microscopy (SEM)

The morphology of the nanocomposites modified electrode (PdNPs, PdNPs-PVP, PdNPs@MIP) surface was studied with scanning electron microscope (FE-SEM) (JEOL; JSM 7610F, Japan). Sample was attached on SEM stubs and then sputter coated with gold before investigated by SEM. Result are presented in Section 4.1.3.

3.4.4 Transmission electron microscopy (TEM)

The morphology of the as-prepared nanocomposites modified electrode surface was performed on a transmission electron microscopy (TEM) (1230 JEOL, Japan). The TEM samples were prepared by dispersing the nanocomposites in deionized water with ultrasonicated for 1 h and then drying a drop of the suspension on a copper grid at room temperature prior to TEM analysis. The morphology of PdNPs, Pd-PVP, and PdNPs@MIP are discussed in Section 4.1.3.

3.4.5 Energy Dispersive X-Ray Spectrometer

Energy dispersive X-ray spectroscopy (EDS) is a standard method for identifying and quantifying elemental compositions in a very small sample of material (even a few cubic micrometers). The elemental compositions were evaluated by energy-dispersive X-ray spectroscopy (EDS) (OXFORD instruments, INCAx-Max20, United Kingdom). Sample was attached on EDS stubs and then sputter coated with gold before investigated by EDS. Result are presented in Section 4.1.3.

3.4.6 X-ray photoelectron spectroscopy

The valance of PdNPs in the as-prepared the PdNPs@MIP composites was investigated by using X-ray photoelectron spectrometer (XPS) (AXIS ULTRA^{DLD}, Kratos Analytical, Manchester, U.K.). Results are discussed in Section 4.1.3.

3.5 The PdNPs@MIP/SPGrE in electrochemistry

3.5.1 Cyclic voltammetry study of NDPhA

The unique electrochemical behavior of NDPhA oxidation was studied at different modified electrode materials. The cyclic voltammograms at the bare SPGrE, PdNPs/SPGrE, PdNPs-PVP/SPGrE, PdNPs@MIP/SPGrE, and PdNPs@NIP/SPGrE were investigated in 0.04 M B-R buffer pH 3.0 and 250 μM NDPhA at a scan rate 0.05 V s^{-1}. The result were discussed in Section 4.1.4.2.

3.5.2 Electrochemical impedance spectroscopy (EIS)

EIS was performed by using an an Autolab potentiostat PGSTAT302N (Metrohm, Switzerland) to measure the impedance spectra of several modified electrodes. Measurement was done at a potential of 0.19 V within the frequency range from 0.1 Hz to 100 kHz in 0.1 M KCl solution containing 5 mM of $K_3[Fe(CN)_6]$. The EIS results are discussed in Section 4.1.4.1**.**

3.5.3 Studies of parameters that effect the selectivity and sensitivity of the PdNPs@MIP sensor

Effect of parameter used in polymerization conditions including, the mole ratio of template: monomer and monomer: cross linker.

3.5.3.1 Optimization of mole ratio of template: monomer

The template (NDPhA): monomer (NIPAM) ratio directly affects the amount of template molecule embedded in the polymer matrix during polymerization. The effect of NDPhA: NIPAM molar ratio was studied in the range from 1:0 to 1:4. The results are discussed in Section 4.2.

3.5.3.2 Optimization of monomer: cross linker

Monomer (NIPAM): cross linker (TRIM) molar ratio was studied in the range from 2: 0 to 2: 14.5. The results are discussed in Section 4.2

3.5.3.3 Optimization of PdNPs-PVP loading

PdNPs-PVP loading was studied in the range from 0 to 30 mg. The results are discussed in Section 4.2.

3.5.3.4 Effect of 0.04 M B-R buffer pH

The effect of pH on the performance of the PdNPs@MIP/SPGrE for NDPhA detection was investigated over the pH range 2.0-8.0 using 0.04 M B-R buffer as supporting electrolyte. The CV plots were recorded using electrolyte solution of varying pH. Results are presented in Section 4.2.

3.5.4 Scan rate dependence study

The cyclic voltammograms of anodic and cathodic peaks current of NDPhA on the PdNPs@MIP/SPGrE were investigated in 0.04 M B-R buffer (pH 3.0) using 250 μM NDPhA solution. The effect of various scan rate 0.05-0.15 V s on the voltammograms were investigated. The results are discussed in Section 4.3.

3.5.5 Enhancement of the NDPhA detection

3.5.5.1 Effect of loading of PdNPs@MIP

The effect of loading of PdNPs@MIP were performed in 0.04 M B-R buffer (pH 3.0) using 100 µM NDPhA solution. The effect of various loading of PdNPs@MIPin the range 3 to 8 mg L^{-1} on the LSASV were investigated The results are discussed in Section 4.4.

3.5.5.2 Effect of deposition time

The Effect of deposition time on the PdNPs@MIP/SPGrE were investigated in 0.04 M B-R buffer (pH 3.0) using 10 µM NDPhA solution. The effect of various deposition time 0 to 300 s on the LSASV were investigated. The results are discussed in Section 4.4.

3.5.6 Analytical features of the PdNPs@MIP/SPGrE

3.5.6.1 Linear calibration curve

Calibration standards of NDPhA were studied by diluting the appropriate amount of standard NDPhA solution in 0.04 M NDPhA pH 3.0 to give working solutions in the range of 0.01 to 100 µM. The LSASV applied a deposition potential of +0.02 V for 60 seconds. Then, the linear sweep scanned from -0.2 to +0.8 V at a scan rate of 50 mV s-1 to remove the deposited NDPhA, and the corresponding current signal was recorded. The results are discussed in Section 4.5.

3.5.6.2 Limit of detection (LOD)

The LOD was calculated based on the standard deviation (S_b) for consecutive measurements of the lowest analyte concentration on the analytical curve (0.01 µM). The detection limit, estimated by three times the standard deviation of blank ($3S_b$), The results are shown in Section 4.5.

3.5.7 Interference study

Substances with similar structures and ions or compounds commonly found in beverage samples were selected as possible interferences for the study. Interfering species such as diphenylamine, ascorbic acid, uric acid, glucose, fructose, citric acid, caffeine, ethanol, $NaNO_3$, and NaCl were selected as the interferences. The concentration of the interference species that provide a peak area change greater than +10% was considered as the tolerance limit. The results are discussed in Section 4.6.

3.5.8 Reproducibility and long-term stability

Reproducibility and long-term stability of the PdNPs@MIP/SPGrE. The electrode-to-electrode reproducibility of MIP sensor was analyzed by comparing current responses to 1.0 µM NDPhA from five different MIP electrodes. The long-term stability of the MIP sensor was tested by storing at room temperature and measuring the current response each day for 7, 14, 21, and 28 days. The results are discussed in Section 4.7.

CHAPTER 4
RESULTS AND DISCUSSION

4.1 Structure and morphological characterization

4.1.1 UV-Visible spectroscopy

The UV-Visible spectroscopy was used to investigate the adsorption spectra of PdNPs and $PdCl_2$. Figure 4.1 shows the absorption spectrum of palladium nanoparticles after successfully reducing $NaBH_4$ compared with those of a $PdCl_2$ solution. $PdCl_2$ solution reveals a strong peak at 420 nm (blue line) related to the Pd^{2+} ion. After reducing Pd^{2+} to Pd^0, the peaks disappeared with a change in color from yellow to dark brown due to excitation of surface plasmon vibration in the PdNPs, formed at a peak range of 370 – 440 nm [78-80].

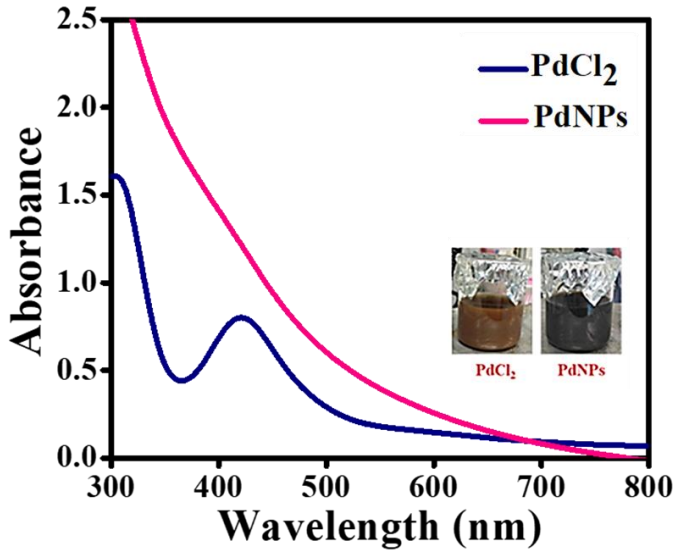

Fig. 4.1 UV-vis spectra of $PdCl_2$ solution (blue line) and PdNPs (pink line) after reduction with 0.1 M $NaBH_4$

4.1.2 FTIR spectroscopy

ATR FTIR spectroscopy was used to confirm the formation of NDPhA recognition sites on the molecularly imprinted polymer coated on the PdNPs core. FTIR spectra (Figure 4.2) were recorded from NDPhA (curve a), PdNPs@MIP before (curve b), and after (curve c) removal of the NDPhA template molecules and PdNPs@NIP (curve d). The bands at 1318, 1292, and 1052 cm^{-1} for NDPhA (curve a) were due to the characteristic stretching vibration bands of N=O (1321 - 1292 cm^{-1}) and N-N (1052 cm^{-1}) [81], respectively. The PdNPs@MIP spectrum before template removal (curve b) shows the absorption bands of the characteristic peaks of NDPhA (star marked in curve b), illustrating the presence of NDPhA in the polymer matrix. After template removal, the spectrum (curve c) bands (at 1318, 1292, and 1052 cm^{-1}) disappear due to loss of NDPhA via ethanol extraction. These results suggest the successful removal of NDPhA from the PdNPs@MIP film. Meanwhile, the film spectra (curves b, c, and d) show absorption characteristic bands of NIPAM (triangle marked in curve d) at 2972, 1640, 1459, and 1387 cm^{-1} that assign to C–N of amide, C=O stretching of amide, C–$(CH_3)_2$ isopropyl groups, and C–H bending in –CH_2– groups and –$C(CH_3)_2$, respectively [82-85]. The result attributed the peaks at 1730 and 1150 cm^{-1} (diamond marked in Fig. S1b, curve d) to symmetric and asymmetric C-O-C stretching of the ester group and C=O stretching of TRIM cross-linker [83]. All the results confirmed the successful fabrication of the PdNPs@MIP.

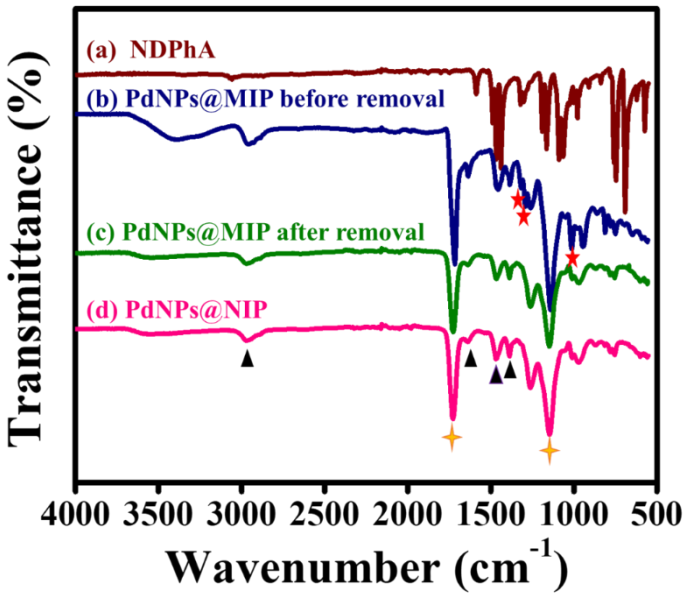

Figure 4.2 FT-IR spectra of a) NDPhA, b) PdNPs@MIP before removal, c) PdNPs@MIP after removal and d) PdNPs@MIP

4.1.3 SEM, TEM, EDS and XPS

SEM and TEM were used to characterize the morphology of PdNPs, PdNPs-PVP, and PdNPs@MIP nanocomposites. EDS and XPS were applied for investigating the Pd atom's composition, elemental fraction, and valence state in the as-prepared PdNPs@MIP.

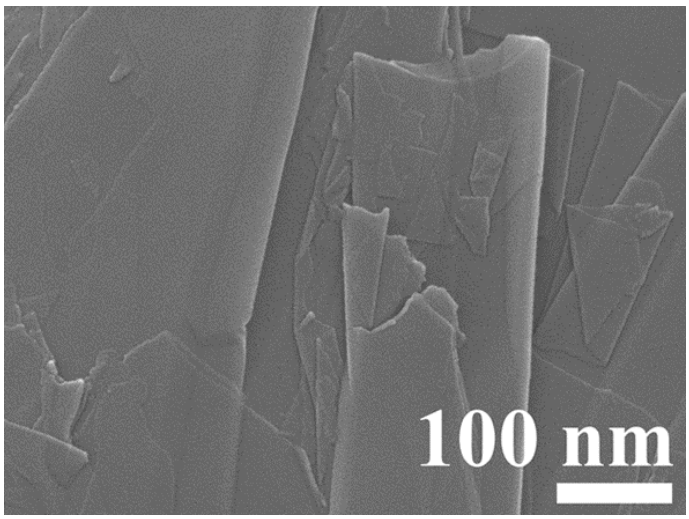

Figure 4.3 SEM image of bare SPGrE

SEM image of bare SPGrE's surface (Fig 4.3) exhibits smooth, thin, and appears nanosheets, which is the typical morphology for graphene. The synthesized PdNPs (Figure 4.4a) appears approximately spherical with an average diameter of 22.0 ± 1.7 nm (count = 20), whereas PdNPs-PVP (Figure 4.4b) is larger than the unmodified PdNPs due to the formation of a PVP layer on the surface of the PdNPs as revealed by SEM. The SEM image (Figure 4.4d) of the PdNPs@MIP exhibits a spherical shape and uniform microsphere with a mean diameter of approximately 2.3 ± 0.8 μm (count = 10). A close-up view of PdNPs@MIP (TEM image, Figure 4.4c) indicated a shell consisting of PdNPs with an average diameter of around 22 nm covered on the sphere surface of MIP particles.

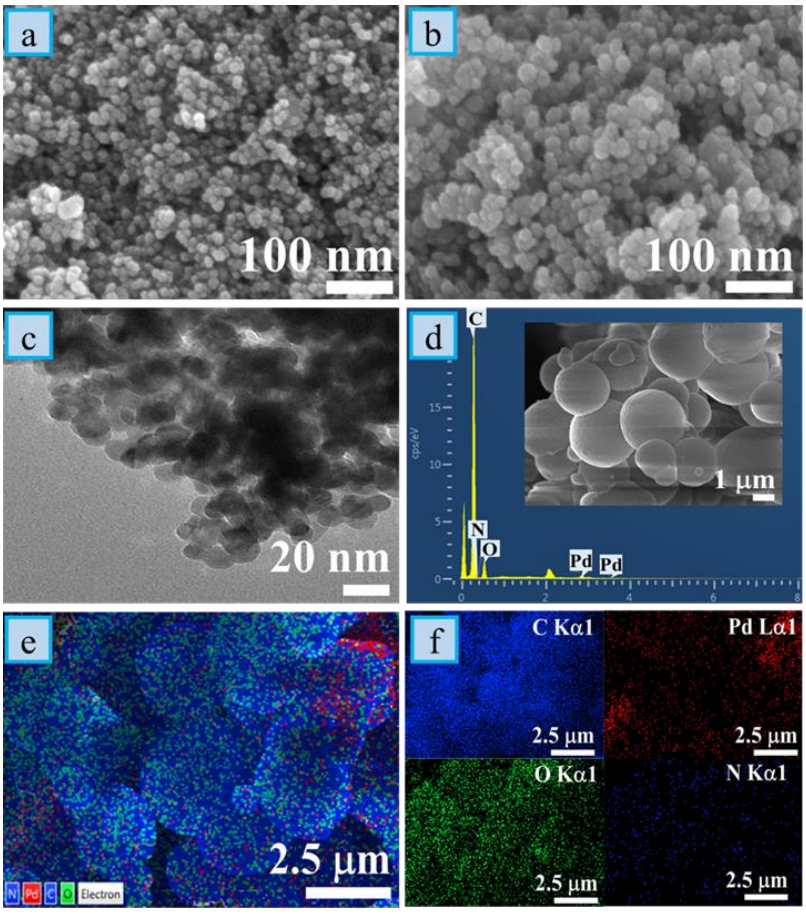

Figure 4.4 SEM images of (a) PdNPs and (b) PdNPs-PVP. TEM images of (c) PdNPs@MIP, (d) EDS of PdNPs@MIP, and (e) mixture of mapping analysis of (f) C, Pd, O, and N elements in the PdNPs@MIP microspheres

The EDS spectrum (Figure 4.4d) reveals the presence of C (66.58 wt.%), N (8.54 wt.%), O (22.24 wt.%), and Pd (2.63 wt.%) atoms. This provides evidence for attachment between the PdNPs core and the organic part corresponding to the polymer matrix synthesized from NIPAM and TRIM. Further, the elemental mapping in Figure 4.4 (e and f) indicates an equal distribution on the PdNPs@MIP microsphere (containing C, N, O, and Pd elements). These results revealed that PdNPs are indeed entirely covered on the MIP microsphere.

XPS revealed the chemical state of Pd in the as-prepared PdNPs@MIP microsphere. The full spectrum of PdNPs@MIP (Figure 4.5a) illustrates three predominant peaks. In the C 1s spectrum (Figure 4.5b), this work attributed the peaks at 284.5, 285.1, 286.2, 287.1, and 288.6 eV to C-C/C-H, C-N, N-C=O, C-O, and O-C=O, respectively. Figure 4.5c shows that the O 1s spectrum of PdNPs@MIP could be deconvoluted into three peaks at 531.8, 533.2, and 534.6 eV, related to the chemical binding energies of N-C=O, C-O, and O-C=O, respectively [86-88]. Furthermore, this work ascribed the 399.3 eV, N1s peak (Figure 4.5d) to the NH_2 in amide functionalities from poly(*N*-Isopropylacrylamide) [86-90]. The spectrum of Pd contains two peaks with binding energies of 336.0 and 341.3 eV for Pd $3d_{5/2}$ and Pd $3d_{3/2}$, respectively (Figure 4.5e), which result from the reduction of Pd^{2+} to Pd^{0} [89]. This observation confirms the successful formation of NDPhA imprinted polymer covering the PdNPs.

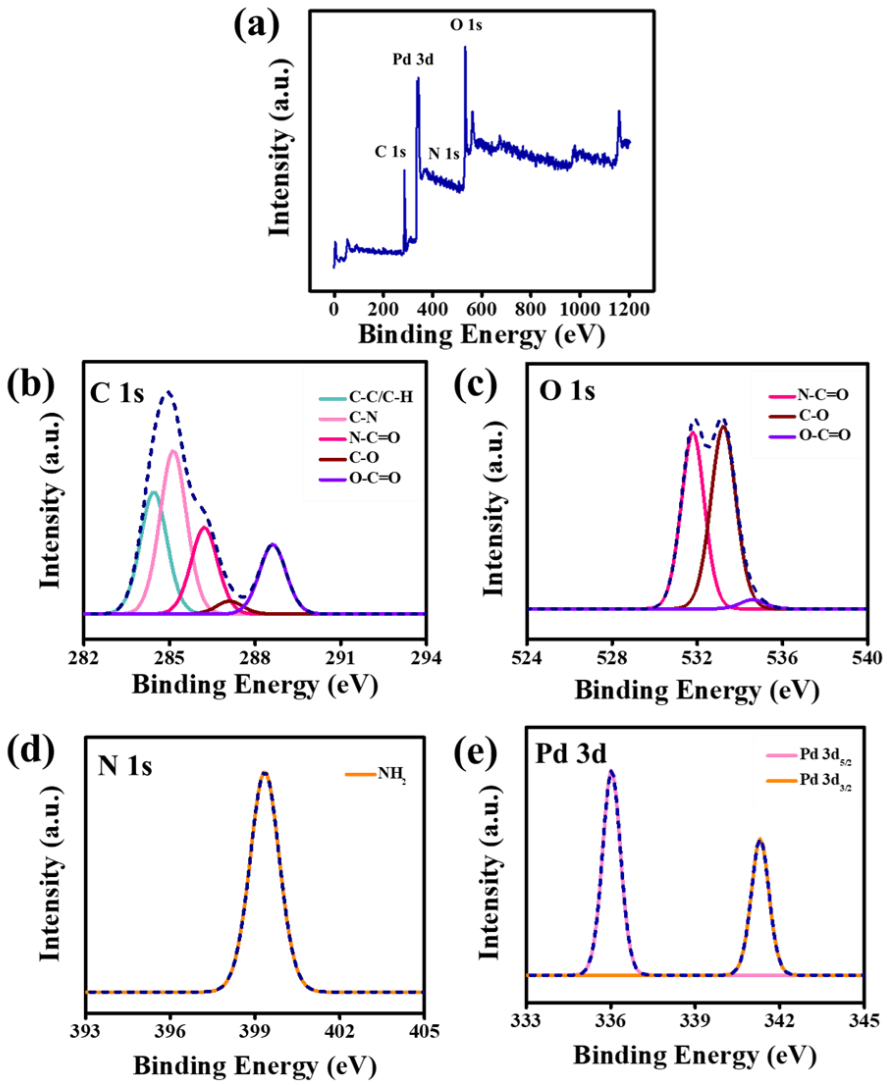

Figure 4.5 XPS survey spectrum of (a) PdNPs@MIP and core level spectra: (b) C 1s, (c) O 1s, (d) N 1s and (d) Pd 3d

4.1.4 Electrochemical characterization

4.1.4.1 Electrochemical impedance spectroscopy

The electron transfer kinetics of the bare and modified electrodes were investigated by using EIS. Figure 4.6 shows the EIS data obtained for a bare SPGrE, PdNPs/SPGrE, PdNPs-PVP/SPGrE, PdNPs@MIP/SPGrE, and PdNPs@MIP/SPGrE. The lowest semicircular diameter was obtained from the PdNPs/SPGrE (R_{ct} = 34.1 Ω), which indicates the fastest electron-transfer kinetics of $[Fe(C.N.)_6]^{3-/4-}$, compared to bare SPGrE (R_{ct} = 1930 Ω), PdNPs-PVP (R_{ct} = 151 Ω,)

PdNPs@MIP (R_{ct} = 175 Ω) and PdNPs@NIP modified electrode (R_{ct} = 360 Ω). The lowest impedance of PdNPs/SPGrE indicates the excellent conductivity enhancement of PdNPs. The highest impedances from the NIP modified electrode indicate the presence of poly(*N*-Isopropylacrylamide) film. This film blocks the electrochemical reaction of $[Fe(CN)_6]^{3-/4-}$ on the electrode surface. The MIP has a lower impedance than the NIP-modified electrode because of NDPhA recognition sites in the MIP films. This permit diffusion of the $[Fe(CN)_6]^{3-/4-}$ redox probe, enhancing the electron transfer.

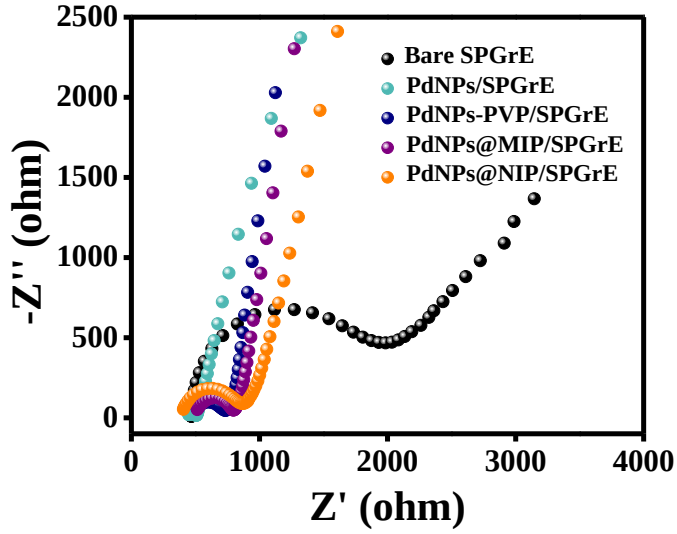

Figure 4.6 Nyquist plot observed for bare SPGrE, PdNPs/SPGrE, PdNPs-PVP/SPGrE, PdNPs@MIP/SPGrE and PdNPs@MIP/SPGrE in 0.1 M KCl containing 5 mM $[Fe(CN)_6]^{3-/4-}$ over the frequency range 0.1 Hz to 100 kHz; amplitude = 10 mV. Inset; Randles equivalent circuit model; here R_s, C_{dl}, R_{ct}, and Z_w stand for the ohmic resistance of electrolyte (R_s), double layer capacitance (C_{dl}), electron transfer resistance (R_{ct}), and Warberg impedance (Z_w)

4.1.4.2 Electrochemical behaviors of different the modified SPGrE

Cyclic voltammetry serves to analyze the electrochemical behavior of NDPhA on the bare SPGrE, PdNPs/SPGrE, PdNPs@MIP/SPGrE, and PdNPs@NIP/SPGrE.

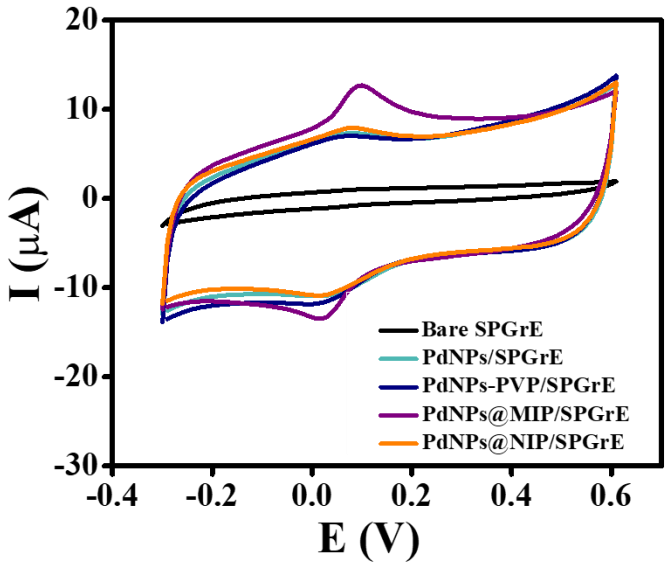

Figure 4.7 CV curve of 250 µM NDPhA on bare SPGrE, PdNPs/SPGrE, PdNPs-PVP/SPGrE, PdNPs@MIP/SPGrE, and PdNPs@NIP/SPGrE in 0.04 M B-R buffer (pH 3.0) supporting solution

As shown in Figure 4.7, the characteristic oxidation peak of NDPhA appears at about + 0.15 V at all the electrodes. Bare SPGrE shows only weak current response, while modified electrodes lead to higher current response. After modifying SPGrE with PdNPs, the anodic peak current of NDPhA increased 3.68 times that at the bare SPGrE due to PdNP's good electrocatalytic activity, high conductivity, and large surface area [28, 90]. Moreover, the peak current at the PdNPs@MIP/SPGrE is 9.20 times higher than the bare SPGrE. Enhancement of anodic peak current is because of the high electrocatalytic activity and conductivity of PdNPs and the formation of hydrogen bonds between specific recognition cavities in the MIP microsphere and NDPhA that improve the accumulation of NDPhA on the electrode surface. However, the PdNPs@NIP/SPGrE exhibits an anodic current peak less than PdNPs@MIP/SPGrE. The absence of NDPhA recognition sites on NIP-modified electrodes generates an

obstruction effect from the polymer that blocks the binding of NDPhA target analyte on the electrode surface. In other words, the higher NDPhA oxidation peak at PdNPs@MIP/SPGrE results from the formation of specific binding sites offered by the successful imprinting process, resulting in a higher electron transfer rate. As a result, the MIP sensor has a greater affinity for the analyte molecules, which is in accord with previous reports [19, 91].

The role of PdNPs for electro-catalytic the oxidation of NDPhA was also demonstrated as in Figure 4.8. It is clearly seen that anodic peak current at PdNPs@MIP/SPGrE is higher than the MIP/SPGrE. Enhancement of peak current is because of the high electrocatalytic activity, specific surface area and the formation of many specific NDPhA recognition cavities in the MIP microsphere that improve the current signal of NDPhA on the electrode surface.

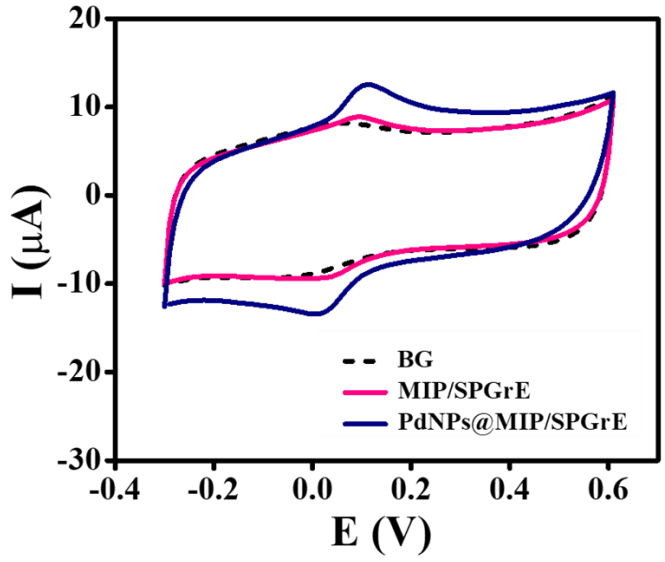

Figure 4.8 CV curves of 250 µM NDPhA on MIP/SPGrE (pink line) and PdNPs@MIP/SPGrE (blue line) in 0.04 M B-R buffer (pH 3.0), the curve of supporting solution (BG) was also shown as dotted line

4.2 Optimization of the sensor preparation

MIPs were synthesized with different template-to-monomer molar ratios and monomer-to-crosslinker molar ratios to optimize the imprinting conditions. The template molecule (NDPhA): monomer (NIPAM) ratio is crucial. It influences the number of imprinted cavities and the binding affinity between NDPhA and recognition sites. This work chose NIPAM as a monomer because it has more amide functional groups, making it possible to obtain a good interaction with NDPhA through hydrogen bonds, to form a non-covalent interaction. Figure 4.9a reveals that the NDPhA oxidation peak current increased the NDPhA : NIPAM molar ratio from 1:0 to 1:2 but slightly decreased at larger currents.

Polymerization is incomplete at low NDPhA : NIPAM ratios, so there are fewer imprinted cavities. A ratio of 1:2 provides the maximum current response and imprinting ability from NIPAM, indicating that the most significant number of imprinting cavities in the polymer network had formed. Above this ratio, the current response decreases. Excess NIPAM monomer produces thicker polymer films and blocks NDPhA molecules from accessing binding sites, thereby reducing the number of specific binding sites. This circumstance is consistent with previous reports [91, 92]. Therefore, this work selected the ratio of 1:2 as the optimal template-to-monomer ratio.

Cross-linker content is also significant in modulating the shape of the polymer matrix and maintaining the imprinted binding site. The effect of the monomer: cross-linker (NIPAM : TRIM) molar ratio on the PdNPs@MIP current response was investigated at 2.0, 2.40, 2:7.5, 2:11, and 2:14.5 (Figure 4.9b). Peak current increases from a ratio of 2:0 up to 2:7.5. Further increases in the mole ratio to 2:14.5 result in a significant decrease in signal. It is also possible that excess TRIM forms hydrogen bonds with NIPAM and with the NDPhA template molecule. This competition can reduce the number of interactions between template molecule and monomer, resulting in fewer recognition cavities in the polymer and decreasing the number of binding sites. In addition, excess TRIM cross-linker forms a rigid polymer that prevents NDPhA from entering cavities in the proper position and orientation, reducing retention efficiency. Therefore, this work chose a molar ratio of 2:7.5 for the monomer and cross-linker to maximize sensitivity.

PdNPs play an important role in electro-catalytic of the NDPhA oxidation and influence the number of NDPhA imprinting sites in the MIP microsphere. Thus, the amount of PdNPs-PVP core on the imprinting conditions was studied. The NDPhA anodic peak current increases with the PdNPs- PVP core from 0 to 20 mg but decreased at higher loading (Figure 4.9c). The increased current response on increasing PdNPs-PVP core may result from an increase in the density of NDPhA imprinting sites per unit surface area on the MIP matrix. Therefore, PdNPs- PVP amount of 20 mg was selected to provide the largest NDPhA anodic peak current as optimal condition for the MIP microsphere synthesized.

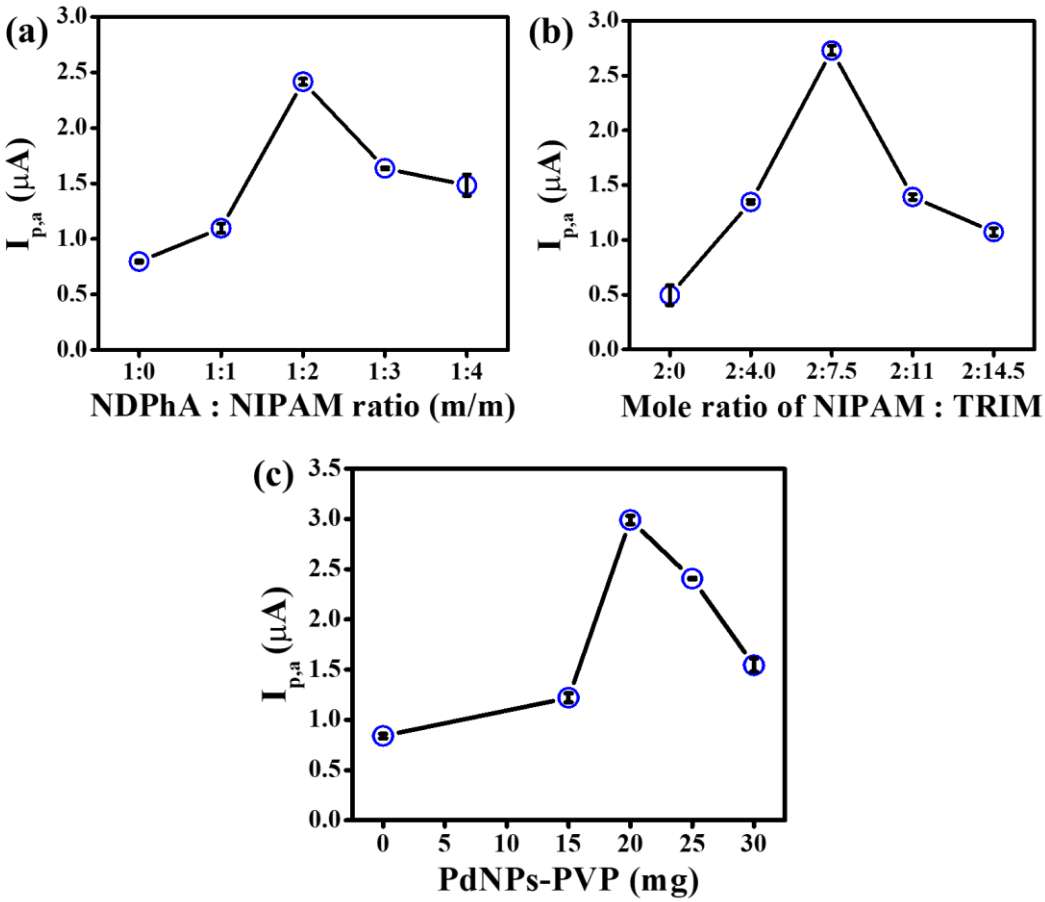

Figure 4.9 Optimization conditions affect the determination of NDPhA. Variation of electrode response for NDPhA (250 µM) with changing of (a) NDPhA: NIPAM mole ratio and (b) NIPAM : TRIM mole ratio and (c) PdNPs-PVP loading (mg), using 0.04 M B-R buffer pH 3.0 as supporting solution

4.3 Mechanism of NDPhA detection on the PdNPs@MIP sensor

The electrochemical behaviors of NDPhA on the proposed PdNPs@MIP/SPGrE was investigated by studying the effects of scan rate (ν) and pH of the electrolyte solution to determine the detection mechanism. This work set the scan rate dependency to between 50 and 150 mVs^{-1} to investigate the number of electrons involved in the oxidation of NDPhA (Figure 4.10a). Figure 4.10b shows a plot of the NDPhA anodic and cathodic peak currents (μA) increasing linearly with the scan rate's square root ($V^{1/2}$ $s^{-1/2}$). Linear regression analysis provides a correlation coefficient (r^2) of 0.9980 ($I_{p,a}$) for oxidation, and 0.9975 ($I_{p,c}$) for reduction reactions. There is a diffusion-controlled reversible electrochemical process at the surface of the PdNPs@MIP/SPGrE. The relationship between the peak potential $E_{p,a}$ and ν is defined by Laviron as Eqn. 4.1 [93, 94].

$$E_{p,a} = E_0 + \frac{RT}{(1-\alpha)nF} ln \frac{(1-\alpha)nF}{RTk_s} + \frac{RT}{(1-\alpha)nF} ln \nu \quad (4.1)$$

Where E_0 represents the formal potential, k_s is the standard rate constant of the reaction, R is the gas constant, T is the temperature, F is the Faraday constant, ν is the scanning rate, α is the transfer coefficient, and n is the electron transfer number. This work can use the slope to calculate the (1 - α) n term. The slope is 0.0527 (Figure 4.10c), taking T = 298 K, F = 96,485 C mol^{-1} and R = 8.314 J mol^{-1} K^{-1}, so, (1 - α) n is 0.4873. This work calculate α according to Bard and Faulkner, in equation (4.2) [95].

$$\alpha = \frac{47.7}{E_{p,a} - E_{p,a/2}} \quad (4.2)$$

Here, $E_{p,a/2}$ is the oxidation peak potential where the current is half the oxidation peak value. Therefore, the transfer coefficient (α) is 0.53 and the electron transfer number (n) 1.03 ≈ 1. One-electron transfer in the oxidation of NDPhA is in accord with a previous report [17].

Moreover, this work can determine the k_s value from the intercept of the straight line between $E_{p,a,}$ and ln ν (Figure 4.10c). The value of E_0 is obtained from the intercept of $E_{p,a}$ vs. ν plot [96, 97]. In this PdNPs@MIP/SPGrE, the intercept is -0.1559 V (Figure 4.10c), and E_0 is 0.0262 V (Figure 4.10d); hence the k_s value calculated according to the

Laviron equation is 593.69 s^{-1}. Using this method, the k_s value obtained from bare SPGrE is 128.63 s^{-1}. The k_s value for PdNPs@MIP/SPGrE is ~5 times higher than that of the bare electrode. This circumstance reveals the higher efficacy of the proposed MIP sensor for significantly promoting the oxidation reaction of NDPhA.

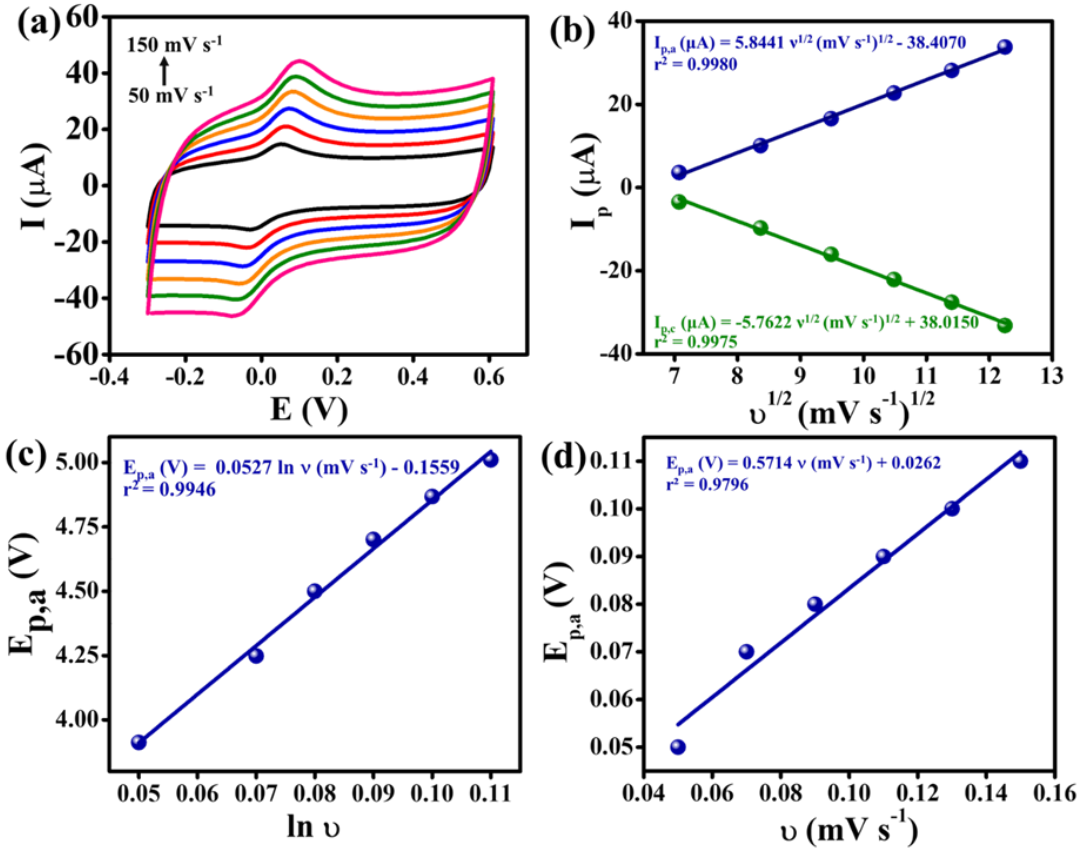

Figure 4.10 (a) the CV curves of 250 µM NDPhA at different scan rates in range 50 to 150 mV s^{-1} on the PdNPs@MIP/SPGrE, using 0.04 M B-R buffer pH 3.0 as supporting electrolyte, (b) the linear plot between redox current (I_p) and the different square root of scan rate ($\nu^{1/2}$), (c) the linear plot of oxidation peak potential ($E_{p,a}$) and the natural logarithm scan rate (ln ν) and (d) the linear plot of oxidation peak potential ($E_{p,a}$) and scan rate (ν)

The electrolyte's pH significantly impacts the binding of NDPhA target molecules to the recognition cavities on the polymer. To investigate the influence of pH, this work

recorded signals of NDPhA using the PdNPs@MIP/SPGrE with B-R buffer electrolyte in the pH range of 2.0 - 8.0 (Figure 4.11a). Figure 4.11b shows the effects of pH on the NDPhA oxidation peak potential ($E_{p,a}$) and peak current ($I_{p,a}$). The NDPhA peak potential shifts toward a less positive value with increasing electrolyte pH, whereas the anodic peak current decreases. The binding strength of NDPhA to the MIP recognition site varies depending on the pH environment. This is because a binding interaction exists between the functional groups in the template molecules and MIP. At different pH levels, the functional groups dissociate to varying degrees, causing the interaction between the functional groups to shift. This leads to a change in the binding strength of template molecules to MIP. The maximum peak current was at pH 3.0. Thus, an electrolyte pH of 3.0 gives the best performance for NDPhA binding and catalytic activity in the oxidation process.

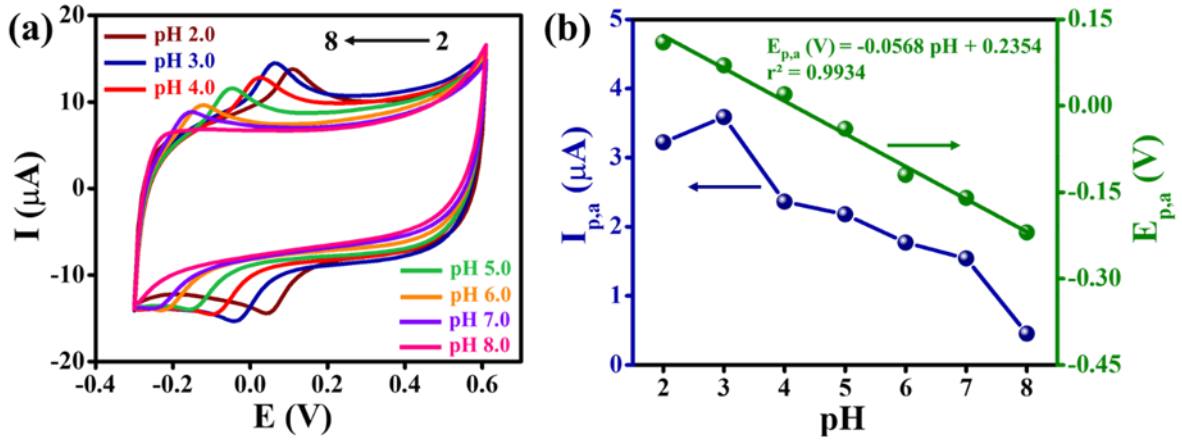

Figure 4.11 (a) CV of 250 µM NDPhA at PdNPs@MIP/SPGrE in 0.04 M B-R buffer electrolyte at different pH ranging from 2.0 to 8.0, and (b) the relation between oxidation peak current ($I_{p,a}$) and peak potential ($E_{p,a}$) vs. pH

The linear equation of the plot between oxidation peak potential against pH (Figure 4.11b) is as follows: $E_{p,a}$ (V) = − 0.0568 pH + 0.2354 (r^2 = 0.9934). According to Nernst theory, this work determined the m/n ratio from Equation (4.3) [98].

$$E_{p,a} = -\left(\frac{0.0570m}{n}\right)pH + b \qquad (4.3)$$

Where n and m represent the total number of electrons (e^-) and protons (H^+), respectively.

The slope of developed sensor (-0.0568) is close to the Nernstian slope (-0.0570), indicating that m/n is estimated to be 1. As a result, Figure 4.12 shows a possible electrochemical mechanism of NDPhA on PdNPs@MIP/SPGrE.

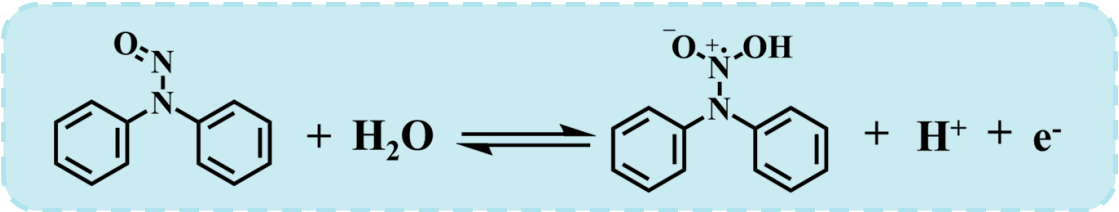

Figure 4.12 The proposed electrochemical oxidation mechanism of NDPhA on the PdNPs@MIP/SPGrE

This proposed mechanism is consistent with the previous works reported for a solid graphited polyurethane composite electrode (GPUE) [18] and boron-doped diamond electrode [99].

4.4 Enhancement of the NDPhA detection

To achieve good sensitivity, this work optimized the effect of PdNPs@MIP on the surface of SPGrE and the deposition time used in linear sweep anodic stripping (LSASV) for enhancing electrochemical responsiveness. Figure 4.13a shows that the response increases with increasing PdNPs@MIP loading, from 3 to 5 mgL^{-1}. However, greater loading generally results in a decreased signal response. The reduced signal might result from the thickness of the modified layer reducing the adsorption efficiency and hindering electron transfer from the binding NDPhA and electrode surface. Thus, the optimal concentration of PdNPs@MIP for modifying the SPGrE is 5 mg L^{-1}.

LSASV is a powerful technique for pre-concentrating the analyte by electro-depositing on the working electrode before stripping for the determination. The deposition potential and time are important parameters to optimize the accumulation process to achieve high sensitivity and precision. In this work, the influence of deposition potential and time on NDPhA oxidation current signals were investigated.

Deposition potential (-0.02, 0.00 and +0.02 V) and the results (data not shown) indicated that NDPhA gave the highest signal at the deposited potential at +0.02 V. For deposition time, the signals ranged from 0 to 300 s for PdNPs@MIP/SPGrE, using a deposition potential of + 0.02 V. Figure 4.13b revealed that anodic stripping peak current increases rapidly with increasing deposition time from 0 to 60 s and then decreases after 60 s. As a result, the optimal deposition time at 60 s to determine NDPhA was fixed.

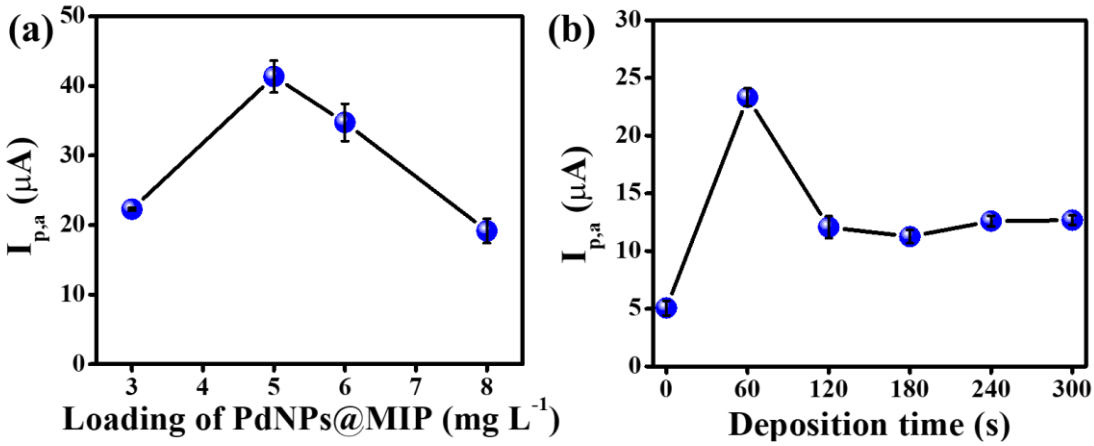

Figure 4.13 Effects of (a) loading of PdNPs@MIP on the oxidation peak current of 100 μM NDPhA at the PdNPs@MIP/SPGrE by LSASV. (b) Effect of deposition time on the oxidation peak current of 10 μM NDPhA at PdNPs@MIP/SPGrE by using LSASV, using 0.04 M B-R buffer pH 3.0 as supporting electrolyte

4.5 Analytical features

This work analyzed the analytical performance of the LSASV detection method with the developed PdNPs@MIP/SPGrE. As demonstrated in Figure 4.14a, the peak current increases with increasing NDPhA concentrations ranging from 0.01 - 100 μM. The calibration plot has its greatest slope at a concentration of less than 0.1 μM. The linear regression equation is given by: Ip,a (μA) = 51.935 ± 5.636 (μM) + 5.505 ± 0.294, r^2 = 0.996 (Figure 4.14b). At high NDPhA concentration, over the range of 0.1-100 μM, the slope of the plot indicates reduced linear sensitivity of 0.821 ± 0.013 (μA s) μM^{-1} with a linear correlation of 0.992 (Figure 4.14c). The detection limit (LOD) determined using three times the standard deviation of the blank ($3S_b$, n = 3) is 0.0013 μM. Table

4.1 compares the analytical characteristics of NDPhA imprinted sensor to those of previously modified electrodes from the literature. The performance of the PdNPs@MIP/SPGrE was comparable to or better than those reported for other NDPhA sensor designs.

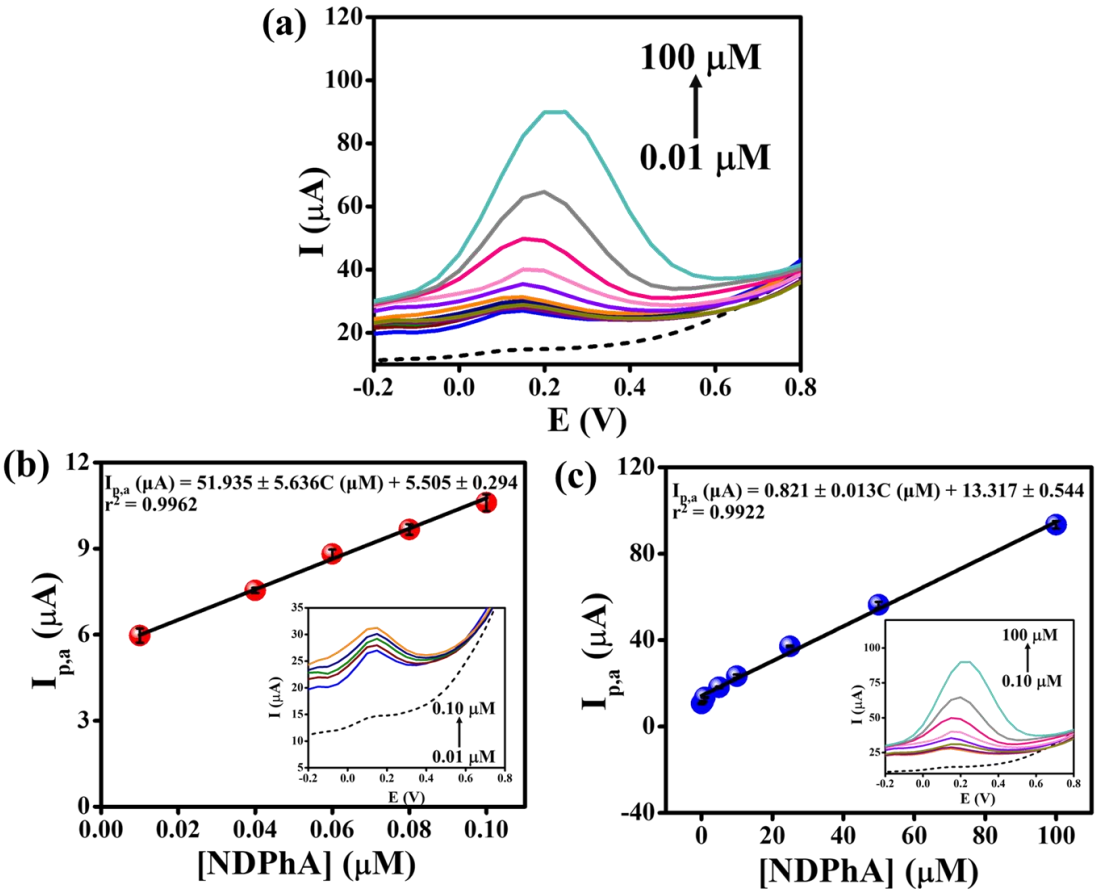

Figure 4.14 (a) LSASV curves of NDPhA on PdNPs@MIP/SPGrE in 0.04 M B-R buffer at different concentrations (0.01, 0.04, 0.06, 0.08, 0.10, 0.50, 1, 5,10, 25, 50, and 100 µM). Linear calibration curve between the oxidation peaks current ($I_{p,a}$) and the concentration of NDPhA in the ranges of (b) 0.01 – 0.10 µM, and (c) 0.1 - 100 µM

Additionally, this sensor detects NDPhA at the lowest potential ($E_{p,a}$ = 0.20 V), reducing the risk of interference from sample constituents. Moreover, the use of PdNPs@MIP/SPGr offers the lowest LOD. These results suggested that the PdNPs@MIP microsphere played an essential role in enhancing electrochemical

activity. PdNPs@MIP/SPGrE sensor provides excellent selectivity and sensitivity, quick analysis, cost-effectiveness, and minute reagent usage. These advantages result from the excellent electrocatalytic activity of the PdNPs core and many NDPhA imprinted sites in the shell. The imprinted sites increase the selective surface area and offer faster electron transfer rates between PdNPs@MIP and the SPGrE surface. This MIP sensor readily prepared the SPGrE by screen-printing and loaded PdNPs@MIP on the electrode surface by drop-casting. Hence the NDPhA imprinted sensor is convenient for large-scale and cost-effective production. Moreover, proposed MIP sensor offers comparable or superior sensing performance with additional advantages of being ready-to-use with straightforward synthesis, flexibility, and mechanical stability. Further, this is the first report of using an NDPhA-recognition imprinted sensor for the selective and sensitive determination of NDPhA using voltammetric measurements in a compact sensor.

Table 4.1 Comparison of the developed MIP sensor with other methods.

Electrode	Modifier	Technique	$E_{p,a}$ (V)	Linearity range (μM)	LOD (μM)	Sample	Reference
DME	-	DPP	-	0.10-2.4	0.032	-	[14]
Au	Porous Au	CV	+ 1.56	10,000-100,000	-	-	[15]
GCE	RuO-CN	AMP, in FIA	+ 1.06	0.20–1.0	0.10	Water	[16]
	PDDA-Gr/PtNPs	DPV	+ 1.34	0.10-50	0.033	Tap water	[17]
	GPUE	SWV	+ 0.75	2.5-18	0.27	Synthetic urine	[18]
SPGrE	PdNPs@MIP	LSASV	+ 0.20	0.01-0.1 0.1-100	0.0013	Beverages	This work

Electrode

DME = Dropping Mercury Electrode, Au = gold disk electrode, GCE = Glassy carbon electrode,

SPGrE = Screen-printed graphene electrode

Modifier

Porous Au = porous gold electrode running in the medium of liquid ionic [$BMIM^+$] [BF_4^-],

RuO-CN= a film of mixed valent ruthenium oxides stabilized by cyano cross-links, PDDA-Gr/PtNPs = graphene and platinum nanoparticles stabilized by poly(diallyldimethylammonium chloride), GPUE = graphite-polyurethane composite,

PdNPs@MIP = palladium nanoparticles coated with a molecularly imprinted polymer.

Technique

DPP = Differential pulse polarography, CV = Cyclic voltammetry, AMP = Amperometry in flow injection analysis,

DPV = Differential pulse voltammetry, SWV = Square wave voltammetry, LSASV = Linear sweep anodic stripping voltammetry

4.6 Enhancing anti-interference ability

This section examined the selective detection of NDPhA on the proposed sensor in the presence of possible interfering species found in beverage samples was examined. The interfering species included ascorbic acid, glucose, fructose, citric acid, caffeine, ethanol, $NaNO_3$, NaCl, and substances with similar structures such as diphenylamine and uric acid. Two different methods in these experiments was used. In the first method, both MIP and NIP electrodes were operated under a rebinding process in a solution of NDPhA or other substances. This work calculated the value of the imprinting factor (IF) from equation (4.4) [100].

$$IF = \frac{i_p\ current\ MIP}{i_p\ current\ NIP} \tag{4.4}$$

The largest IF values confirm good imprinting of MIP. On the other hand, IF values close to 1 infer that the imprinting effect is almost insignificant, which means that the interaction between the MIP and the template is somewhat unspecific, more involved to surface interactions than to any generated recognition cavities [21].

Figure 4.15a shows responses for PdNPs@MIP/SPGrE (front row, purple bar) and PdNPs@NIP/SPGrE (middle row, orange bar) when exposed to solutions containing the respective NDPhA or other substances at a concentration of 1 µM. The IF values of this work (Figure 4.15a, back row, blue bar) for NDPhA is 10.15. For other compounds, it is in the range of 0.41 - 1.05, so the IF value for the target NDPhA is much higher than that obtained from competing compounds. These results thus clearly demonstrate appreciable selectivity of the developed sensor. The electrode selectivity was enhanced because PdNPs@MIP has imprinted cavities complementary in size conformation and shape to NDPhA molecules. Therefore, specific polymer recognition sites will allow only NDPhA molecules to bind. Other compounds with different structures from the NDPhA target cannot diffuse or bind strongly to the recognition sites.

In the second method, a current signal of 1.0 µM NDPhA in the presence of varying concentrations of the interferents, as mentioned above, was investigated with the MIP electrode. As shown in Figure 4.15b, the $I_{p\,a}$ changed less than 10% in the presence of a 50-fold excess of diphenylamine, a 250-fold excess of ascorbic acid and uric acid, and a 1,000-fold excess of glucose, fructose, citric acid, caffeine, ethanol, $NaNO_3$, and NaCl.

Only NDPhA provides a strong current response at the PdNPs@NIP/SPGrE electrode (Figure 4.15a). Other species did not produce any substantial current. These findings suggested that the NDPhA molecules effectively transferred to the polymeric network, and the PdNPs@MIP can detect the NDPhA molecules preferentially among other substances.

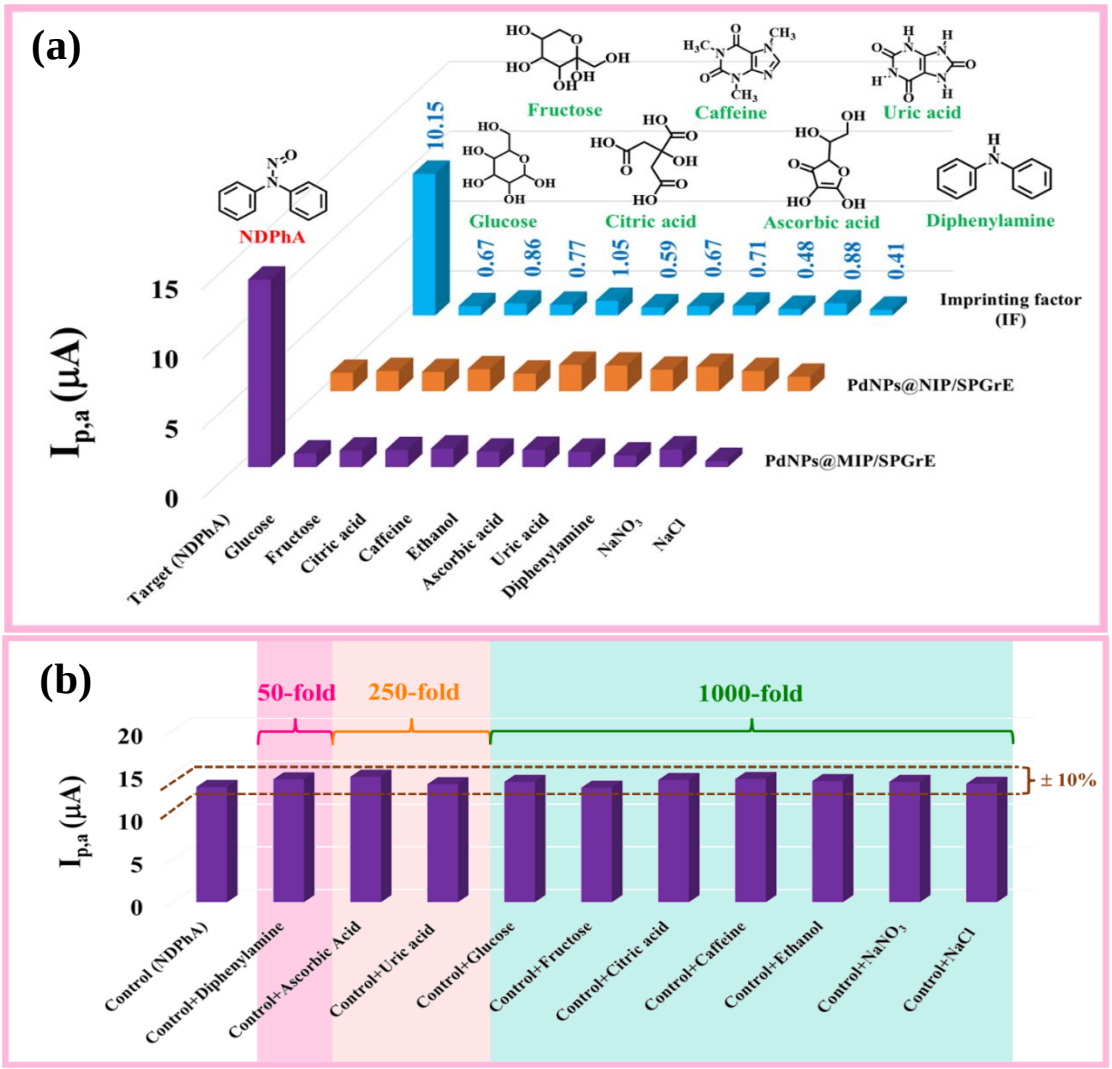

Figure 4.15 (a) The selectivity of the imprinted (PdNPs@MIP/SPGrE) and non-imprinted (PdNPs@NIP/SPGrE) sensors for NDPhA and foreign interferences. (b) Selectivity evaluation of the proposed MIP sensor for NDPhA at 1 μM, diphenylamine at 50 μM, ascorbic acid and uric acid at 250 μM, glucose, fructose, citric acid, caffeine, ethanol, $NaNO_3$, and NaCl at 1000 μM

4.7 Reproducibility and stability

The MIP sensor analyzed the reproducibility of the fabricated NDPhA imprinted sensor by comparing the current response of 1 µM NDPhA for five different PdNPs@MIP/SPGrE electrodes (Figure 4.16a). All NDPhA imprinted sensors responded with similar currents, with an RSD of 1.67%. Additionally, the stability of the NDPhA imprinted sensor by measuring the current signal of 1 µM NDPhA at various intervals over four weeks was investigated. The results (Figure 4.16b) showed that after 28 days, the signal of the NDPhA imprinted sensor retains 81 % of its initial current. These results demonstrate that the imprinted sensor possesses good reproducibility and stability for detecting NDPhA.

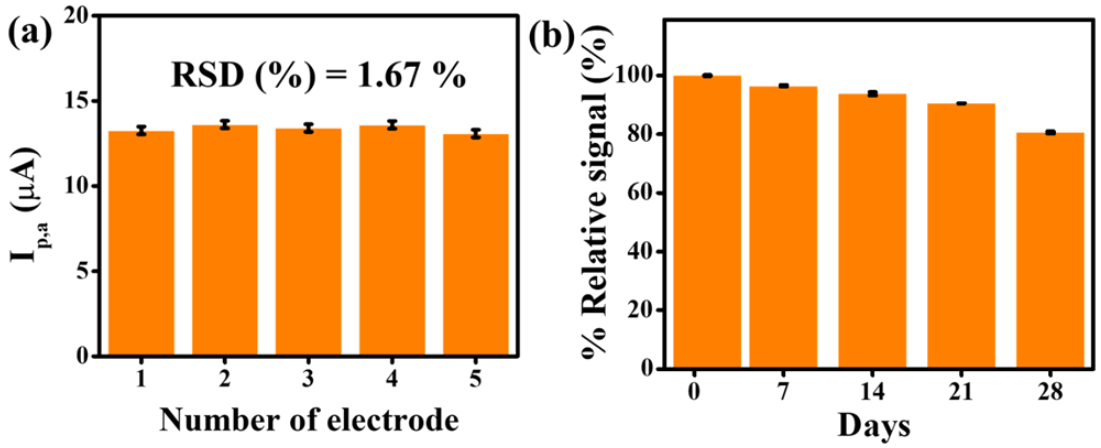

Figure 4.16 (a) Reproducibility of five independent PdNPs@MIP/SPGrE electrodes and (b) storage stability for 30 days (every seven days per measurement). The obtained results were performed in 1.0 µM NDPhA containing 0.04 M B-R buffer pH 3.0

4.8 Real sample analysis

The PdNPs@MIP/SPGrE further tested the accuracy and application of the PdNPs@MIP sensor in the quantitative analysis of NDPhA in six beverage samples, including beer, wines (dark and red wines), green tea, orange juice, apple juice, and a synthetic sample. This work used HPLC coupled with a photodiode array detector set at 280 nm as a comparison method to quantify the set of samples. In addition, sample recoveries (spiked levels of 0.05 and 0.10 µM) to validate the analysis were investigated.

Table 4.2 compares the results of NDPhA concentrations in beverages and calculated recovery values as analyzed by the MIP sensor and HPLC. The measurements obtained from the two methods are in good agreement. The recoveries of developed MIP sensor are in the acceptable range (92.00% to 98.00%) with sustainable repeatability (%RSD less than 4.91%). Relative differences are in the range of -3.15% to 4.26%. These results indicate no significant matrix interference in the analyzed samples. Therefore, this work conclude that the proposed MIP sensor is sufficiently accurate, precise, and suitable for the NDPhA determination in beverage samples.

This work further evaluated the accuracy and precision of the proposed MIP sensor in terms of intra-day and inter-day analysis. The NDPhA content of certified reference materials (CRM31032/607) was determined using MIP sensor. As shown in Table 4.3, good intra-day and inter-day accuracy (%bias) in CRM, *e.g.*, -0.74% for intra-day and -1.01% for inter-day analysis, are obtained. These results reflect that the proposed PdNPs@MIP/SPGrE sensor is accurate, precise, and appropriate for the determination of NDPhA in real samples.

Table 4.2 Comparison of NDPhA determination in beer, wines (dark and red wines), green tea, and juices (orange and apple juices) using the proposed MIP sensor and the reference values obtained from HPLC.

Sample	Added (μM)	Proposed MIP sensor			HPLC			Relative difference (%)
		Found (μM)	% Recovery	%RSD	Found (μM)	% Recovery	%RSD	
Beer	- 0.05 0.10	<LOD 0.047 0.097	- 94.00 97.00	- 1.39 1.13	<LOD 0.048 0.096	- 96.00 96.00	- 1.19 2.41	- - 2.08 +1.04
Dark wine	- 0.05 0.10	<LOD 0.049 0.094	- 98.00 94.00	- 2.06 4.22	<LOD 0.049 0.093	- 98.00 93.00	- 2.49 4.43	- 0.00 + 1.08
Red wine	- 0.05 0.10	<LOD 0.047 0.092	- 94.00 92.00	- 2.01 3.89	<LOD 0.047 0.095	- 94.00 95.00	- 1.83 2.45	- 0.00 -3.15
Green tea	- 0.05 0.10	<LOD 0.049 0.098	- 98.00 98.00	- 1.16 2.53	<LOD 0.048 0.099	- 96.00 99.00	- 1.29 2.78	- + 2.04 - 1.01
Orange juice	- 0.05 0.10	<LOD 0.048 0.089	- 96.00 89.00	- 3.98 0.51	<LOD 0.047 0.090	- 94.00 90.00	- 1.37 2.23	- + 2.13 - 1.11
Apple juice	- 0.05 0.10	<LOD 0.048 0.098	- 96.00 98.00	- 3.21 4.91	<LOD 0.049 0.094	- 98.00 94.00	- 4.94 2.74	- - 2.04 + 4.26
Synthetic sample	- 0.05 0.10	0.050 0.099 0.145	- 98.00 95.00	- 1.80 1.62	0.049 0.098 0.144	- 98.00 95.00	- 1.71 1.10	+ 2.04 + 1.02 + 0.69

% Relative difference = ($[NDPhA]_{MIP\ sensor} - [NDPhA]_{HPLC}$) / ($[NDPhA]_{HPLC}$) × 100

Table 4.3 Intra-day and Inter-day assay precision and accuracy for determination of NDPhA in certified reference materials (CRM) using the proposed MIP sensor.

CRM	Proposed MIP sensor		Bias (%)
	Found (μM)	RSD (%)	
Intra-day	10,046.667 ± 75.719	0.75	-0.74
Inter-day	10,019.998 ± 84.855	0.85	-1.01

CRM31032/607, with the certified value of NDPhA at 10,122.087 ± 94.340 μM.

CHAPTER 5
CONCLUSION

This research successfully developed and utilized a novel NDPhA compact electrochemical sensor based on palladium nanoparticles covered with a molecularly imprinted polymer (PdNPs@MIP) for NDPhA determination in beverages. The screen-printed graphene electrode (SPGrE) was easily manufactured, and the synthesized PdNPs@MIP was dropped cast on the electrode surface to create the NDPhA - imprinted sensor. The 3 D-imprinting on the surface of PdNPs was effectively accomplished by successively coating the surface of PdNPs with PVP, followed by MIP. NDPhA imprinted polymer was successfully synthesized on the PdNPs core using NDPhA as template, n-Isopropylacrylamide (NIPAM) as the monomer, trimethylolpropane trimethacrylate (TRIM) as cross-linker, and 2,2'-azobis(2-methylpropionitrile) (AIBN) as initiator. Polymerization conditions of MIP using PdNPs nanoparticle core at 20 mg and the template: monomer: cross-linker (NDPhA: NIPAM: TRIM) ratio of 1: 2: 7.5 were performed. The as-prepared micro-size spherical PdNPs@MIP are homogeneous, have strong electro-catalytic activity, and have a large number of NDPhA imprinted sites. This is the first report of employing an NDPhA recognition imprinted sensor to determine NDPhA selectively and sensitively using voltammetric measurements on a compact sensor. Results from SEM and TEM revealed that the synthesized PdNPs appears approximately pherical with an average diameter of 22.0 ± 1.7 nm (count = 20), whereas PdNPs-PVP is larger than the unmodified PdNPs due to the formation of a PVP layer on the surface of the PdNPs. The PdNPs@MIP shows a spherical shape and uniform microsphere with a mean diameter of around 2.3 ± 0.8 μm (count = 10). The presence of Pd^0 species in the PdNPs@MIP is confirmed by XPS analysis. Furthermore, FT-IR confirmed the success of MIP coating on PdNPs as well as the formation of NDPhA recognition sites on polymer films. The compact NDPhA imprinted sensor was constructed by coating the SPGrE surface with PdNPs@MIP. Quantitative analysis was operated by linear sweep anodic stripping voltammetry (LSASV) using a deposition potential of +0.02 V for 60 s. The linear working ranges for NDPhA measurements were

0.01 - 0.1 μM (r^2 = 0.996) and 0.1 – 100 μM (r^2 = 0.992) with corresponding sensitivities of 51.935 and 0.821 (μA s) μM^{-1}, respectively. The system provides a good precision of %RSD 1.67% with an estimated detection limit ($3S_b$, n = 3) of 0.0013 μM. The certified reference material (CRM) has intraday and interday accuracy (% bias) of -0.74 % and -1.01 %, respectively. The proposed MIP sensor has outstanding sensing performance while also being ready-to-use, cost-effective, simple to synthesize, flexible, mechanically stable, and suitable for large-scale production. The PdNPs@MIP/SPGrE performed well, with a low detection limit, broad linearity, high reproducibility, and stability. The electrocatalytic properties of the PdNPs core and a large number of NDPhA imprinted sites in the shell enhance the selective surface area and offer fast electron transfer rates, resulting in these exceptional features. Furthermore, the designed sensor detects NDPhA at a very low potential of 0.20 V, which reduces the possibility of interference from sample components and improves the sensor's anti-interference capabilities for determining NDPhA in a complex matrix. The offered MIP sensor presents high accuracy, high precision, and excellent performance when applied to the determination of NDPhA in beverages.

REFERENCES

REFERENCES

[1] Fan, C. C. and Lin, T. F. "N-nitrosamines in drinking water and beer: Detection and risk assessment", **Chemosphere**. 200: 48-56; June, 2018.

[2] Lachenmeier, D. W. and Fügel, D. "Reduction of nitrosamines in beer-review of a success story", **Brewingscience - Monatsschrift Für Brauwissenschaft**. 60: 84-89; June, 2007.

[3] Li, W. and et al. "Online coupling of tandem liquid-phase extraction with HPLC-UV for the determination of trace N-nitrosamines in food products", **Analytical Methods.** 10(15): 1733-1739; March, 2018.

[4] Lu, S. and et al. "Facile and sensitive determination of N-nitrosamines in food samples by high-performance liquid chromatography via combining fluorescent labeling with dispersive liquid-liquid microextraction", **Food chemistry**. 234: 408-415; November, 2017.

[5] Benedé, J. L. and et al. "Stir bar sorptive-dispersive microextraction mediated by magnetic nanoparticles–nylon 6 composite for the extraction of hydrophilic organic compounds in aqueous media", **Analytica chimica acta**. 926: 63-71; July, 2016.

[6] Miralles, P., Alberto, C., and Amparo, S. "Determination of N-nitrosamines in cosmetic products by vortex-assisted reversed-phase dispersive liquid-liquid microextraction and liquid chromatography with mass spectrometry", **Journal of separation science.** 41(15): 3143-3151; August, 2018.

[7] Ishizaki, A., and Hiroyuki, K. "A sensitive method for the determination of tobacco-specific nitrosamines in mainstream and sidestream smokes of combustion cigarettes and heated tobacco products by online in-tube solid-phase microextraction coupled with liquid chromatography-tandem mass spectrometry", **Analytica Chimica Acta**. 1075: 98-105; October, 2019.

[8] Zhou, Y. and et al. "Development of a heart-cutting supercritical fluid chromatography-high-performance liquid chromatography coupled to tandem mass spectrometry for the determination of four tobacco-specific nitrosamines in mainstream smoke", **Analytical and bioanalytical chemistry.** 411(13): 2961-2969; March, 2019.

REFERENCES (CONTINUED)

[9] Giménez-Campillo, C. and et al. "Ultrasound Assisted Extraction Approach to Test the Effect of Elastic Rubber Nettings on the N-Nitrosamines Content of Ham Meat Samples", **Foods**. 10(11): 2564; October, 2021.

[10] Ramezani, H. and et al. "Rapid determination of nitrosamines in sausage and salami using microwave-assisted extraction and dispersive liquid–liquid microextraction followed by gas chromatography–mass spectrometry", **European Food Research and Technology.** 240(2): 441-450; October, 2015.

[11] Hu, Y. and et al. "Dual-functional imprinted magnetic nanoprobes for fluorescence detection of N-nitrosodiphenylamine", **Analytical Methods**. 10(20): 2384-2389; April, 2018.

[12] Li, Z. and et al. "Molecularly imprinted solid phase extraction coupled with gas chromatography-mass spectrometry for determination of N-Nitrosodiphenylamine in water samples", **Chemosphere.** 212: 872-880; December, 2018

[13] Li, Z. and et al. "A novel molecularly imprinted polymer-solid phase extraction method coupled with high performance liquid chromatography tandem mass spectrometry for the determination of nitrosamines in water and beverage samples", **Food chemistry.** 292: 267-274; September, 2019.

[14] Samuelsson, R. "Pulse polarographic determination of nitrosamines: Part 2. Methods for the Determination of N-Nitrosodiphenylamine and N-Nitrosodibutylamine", **Analytica Chimica Acta.** 108: 213-219; July, 1979

[15] Yang, H. L. and et al. "Electrochemical determination of NDPhA via its electrocatalysis at porous Au electrode in room temperature ionic liquid", **Electroanalysis: An International Journal Devoted to Fundamental and Practical Aspects of Electroanalysis.** 20(18): 2003-2008; September, 2008.

[16] Gorski, W., and James A. C. "Amperometric determination of N-Nitrosamines in aqueous solution at an electrode coated with a ruthenium-based inorganic polymer", **Analytical Chemistry.** 66(17): 2771-2774; September, 1994.

REFERENCES (CONTINUED)

[17] Peng, Xiuying and et al. "Electrochemical sensor for facile detection of trace N-nitrosodiphenylamine based on poly (diallyldimethylammonium chloride)-stabilized graphene/platinum nanoparticles", **New Journal of Chemistry.** 43(2): 820-826; November, 2019.

[18] Martoni, L. V. and et al. "Electrochemical behavior of N-Nitrosodiphenylamine and its determination in synthetic urine samples using a graphite-polyurethane composite electrode", **Journal of Electroanalytical Chemistry.** 857: 113747; January, 2020.

[19] Wang, Y. and et al. "$CuCo_2O_4$/N-Doped CNTs loaded with molecularly imprinted polymer for electrochemical sensor: Preparation, characterization and detection of metronidazole", **Biosensors and Bioelectronics.** 142: 111483; October, 2019.

[20] Pandit, S.G. and et al. "Safety efficacy and chemical profiling of water-soluble Talaromyces purpureogenus CFRM02 pigment", **Food Chemistry.** 310: 125869; April, 2020.

[21] Yue, X. and et al. "Selective electrochemical determination of tertiary butylhydroquinone in edible oils based on an in-situ assembly molecularly imprinted polymer sensor", **Food chemistry.** 289: 84-94; August, 2019.

[22] Herrera-Chacón, A., Xavier C., and Manel D. V. "Molecularly imprinted polymers-towards electrochemical sensors and electronic tongues", **Analytical and Bioanalytical Chemistry.** 413(24): 6117-6140; April, 2021.

[23] Somnet, K. and et al. "Ready-to-use paraquat sensor using a graphene-screen printed electrode modified with a molecularly imprinted polymer coating on a platinum core", **Analyst.** 146(20): 6270-6280; September, 2021.

[24] Fresco-Cala, B., Batista, A. D., and Cárdenas, S. "Molecularly imprinted polymer micro-and nano-particles: A review", **Molecules.** 25(20): 4740; October, 2020.

REFERENCES (CONTINUED)

[25] Mamipour, Z., Nematollahzadeh, A., & Kompany-Zareh, M. "Molecularly imprinted polymer grafted on paper and flat sheet for selective sensing and diagnosis: a review", **Microchimica Acta.** 188(8): 1-21; July, 2021.

[26] Lahcen, A. A., and Amine, A. "Recent advances in electrochemical sensors based on molecularly imprinted polymers and nanomaterials", **Electroanalysis.** 31(2): 188-201; December, 2019.

[27] Chen, Jianrong and et al. "A novel composite of molecularly imprinted polymer-coated PdNPs for electrochemical sensing norepinephrine", **Biosensors and Bioelectronics.** 65: 366-374; March, 2015.

[28] Uberman, P. M. and et al. "Electrochemical synthesis of palladium nanoparticles in PVP solutions and their catalytic activity in Suzuki and Heck reactions in aqueous medium", **RSC Advances.** 4(24): 12330-12341; February, 2014.

[29] Li, J. and et al. "High-sensitivity paracetamol sensor based on Pd/graphene oxide nanocomposite as an enhanced electrochemical sensing platform", **Biosensors and Bioelectronics.** 54: 468-475; April, 2014.

[30] Park, J. E. and et al. "Distribution of seven N-nitrosamines in food", **Toxicological research.** 31(3): 279-288; December, 2015.

[31] Fan, T. Y. and et al. "Comprehensive analytical procedures for the determination of volatile and non-volatile, polar and non-polar N-nitroso compounds", **IARC Scientific Publications.** 19: 3-17; January, 1978.

[32] Bartsch, H. **Relevance of N-nitroso compounds to human cancer: exposures and mechanisms.** London: R. & International Agency for Research on Cancer, 1987

[33] Spichiger, K., and Ursula E. **Chemical sensors and biosensors for medical and biological applications.** Berlin: Wiley-VCH, 2008.

[34] Hulanicki, A., Glab, S., and Ingman, F. O. L. K. E. "Chemical sensors: definitions and classification", **Pure and applied chemistry.** 63(9): 1247-1250; January, 1991.

[35] Hierlemann, A. and Henry B. "CMOS-based chemical microsensors", **Analyst.** 128(1): 15-28; December, 2003.

REFERENCES (CONTINUED)

[36] J. Janata. **Principles of Chemical Sensor.** New York: Plenum Press, 1989.

[37] J. Janata and R.J. Huber. **Solid State Chemical Sensors.** San Diego: Academic Press, 1985.

[38] Fazio, E. and et al. "Metal-oxide based nanomaterials: Synthesis, characterization and their applications in electrical and electrochemical sensors", **Sensors.** 21(7): 2494; April, 2021.

[39] Wang, J. "Amperometric biosensors for clinical and therapeutic drug monitoring: a review", **Journal of pharmaceutical and biomedical analysis.** 19(1-2): 47-53; February, 1999.

[40] Shetti, N. P. and et al. "Graphene–clay-based hybrid nanostructures for electrochemical sensors and biosensors", **Graphene-Based Electrochemical Sensors for Biomolecules.** 235-274; October, 2019.

[41] Brett, C., and Oliveira-Brett, A. M. "Electrochemical sensing in solution-origins, applications and future perspectives", **Journal of Solid State Electrochemistry.** 15(7): 1487-1494; June, 2011.

[42] Heyrovsky, J. "Electrolysis with the dropping mercury electrode", **Chemicke Listy.** 16: 256-304, 1922.

[43] Kolthoff, I. M. and Lingane, J. J. **Polarography.** New York: Interscience, 1952.

[44] Heyrovský, J. and Zuman, P. **Practical Polarography.** New York: Academic Press, 1968.

[45] Wulff, G. "The use of polymers with enzyme-analogous structures for the resolution of racemates", **Angewandte Chemie International edition in English.** 11(4): 341, 1972.

[46] Wulff, G., Gross, T., and Schönfeld, R. "Enzyme models based on molecularly imprinted polymers with strong esterase activity", **Angewandte Chemie International Edition in English.** 36(18): 1962-1964; October, 1997.

[47] Algieri, C. and et al. "Bio-mimetic sensors based on molecularly imprinted membranes", **Sensors.** 14(8): 13863-13912; July, 2014.

REFERENCES (CONTINUED)

[48] Wackerlig, J., and Schirhagl, R. "Applications of molecularly imprinted polymer nanoparticles and their advances toward industrial use: a review", **Analytical chemistry.** 88(1): 250-261; November, 2016.

[49] Bole, A. L., and Manesiotis, P. "Advanced materials for the recognition and capture of whole cells and microorganisms", **Advanced Materials.** 28(27): 5349-5366; December, 2016.

[50] Zeng, Z. and et al. "Synthetic polymer nanoparticles with antibody-like affinity for a hydrophilic peptide", **ACS nano.** 4(1): 199-204; December, 2010.

[51] Baggiani, C. and et al. "A connection between the binding properties of imprinted and nonimprinted polymers: a change of perspective in molecular imprinting", **Journal of the American Chemical Society.** 134(3): 1513-1518; December, 2012.

[52] Adumitrăchioaie, A. and et al. "Electrochemical methods based on molecularly imprinted polymers for drug detection. A review", **international journal of electrochemical science.** 13: 2556-2576; February, 2018.

[53] Wulff, G. and et al. "Enzyme-analogue built polymers, 4. On the synthesis of polymers containing chiral cavities and their use for the resolution of racemates", **Die Makromolekulare Chemie: Macromolecular Chemistry and Physics.** 178(10): 2799-2816; October, 1977.

[54] Renedo, O. D., Alonso-Lomillo, M. A., and Martínez, M. A. "Recent developments in the field of screen-printed electrodes and their related applications", **Talanta.** 73(2): 202-219; September, 2007.

[55] Hart, J. P. and et al. "Some recent designs and developments of screen-printed carbon electrochemical sensors/biosensors for biomedical, environmental, and industrial analyses", **Analytical letters.** 37(5): 789-830; August, 2004.

[56] Li, M. and et al. "Recent developments and applications of screen-printed electrodes in environmental assays-A review", **Analytica chimica acta.** 734: 31-44; July, 2012.

REFERENCES (CONTINUED)

[57] Lucarelli, F. and et al. "Electrochemical DNA biosensor for analysis of wastewater samples", **Bioelectrochemistry.** 58(1): 113-118; November, 2002.

[58] Yi, W. and et al. "Electrochemical detection of chloramphenicol using palladium nanoparticles decorated reduced graphene oxide", **Microchemical Journal.** 148: 774-783; July, 2019.

[59] Atiweena, K. and et al. "Palladium nanoparticles decorated on reduced graphene oxide rotating disk electrodes toward ultrasensitive hydrazine detection: effects of particle size and hydrodynamic diffusion", **Analytical Chemistry.** 86: 12272–12278; November, 2014.

[60] Chappa, S. and et al. "Egg-shell membrane mimicking synthetic polymer membrane supported palladium nanoparticles for catalyzing reduction of uranyl (VI) ions", **Applied Catalysis B: Environmental.** 203: 53–64; April, 2017.

[61] Shao, M. and et al. "Structural dependence of oxygen reduction reaction on palladium nanocrystals", **Chemical Communications.** 47(23): 6566-6568; May, 2011.

[62] J. Zhang, J. Wu, H. Zhang. **PEM Fuel Cell Testing and Diagnosis**. Kidlington: Elsevier, 2013.

[63] Lyle, S. J., and Yassin, S. S. "Polarographic studies of metal ion complexes of Ampicillin and Amoxycillin", **Analytica chimica acta.** 274(2): 225-230; March, 1993.

[64] Uslu, B., and Biryol, I. "Voltammetric determination of amoxicillin using a poly (N-vinyl imidazole) modified carbon paste electrode", **Journal of pharmaceutical and biomedical analysis.** 20(3): 591-598; July, 1999.

[65] Biryol, I., Uslu, B., and Küçükyavuz, Z. "Voltammetric determination of amoxicillin using a carbon paste electrode modified with poly (4-vinyl pyridine)", **STP pharma sciences.** 8(6): 383-386; 1998.

REFERENCES (CONTINUED)

[66] Kit-Anan, W. and et al. "Disposable paper-based electrochemical sensor utilizing inkjet-printed Polyaniline modified screen-printed carbon electrode for Ascorbic acid detection", **Journal of Electroanalytical Chemistry.** 685: 72–78; October, 2012.

[67] Karuwan, C. and et al. "Screen-printed graphene-based electrochemical sensor for microfluidic device", **Analytical Methods.** 9: 3689-3695; May, 2017.

[68] Pasakon, P. and et al. "A high-performance, disposable screen-printed carbon electrode modified with multi-walled carbon nanotubes/graphene for ultra-trace level electrochemical sensors", **Journal of Applied Electrochemistry.** 49: 214-227; November, 2019.

[69] Kampeera, J. and et al. "Point-of-care rapid detection of Vibrio parahaemolyticus in seafood using loop-mediated isothermal amplification and graphene-based screen-printed electrochemical sensor", **Biosensors and Bioelectronics.** 132: 271-278; May, 2019.

[70] De Oliveira, R. T. S. and et al. "Electroanalytical Determination of N-Nitrosamines in Aqueous Solution Using a Boron-Doped Diamond Electrode", **Electroanalysis.** 20: 396-401; February, 2008.

[71] Shah, K. A., Halquist, M. S., and Karnes, H. T. "A modified method for the determination of tobacco specific nitrosamine 4-(methylnitrosamino)-1-(3-pyridyl)-1-butanol in human urine by solid phase extraction using a molecularly imprinted polymer and liquid chromatography tandem mass spectrometry", **Journal of Chromatography B: Biomedical Sciences.** 877: 1575–1582; May, 2009.

[72] Cetó, X. and et al. "Electrochemical detection of N-nitrosodimethylamine using a molecular imprinted polymer", **Sensors and Actuators B: Chemical.** 237: 613–620; December, 2016.

[73] Zheng, X. and et al. "Preparation of hollow porous molecularly imprinted polymers for N-nitrosamine adsorption", **Materials Letters.** 211: 21-23; January, 2018.

REFERENCES (CONTINUED)

[74] Kamsong, W. and et al. "Highly sensitive and disposable screen-printed ionic liquid/graphene based electrochemical sensors", **Electrochemistry Communications.** 107209; February, 2022.

[75] Ullah, I., et al. "Synthesis, structural characterization and catalytic application of citrate-stabilized monometallic and bimetallic palladium@ copper nanoparticles in microbial anti-activities", **International Journal of Nanomedicine.** 12: 8735; December, 2017.

[76] Savotha, M., Dhineshbabu, N., and Sriram, R. G. "Iron-Polyvinylpyrrolidone (Fe-PVP) nanocomposite coated Inductive Proximity Sensor", **Applied science letters.** 1: 62–67; July, 2015.

[77] Nontawong, Nongyao, and et al. "Novel amperometric flow-injection analysis of creatinine using a molecularly-imprinted polymer coated copper oxide nanoparticle-modified carbon-paste-electrode", **Journal of pharmaceutical and biomedical analysis.** 175: 112770; October, 2019.

[78] Siddiqi, K. S., and Husen, A. "Green synthesis, characterization and uses of palladium/platinum nanoparticles", **Nanoscale research letters.** 11(1): 1-13; November, 2016.

[79] Arsiya, F., Sayadi, M. H., and Sobhani, S. "Green synthesis of palladium nanoparticles using Chlorella vulgaris", **Materials Letters.** 186: 113-115; January, 2017.

[80] Sheny, D. S., Philip, D., and Mathew, J. "Rapid green synthesis of palladium nanoparticles using the dried leaf of Anacardium occidentale", **Spectrochimica Acta Part A: Molecular and Biomolecular Spectroscopy.** 91: 35-38; June, 2012.

[81] Piskorz, M., and T. Urbanski. "Ultraviolet and infrared spectra of some nitrosamines", **Bulletin L'Académie Polonaise des Science.** 11(11); August, 1963.

REFERENCES (CONTINUED)

[82] Bucatariu, S. and et al. "Synthesis and characterization of thermosensitive poly (N-isopropylacrylamide-co-hydroxyethylacrylamide) microgels as potential carriers for drug delivery", **Journal of Polymer Research.** 21(11): 1-12; October, 2014.

[83] Xu, H., and et al. "Development of poly (N-isopropylacrylamide)/alginate copolymer hydrogel-grafted fabrics embedding of berberine nanosuspension for the infected wound treatment", **Journal of Biomaterials Applications.** 28(9): 1376-1385; October, 2014.

[84] Kim, Y., and et al. "Dual stimuli-triggered nanogels in response to temperature and pH changes for controlled drug release", **Nanoscale Research Letters.** 14(1): 1-9; March, 2019.

[85] Zou, G. and et al. "Temperature-sensitive poly (N-isopropylacrylamide)/konjac glucomannan/graphene oxide composite membranes with improved mechanical property, swelling capability, and degradability", **International Journal of Polymer Science.** 2018: 7906747; April, 2018.

[86] Yang, X. and et al. "Plasma-initiated polymerization of N-isopropylacrylamide and functionalized with dopamine for the adhesion to Hela cells", **Polymer Bulletin.** 77(2): 963-974; April, 2020.

[87] Meng, X. and et al. "Preparation and Properties of Polyvinylidene Fluoride Nanocomposited Membranes based on Poly (N-Isopropylacrylamide) Modified Graphene Oxide Nanosheets", **Polymers.** 11(3): 473; March, 2019.

[88] Thomas, H. R. and et al. "One-step grafting of polymers to graphene oxide", **Polymer chemistry**. 6(48): 8270-8274; October, 2015.

[89] Gholinejad, M., Bahrami, M., and Nájera, C. "A fluorescence active catalyst support comprising carbon quantum dots and magnesium oxide doping for stabilization of palladium nanoparticles: Application as a recoverable catalyst for Suzuki reaction in water", **Molecular Catalysis.** 433: 12-19; May, 2017.

REFERENCES (CONTINUED)

[90] Gao, L. and et al. "Novel strategy for preparation of graphene-Pd, Pt composite, and its enhanced electrocatalytic activity for alcohol oxidation", **Langmuir.** 29(3): 957-964; December, 2013.

[91] Nontawong, N. and et al. "Smart sensor for assessment of oxidative/nitrative stress biomarkers using a dual-imprinted electrochemical paper-based analytical device", **Analytica Chimica Acta.** 1191: 339363; January, 2022.

[92] Gökçeören, A. T., Şenkal, B. F., and Erbil, C. "Effect of crosslinker structure and crosslinker/monomer ratio on network parameters and thermodynamic properties of Poly (N-isopropylacrylamide) hydrogels", **Journal of Polymer Research.** 21(3): 1-12; February, 2014.

[93] Liu, Y. and et al. "Preparation of molecularly imprinted polymeric microspheres based on distillation–precipitation polymerization for an ultrasensitive electrochemical sensor", **Analyst.** 142(7): 1091-1098; February, 2017.

[94] Fatahi, A., Malakooti, R., and Shahlaei, M. "Electrocatalytic oxidation and determination of dexamethasone at an Fe_3O_4/PANI-Cu II microsphere modified carbon ionic liquid electrode", **RSC Advances.** 7(19): 11322-11330; February, 2017.

[95] Bard, A. J., and Faulkner, L. R. "Fundamentals and applications. Electrochem", **Methods.** 2(482): 580-632, 2001.

[96] Wu, Y., Ji, X., and Hu, S. "Studies on electrochemical oxidation of azithromycin and its interaction with bovine serum albumin", **Bioelectrochemistry.** 64(1): 91-97; August, 2004.

[97] Parvin, M. H. and et al. "Highly sensitive and selective electrochemical sensor for detection of vitamin B12 using an Au/PPy/FMNPs@ TD-modified electrode", **Sensors and Actuators B: Chemical.** 261: 335-344; May, 2018.

REFERENCES (CONTINUED)

[98] Ensafi, A. A., Nasr-Esfahani, P., and Rezaei, B. "Metronidazole determination with an extremely sensitive and selective electrochemical sensor based on graphene nanoplatelets and molecularly imprinted polymers on graphene quantum dots", **Sensors and Actuators B: Chemical.** 270: 192-199; October, 2018.

[99] de Oliveira, R. T. S. and et al. "Electroanalytical Determination of N-Nitrosamines in Aqueous Solution Using a Boron-Doped Diamond Electrode", **Electroanalysis: An International Journal Devoted to Fundamental and Practical Aspects of Electroanalysis.** 20(4): 396-401; February, 2008.

[100] Hatamluyi, B. and et. al. "Ultra-sensitive molecularly imprinted electrochemical sensor for patulin detection based on a novel assembling strategy using Au@ Cu-MOF/N-GQDs", **Sensors and Actuators B: Chemical.** 318: 128219; September, 2020.

APPENDICES

APPENDIX A

Optimization conditions of polymerization

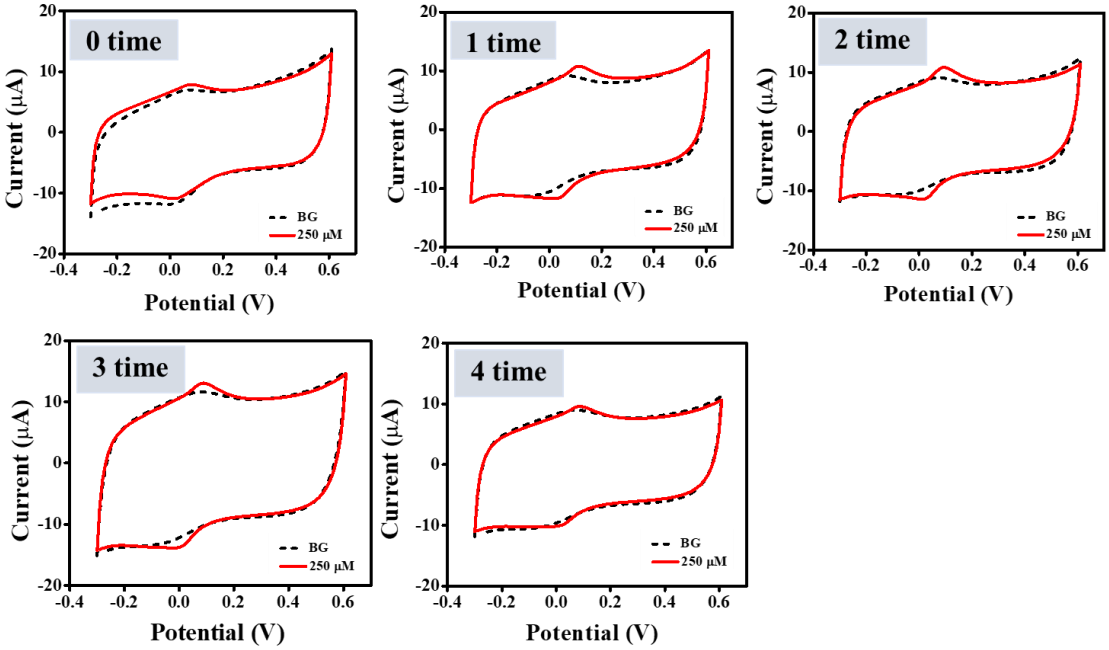

Figure A1. Optimization conditions affect the determination of NDPhA. Variation of electrode response for NDPhA (250 µM) with changing of mole of template molecule

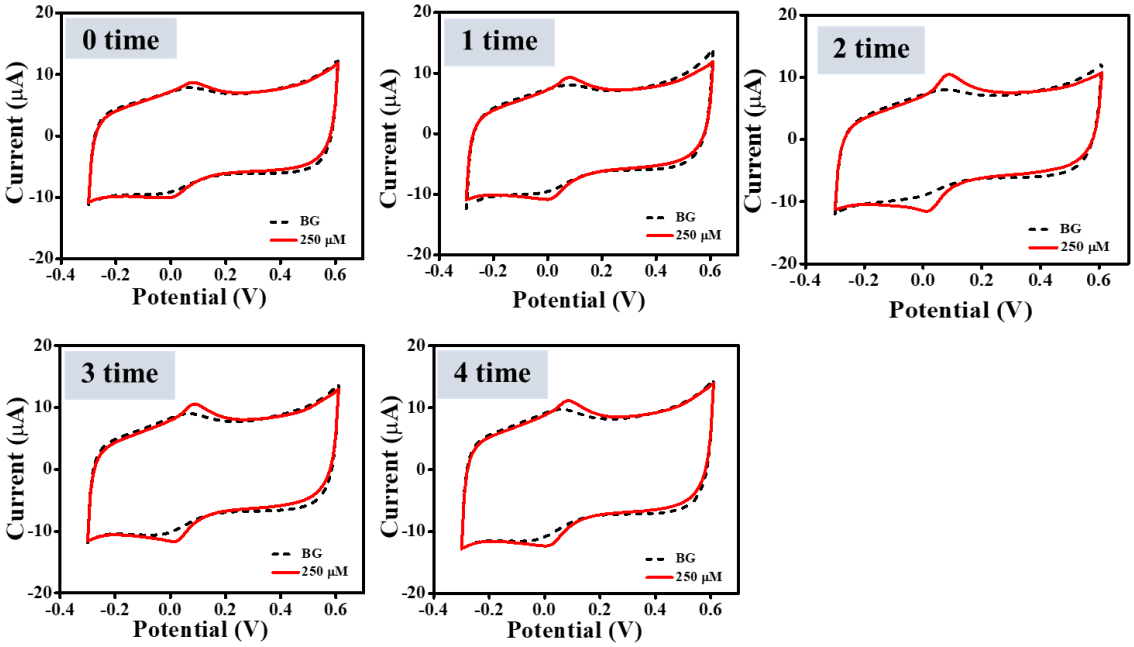

Figure A2. Optimization conditions affect the determination of NDPhA. Variation of electrode response for NDPhA (250 µM) with changing of mole of monomer

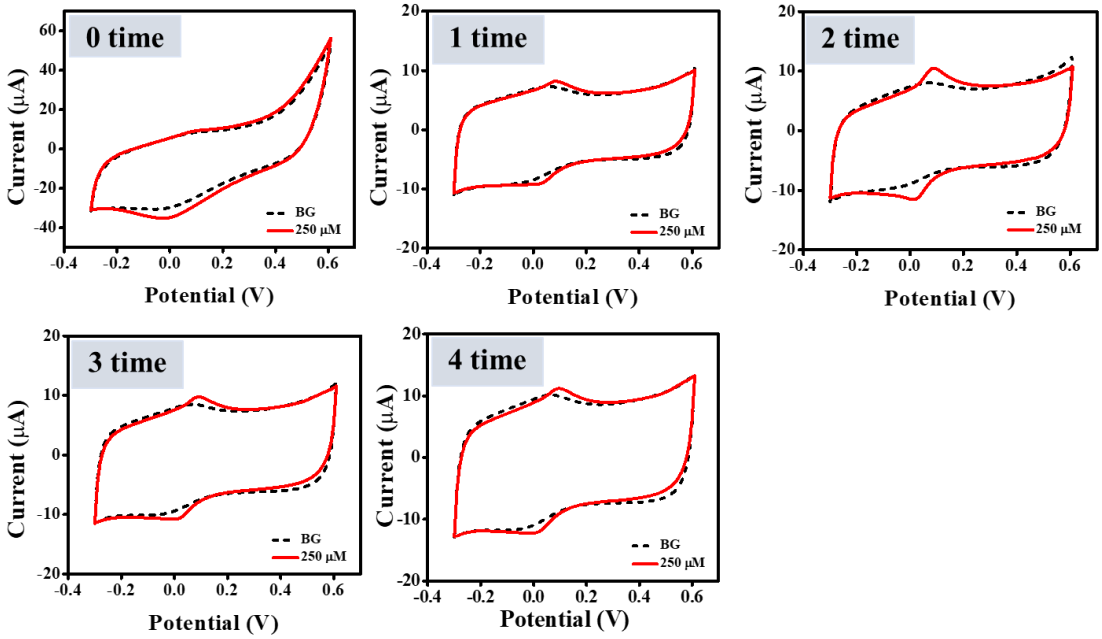

Figure A3. Optimization conditions affect the determination of NDPhA. Variation of electrode response for NDPhA (250 µM) with changing of mole of cross-linker

APPENDIX B

HPLC for NDPhA determination

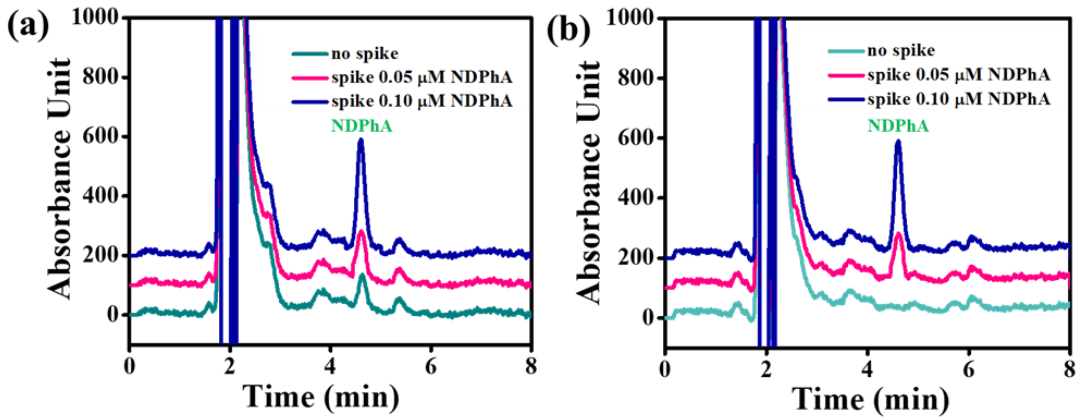

Figure B1. Examples of the HPLC chromatograms of (a) the synthetic sample (green line) and spiked synthetic samples (pink and blue lines, 0.05 and 0.10 µM) and (b) beer (green line) and spiked beer (pink and blue lines, 0.05 and 0.10 µM). The Separation under the following conditions: Inertsil ODS-3 (150 × 3.9 mm, 5 µm) separation column, isocratic elution with methanol: water (7.5 : 2.5 v/v) mobile phase, 1.0 mL min^{-1} flow rate, 20 µL injection volume. Absorbances were detected at 280 nm, and the column temperature was 25 ˚C

APPENDIX C
CONFERENCES

CONFERENCES

Poster presentations

1. **Kanpitcha Somnet**, Nongyao Nontawong, Suphatsorn Thimoonnee, Chanpen Karuwan and Maliwan Amatatongchai "Novel Paraquat Sensor Using Platinum Nanoparticles Coated with a Molecularly-Imprinted Polymer Modified Graphene-Screen Printed Electrode" Pure and Applied Chemistry International Conference (PACCON 2020), 13-14 February 2020, Bangkok, Thailand.

2. Pattawan Soravech, **Kanpitcha Somnet**, Suphatsorn Thimoonnee, and Maliwan Amatatongchai "Development of N-Nitrosamines electrochemical sensor using a glassy carbon electrode modified with single–walled carbon nanotubes with amide functionalized and graphene quantum dots-gold nanoparticle nanocomposites" UBU SCI-TECH SYMPOSIUM 2022: Science and Technology for Sustainable Technopreneurship, 18 March 2022, Ubon Ratchathani, Thailand.

3. Sutina Rattanapul, **Kanpitcha Somnet**, Nongyao Nontawong and Maliwan Amatatongchai "Development of a sensitive electrochemical sensor based on graphene quantum dots/gold nanoparticles modified graphite electrode for the determination of guanosine" UBU SCI-TECH SYMPOSIUM 2022: Science and Technology for Sustainable Technopreneurship, 18 March 2022, Ubon Ratchathani, Thailand.

Oral presentations

1. **Kanpitcha Somnet**, Maliwan Amatatongchai, Chanpen Karuwan, Wichayaporn Kamsong and Adisorn Tuantranont "Development of a selective paraquat sensor based on graphene screen printed electrode modified with platinum nanoparticles coated with molecularly imprinted polymer" YSTP & TGIST Project Progress Presentation by NSTDA Scholarships, 22 january 2020, Thailand Science Park Convention Center, National Science and Technology Development Agency (NSTDA), Pathum Thani, Thailand.

Publications

1. **Kanpitcha Somnet**, Suphatsorn Thimoonnee, Chanpen Karuwan, Wichayaporn Kamsong, Adisorn Tuantranont and Maliwan Amatatongchai "Ready-to-use paraquat sensor using a graphene-screen printed electrode modified with a molecularly imprinted polymer coating on a platinum core" Analyst, Volume: 146, 12 September 2021, Page 6270–6280.

2. **Kanpitcha Somnet**, Pattawan Soravech, Chanpen Karuwan, Adisom Tuantranont and Maliwan Amatatongchai "A compact N-nitrosodiphenylamine imprinted sensor based on a Pd nanoparticles-MIP microsphere modified screen-printed graphene electrode" Journal of Electroanalytical Chemistry, Volume: 914, 12 April 2022, page 116302.

Outstanding

1. Outstanding Poster Presentation Awards in Analytical Session in Pure and Applied Chemistry International Conference (PACCON 2020), 13-14 February 2020, Bangkok, Thailand, in title "Novel Paraquat Sensor Using Platinum Nanoparticles Coated with a Molecularly-Imprinted Polymer Modified Graphene-Screen Printed Electrode".

PACCON
Pure and Applied Chemistry International Conference
CHEMISTRY FOR CATALYZING SUSTAINABILITY AND PROSPERITY
FEBRUARY 13 - 14, 2020 || IMPACT FORUM, MUANG THONG THANI, NONTHABURI , THAILAND

Novel Paraquat Sensor Using Platinum Nanoparticles Coated with a Molecularly-Imprinted Polymer Modified Graphene-Screen Printed Electrode

Kanpitcha Somnet[1], Nongyao Nontawong[1], Suphatsorn Thimoonnee[1], Chanpen Karuwan[2] and Maliwan Amatatongchai [1]*

[1]Department of Chemistry and Center of Excellence for Innovation in Chemistry, Faculty of Science, Ubon Ratchathani University , Thailand.
[2]Graphene and Printed Electronics for Dual -Use Applications Research Division (GPERD), National Science and Technology Developmen t Agency (NSTDA), Thailand.

*E-mail: maliwan.a@ubu.ac.th or amaliwan@gmail.com

ABSTRACT

This work proposed the fabrication of a novel electrochemical sensor based on screen printed graphene paste electrode (SPGrE) modified with platinum nanoparticles coated with molecularly imprinted polymer (PtNPs@MIP) for sensitive and cost effective detection of paraquat (PQ) herbicide. The PtNPs@MIP was synthesized by successively coating the surface of PtNPs with SiO_2 and vinyl end groups. Then, the vinyl groups were terminated with molecularly imprinted polymer (MIP) shell. MIP was attached to the PtNPs cores using methacrylic acid (MAA) monomer, ethylene glycol dimethacrylate (EGDMA) as crosslinker and 2,2'-azobisisobutyronitrile (AIBN) as initiator. PtNPs@MIP was coated on the SPGrE surface for establishing the PQ sensor. Cyclic voltammetry (CV) was used to study the electrochemical mechanism of PQ on the MIP sensor. Quantitative analysis was performed by anodic stripping voltammetry (ASV). The MIP sensor provide linearity ranged from 0.05 to 1,000 µM and low detection limit of 0.02 µM. The imprinted sensor gave a highly sensitive and selective towards PQ. The as-prepared imprinted sensor can be alternative approach determination of paraquat residuals in vegetables and fruits for food safety.

EXPERIMENTAL

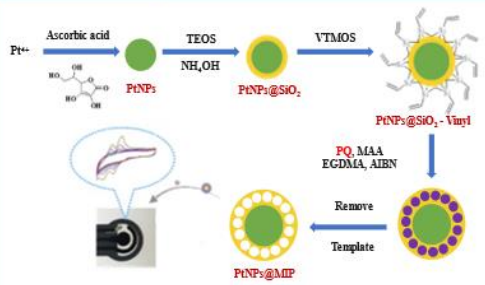

Scheme. 1. Preparation of the paraquat (PQ) sensor (PtNPs@MIP/SPGrE)

Electrochemical behavior of paraquat

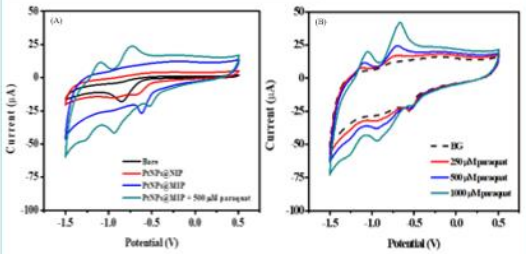

Fig. 2 (A) CV of different modified electrodes in the blank K_2SO_4 solution and PtNPs@MIP in 500 µM paraquat solution (green line) and (B) CV of PtNPs@MIP in 250, 500 and 1,000 µM paraquat containing 0.1 M K_2SO_4 solution.

RESULTS

Characterization

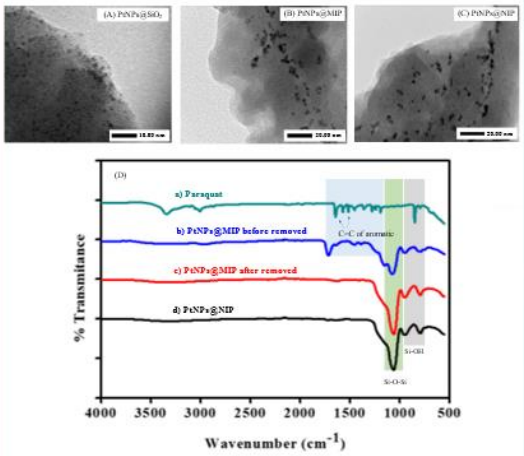

Fig. 1. TEM images of (A) PtNPs@SiO_2, (B) PtNPs after removal template, (C) PtNPs@NIP and (D) FT -IR spectra of a) paraquat, b) PtNPs@MIP before removal template, c) PtNPs@MIP after removal template and d) PtNPs@NIP

Analytical Characterization

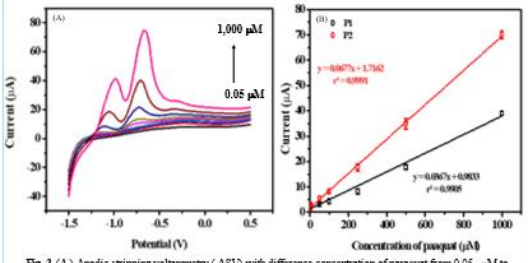

Fig. 3 (A) Anodic stripping voltammetry (ASV) with difference concentration of paraquat from 0.05 µM to 1,000 µM at PtNPs@MIP sensor and (B) Corresponding calibration curve of paraquat.

CONCLUSION

We designed a MIP sensor for sensitive and selectively detection of paraquat. TEM and FT -IR results confirm the formation of PtNPs@MIP via the synthesized composites. The developed sensor shows linearity ranged from 0.05 to 1,000 µM with the LOD of 0.02 µM. The MIP sensor provides an acceptable accuracy and precision for the detection of paraquat.

REFERENCES

[1] M. Amatatongchai, W. Sroysee, P. Sodkrathok, N. Kesangam, S. Chairum, P. Jarujamrus, Anal. Chim. Acta 1076 (2019) 64-72.
[2] X. Shan, J . de D. Habimana, J. Ji, J. Sun, F. Pi, Y. Zhang , X. Sun, J. of Solid State Electrochem 23 (2019) 1211–1220.

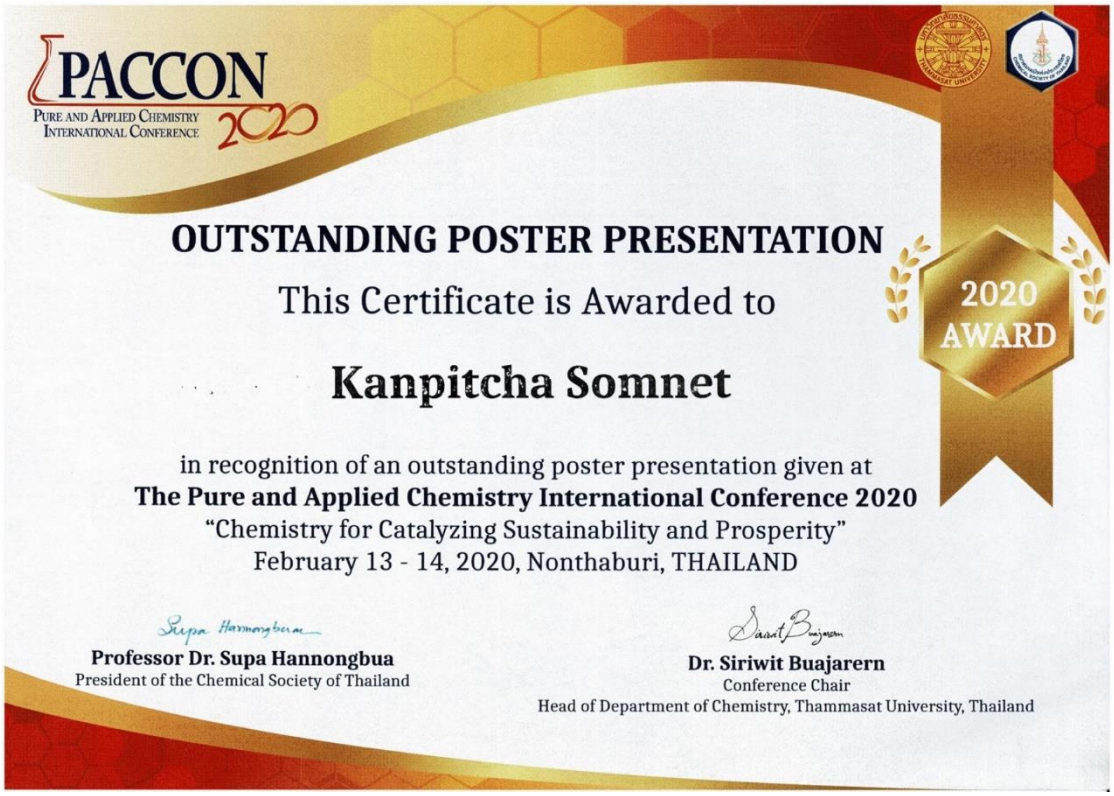

PACCON
PURE AND APPLIED CHEMISTRY INTERNATIONAL CONFERENCE 2020

OUTSTANDING POSTER PRESENTATION

This Certificate is Awarded to

2020 AWARD

Kanpitcha Somnet

in recognition of an outstanding poster presentation given at
The Pure and Applied Chemistry International Conference 2020
"Chemistry for Catalyzing Sustainability and Prosperity"
February 13 - 14, 2020, Nonthaburi, THAILAND

Professor Dr. Supa Hannongbua
President of the Chemical Society of Thailand

Dr. Siriwit Buajarern
Conference Chair
Head of Department of Chemistry, Thammasat University, Thailand

Analyst

ROYAL SOCIETY OF CHEMISTRY

PAPER

View Article Online
View Journal | View Issue

Cite this: *Analyst*, 2021, **146**, 6270

Ready-to-use paraquat sensor using a graphene-screen printed electrode modified with a molecularly imprinted polymer coating on a platinum core†

Kanpitcha Somnet,[a] Suphatsorn Thimoonnee,[a] Chanpen Karuwan,[b] Wichayaporn Kamsong,[b] Adisorn Tuantranont[b] and Maliwan Amatatongchai *[a]

Received 16th July 2021,
Accepted 12th September 2021

DOI: 10.1039/d1an01278a

rsc.li/analyst

We propose the fabrication of a novel ready-to-use electrochemical sensor based on a screen-printed graphene paste electrode (SPGrE) modified with platinum nanoparticles and coated with a molecularly imprinted polymer (PtNPs@MIP) for sensitive and cost-effective detection of paraquat (PQ) herbicide. Successive coating of the PtNPs surface with SiO_2 and vinyl end-groups formed the PtNPs@MIP. Next, we terminated the vinyl groups with a molecularly imprinted polymer (MIP) shell. MIP was attached to the PtNPs cores using PQ as the template, methacrylic acid (MAA) as the monomer, ethylene glycol dimethacrylate (EGDMA) as the cross-linker, and 2,2′-azobisisobutyronitrile (AIBN) as the initiator. Coating the SPGrE surface with PtNPs@MIP furnished the PQ sensor. We studied the electrochemical mechanism of PQ on the MIP sensor using cyclic voltammetry (CV) experiments. The PQ oxidation current signal appears at −1.08 V and −0.71 V *vs.* Ag/AgCl using 0.1 M potassium sulfate solution. Quantitative analysis was performed by anodic stripping voltammetry (ASV) using a deposition potential of −1.4 V for 60 s and linear sweep voltammetric stripping. The MIP sensor provides linearity from 0.05 to 1000 μM (r^2 = 0.999), with a lower detection limit of 0.02 μM (at −0.71 V). The compact imprinted sensor gave a highly sensitive and selective signal toward PQ. The ready-to-use MIP sensor can provide an alternative approach to the determination of paraquat residue on vegetables and fruits for food safety applications.

1. Introduction

Paraquat (PQ), 1,1′-dimethyl-4,4′-bipyridinium, is a widely used herbicide used to destroy or control weeds in several countries throughout south-east ASIA, including Thailand.[1,2] It is a quick-action, non-selective herbicide that is undesirably persistent in the environment. It poses a great risk to an ecosystem's health due to its high-water solubility (*ca.* 620 g L^{-1} at 25 °C).[3] Additionally, PQ is hazardous to human health, with an LD_{50} of 35 mg kg^{-1}.[4] The US Environmental Protection Agency (EPA) classifies PQ as a hazardous chemical and establishes a maximum contaminant level of 3 μg L^{-1} for PQ in drinking water.[5,6] Therefore, its detection is necessary for drinking water and farm-produced products. Quantitative analysis of PQ generally uses spectrophotometry,[5,6] and chromatographic methods include gas chromatography/mass spectrometry,[7,8] or high-performance liquid chromatography coupled with a UV detector,[9–11] mass spectrometry,[12] immunoassay,[13,14] fluorescent probe titration,[15] surface-enhanced Raman spectroscopy,[16] flow injection colorimetric assay,[17] and capillary electrophoresis.[18,19] Although these techniques provide high selectivity and sensitivity and are suitable for PQ analysis, the methods are somewhat time-consuming. They require expert operators,[7,8,12] requiring sophisticated instrumentation,[7–12] and miniaturization limitations. Therefore, developing a practical approach to detect PQ is critical. The challenges of the development are mainly in two aspects. The first is the selectivity and sensitivity of the analysis for practically used in real samples and the second is the miniaturization of the analysis for on-site analysis. Electrochemical sensors are a promising method for portable, sensitive, selective, and rapid PQ determination.[2,20–22]

MIPs have become outstanding selective elements, comparable to biological/natural receptors, such as DNA, antibodies, and enzymes. While these biological products offer satisfactory

[a]*Department of Chemistry and Center of Excellence for Innovation in Chemistry, Faculty of Science, Ubon Ratchathani University, Ubon Ratchathani 34190, Thailand. E-mail: maliwan.a@ubu.ac.th*
[b]*Graphene sensor laboratory (GPL), Graphene and Printed Electronics for Dual-Use Applications Research Division (GPERD), National Science and Technology Development Agency (NSTDA), Pathum Thani 12120, Thailand*

†Electronic supplementary information (ESI) available. See DOI: 10.1039/d1an01278a

to excellent affinity and selectivity to their target analyte, they are often affected by poor durability and repeatability at high temperature, pressure, in organic solvents, low stability in low or high pH solutions, and high production cost. Therefore, synthetic receptors (also called plastic antibodies) have recently been increasingly studied to overcome these drawbacks.[23,24] MIPs offer high analyte selectivity and are ideal for creating specific or recognition sites that are chemically and sterically complementary to a target molecule. MIP-based sensors offer a promising electroanalytic approach because they are cost-effective and straightforward to synthesize. They provide high selectivity to the target analyte and have excellent mechanical strength and long-term stability. To date, MIPs dependent on the application come in different shapes, such as monoliths, thin film, or nanoparticles. Nanoscale MIPs have been reported to overcome the drawbacks from bulk imprinting include recognition site heterogeneity, template leakage, mass transfer limitation, and solubilities.[23,24] Creating a three-dimensional MIP imprinting site on the nanocomposite produces a larger surface/mass ratio, more easily accessible recognition sites and, lower heterogeneities and better solubilities. Moreover, good electrical properties and excellent conductivity of nanomaterials combined with the comparable selectivity of MIPs will endow the sensor with powerful performance for the target analytes.

Additionally, core–shell surface molecular imprinting technology improves target molecule recognition, reduces non-specific adsorption, increases the relative adsorption capacity and selectivity, and accelerates the electrodes' mass transfer rate. This approach works in MIP sensors based on parathion-methyl imprinting on magnetite-gold (Fe_3O_4@Au) core,[25] carbofuran imprinting on Fe_3O_4@Au,[26,27] and for reduced graphene oxide-gold (rGO@Au)[28] cores. MIP provides greatly improved specificity of molecular recognition for the determination of PQ.[29] The paraquat-MIP constructed on a glassy carbon electrode, modified with gold nanocross–chitosan composites, was selective, stable, and sensitive for indirect measurements because of the hindered electron transfer of the $[Fe(CN)_6]^{-3/-4}$ ion pair onto the electrode surface. However, it remains necessary to improve sensitivity and selectivity, and provide a ready-to-use sensor for on-site monitoring.

Herein, we report a novel and ready-to-use sensor based on a screen-printed graphene-paste electrode, modified with platinum nanoparticles coated with a molecularly imprinted polymer (PtNPs@MIP/SPGrE), for sensitive and selective detection of PQ herbicide. This is the first time that PQ imprinted polymer is synthesized on the surface of PtNPs. Our novel PtNPs@MIP is cost-effective with straightforward synthesis, and offers excellent mechanic stability. The PtNPs@MIP was easily loaded on the electrode surface by drop casting and the compact PQ sensors could be convenient for mass production in a short time at much lower cost. We used the PtNPs@MIP nanocomposite to modify an SPGrE to create the new, highly sensitive, selective, compact, cost-effective and ready-to-use PQ sensor. PtNPs cores provided attachment sites for MIPs, and the resulting PtNPs@MIP materials exhibited enhanced electrocatalytic performance. MIP coated PtNP cores improve sensitivity, selectivity, and electron transfer of the fabricated graphene-based electrode. Adding PtNPs@MIP to the sensor substantially increases electrical conductivity, improves the electrode's electrocatalytic properties, and enhances electrode selectivity toward PQ detection. We prepared PtNPs@MIP by successively coating the surface of PtNPs with tetraethoxysilane (TEOS) to afford nano-porous silica-coated PtNPs. The addition of vinyl trimethoxy silane (VTMOS) forms polymerizable vinyl end-groups before finally attaching the MIP shell to the PtNPs-vinyl core surface. We first developed a compact MIP-sensor based on platinum nanoparticles coated with a MIP for PQ's quantitative determination using an SPGrE. The portable ready-to-use MIP sensor was controlled using a commercial mini-potentiostat and a tablet. The sensitive and selective detection of PQ made on-site analysis both convenient and environmentally friendly.

2. Experimental

2.1 Chemicals and reagents

All chemicals were analytical grade. We used deionized-distilled water (water Pro-Ps, USA) for standard and reagent preparation. Hydrogen hexachloroplatinate(IV) ($H_2PtCl_6{\cdot}xH_2O$, Pt >40%), hexadecyl trimethyl ammonium bromide (CTAB) were purchased from Acros Organics (Geel, Belgium). Tetraethoxysilane (TEOS) and ammonia (25%) were obtained from Acros Organics (New Jersey, USA). Ascorbic acid ($C_6H_8O_6$), potassium iodide (KI), methacrylic acid (MAA), ethylene glycol dimethacrylate (EGDMA), 2,2′-azobisisobutyronitrile (AIBN), vinyl trimethoxy silane (VTMOS), paraquat (PQ), and a certified reference material of PQ in drinking water (CRM-QC 1435) were purchased from Sigma-Aldrich (St Louis, USA). We prepared a stock standard solution of PQ (5 mM) in DI water.

2.2 Apparatus

2.2.1 Fabrication of screen-printed graphene electrode (SPGrE). We fabricated the SPGrE using procedures described by Karuwan *et al.*[30] and Pasakon *et al.*[31] Graphene was selected as an electrode material because of its large surface area (2630 $m^2\ g^{-1}$), and excellent electrical conductivity (7200 S m^{-1}) compared to other carbon-based materials, such as carbon nanotubes (CNTs) and graphite.[30,31] Disposable electrochemical analytical devices were prepared using a MK-MINI screen printer (Minami, Japan). Commercial graphene ink (Serve Science Ltd, Thailand) was screen printed onto clear polyvinyl chloride (PVC) (Navanakornplastic Co. Ltd, Pathum Thani, Thailand) sheets through a silk-screen printing mesh (mesh size 120 μm) for two cycles. A reference area was screen-printed with Ag/AgCl ink (Gwent Electronic Materials Ltd, Pontypool, UK) on the PVC sheet for two cycles. Finally, we printed a detection area with insulating ink on the PVC sheet for two cycles and then baked the PVC sheet at 60 °C for 1 h to remove any solvent.

2.2.2 Electrochemical measurements. Electrochemical measurements were performed in batches using an EmStat3

potentiostat (5.0 × 6.7 × 2.8 cm) (PalmSens BV, The Netherlands) using "PSTrace for windows" equipped with multi-trace software. The active surface area for the SPGrE (4 mm diameter) was approximately 0.126 cm^2. The conventional three-electrode cell assembly consisted of a working electrode (PtNPs@MIP/SPGrE), a reference electrode (Ag/AgCl), and a counter electrode (SPGrE). Cyclic voltammograms (CV) were recorded at a scan rate of 50 mV s^{-1} and over a potential range between −1.5 and +0.5 V, using 0.1 M potassium sulfate-supporting electrolyte solution. Quantitative analysis was performed by anodic stripping voltammetry (ASV). The sample or standard solution was dropped into the detection zone. Then, a deposition potential of −1.4 V was applied for 60 s. The linear sweep was recorded from −1.5 to 0.5 V with the scan rate of 50 mV s^{-1}.

2.2.3 Characterization. The nanocomposite structure and composition were investigated by ATR FT-IR, recorded with a spectrum II spectrometer (PerkinElmer, USA), over a wavenumber range of 4000–500 cm^{-1}. Morphology and sizes of PtNPs@MIP nanocomposites were investigated using TEM (JEM-1230; JEOL, Japan) and SEM (JEOL, JSM-6460LV, Japan) equipment, operated under vacuum at an accelerating voltage of 20 kV.

2.3 Preparation of the paraquat sensor (PtNPs@MIP/SPGrE)

Fig. 1A shows a schematic of the synthesized PtNPs@MIP. At first, coating SiO_2 on the surface of PtNPs using a sol–gel technique provides PtNPs@SiO_2. Next, vinyl groups are added to the PtNPs@SiO_2 surface to create PtNPs@SiO_2-vinyl before terminating the vinyl groups with an MIP shell. Overall, we attached MIP to the PtNPs cores using PQ as the template molecule, MAA as a monomer, EGDMA as a cross-linker, and AIBN as an initiator. Removal of the PQ template with DI water provided PtNPs@MIP.

(i) Preparation of PtNPs@SiO_2-vinyl

Platinum nanoparticles (PtNPs) were selected as cores to create recognition sites in order to enhanced high specific surface area, superb high mass transport, and good biocompatibility. We used a recent report describing the synthesis of platinum nanoparticles (PtNPs).[32] Firstly, a Pt seed solution was prepared by mixing H_2PtCl_6 (1 mL, 10 mM) with hexadecyl trimethyl ammonium bromide (CTAB) solution (20 mL, 12.5 mM). The stirred mixture was heated at 95 °C for 5 min before ascorbic acid (160 μL, 100 mM) was added to the solution. Stirring continued for 20 min before the solution was cooled to room temperature and stored in darkness at 4 °C.

PtNPs were synthesized by adding a Pt seed solution (80 μL) and H_2PtCl_6 (125 μL, 10 mM) to CTAB solution (5 mL, 100 mM), containing KI (5 μL, 1 mM), and freshly prepared ascorbic acid (50 μL, 100 mM) was next added. The mixture was stored at 50 °C for 8 h before centrifuging the resulting solution at 9000 rpm for 5 min to remove any residual solution. Drying at 50 °C for two hours provided the PtNPs.

We prepared the PtNPs@SiO_2 nanocomposites by a method described in our previous work[33] with some modifications. In brief, PtNPs (40 mg) were dispersed into ethanol (30 mL) in an ultrasonic bath for 30 min. Then, NH_3 (2 mL) was added dropwise to the solution under vigorous mechanical stirring, and 800 μL of TEOS was dropped into the solution. Stirring continued for 3 h at room temperature. After that, the resulting solution containing PtNPs@SiO_2 nanocomposites was centrifuged, washed with water, and dried in an oven at 50 °C for 2 h.

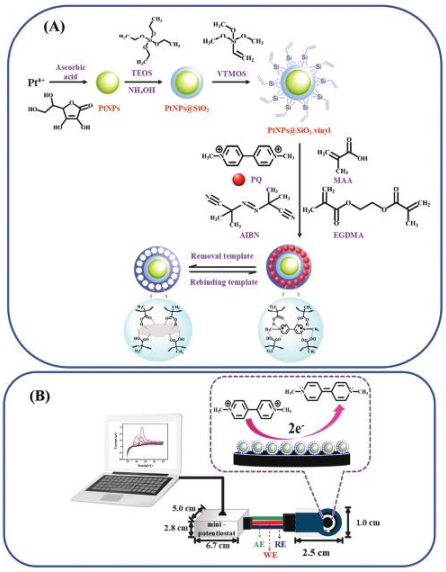

Fig. 1 (A) Preparation of PtNPs@MIP and the fabrication of the MIP sensor (PtNPs@MIP/SPGrE) for paraquat (PQ). (B) The layout of the designed ready-to-use PQ sensor, the set up and the detection mechanism of the electrochemical determination of PQ. Electrochemical measurements were performed using a mini-potentiostat and a conventional three-electrode cell assembly consisted of a working electrode (PtNPs@MIP/SPGrE) (4 mm diameter), a reference electrode (Ag/AgCl), and a counter electrode (SPGrE).

We functionalized PtNPs@SiO_2 nanocomposite surfaces with vinyl end-groups. Firstly, 40 mg of PtNPs@SiO_2 were dispersed into 30 mL of ethanol in an ultrasonic bath for 30 min. Next, 2 mL of NH_3 was added dropwise to the solution under vigorous mechanical stirring. VTMOS (1000 μL) was dropped into the solution, and the stirring continued for 8 h at room temperature. After centrifuging and washing with water and methanol, the nanocomposites were soaked in 1 M HCl for 12 h to eliminate any residual materials that remained uncoated with silica. Finally, the PtNPs@SiO_2-vinyl nanocomposites were centrifuged, washed with water, and dried in an oven at 50 °C for 2 h.

(ii) Preparation of PtNPs@MIP

We prepared PtNPs@MIP nanocomposites by a three-dimensional imprinted protocol applied for CNTs, as

described in our previous work,[33] with appropriate modifications. Briefly, 40 mg of PtNPs@SiO_2-vinyl nanocomposites were dispersed into 25 mL of chloroform in a 50 round-bottomed flask in an ultrasonic bath for 30 min. Next, after combining 0.26 mmol of PQ template and 1.20 mmol of MAA functional monomer, the mixture was sonicated for 10 min and then allowed to react for 6 h at room temperature. EGDMA (1.20 mmol) cross-linker and 0.02 mmol of AIBN initiator were refluxed under nitrogen for 24 h. Centrifuging and washing with ethanol eliminated excess reagent, then stored in a desiccator for 24 h. Finally, the PQ template was removed by sonicating for 1 h in water, centrifuged, and the resulting PtNPs@MIP were stored in a desiccator.

(iii) Preparation of PtNPs@MIP/SPGrE

We prepared the PtNPs@MIP/SPGrE by dispersing 6 mg of PtNPs@MIP into 1000 μL of dimethylformamide in an ultrasonic bath for 1 h. Then, drop-cast the PtNPs@MIP (2.5 μL) on the surface of the SPGrE and left overnight to allow the solvent to evaporate at ambient temperatures.

Fig. 1B shows the layout of the designed ready-to-use PQ sensor (1.0 × 2.5 cm), the set up and the detection mechanism of the electrochemical determination of PQ. Electrochemical measurements were performed using a mini-potentiostat (5.0 × 6.7 × 2.8 cm) and a conventional three-electrode cell assembly consisted of a working electrode (PtNPs@MIP/SPGrE) (4 mm diameter), a reference electrode (Ag/AgCl), and a counter electrode (SPGrE).

2.4 Sample preparation

We purchased seven vegetables (yardlong bean, cabbage, lettuce, cucumber, kale, onion and tomato) from a local market in Ubon Ratchathani Province, Thailand, as samples for PQ analysis using a spiked recovery experiment. Sample extractions were prepared by a method adapted from previous reports.[34] We cut fresh vegetables into small pieces. Samples (20 g) and water (50 mL) were homogenized in a blender for 3 min and then sonicated for 1 h. Filtering the homogenized samples was carried out using Whatman no. 1 Filter paper. For recovery experiments, 20 g of sample was immersed in 50 mL of PQ standard (5 or 10 μM) for 30 min. After the immersion, the vegetable samples were homogenized, sonicated and finally extracted as the same procedure.

3. Results and discussion

3.1 Characterization

We used a transmission electron microscope (TEM) to investigate the surface morphology of PtNPs@MIP. Fig. 2 shows TEM images of (A) PtNPs and (C) PtNPs@MIP. PtNPs were prepared by reducing Pt^{4+} to Pt^0 with ascorbic acid and potassium iodide in the presence of CTAB as a stabilizing agent.[32] The average diameter of the as-prepared PtNPs was 2.20 ± 0.35 nm (count = 20). The TEM image in Fig. 2C shows the thickness of PtNPs@MIP as approximately 4.14 ± 0.46 nm, indicating the formation of an MIP coated PtNPs core. The EDS result of

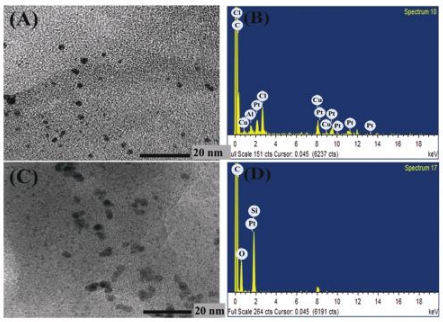

Fig. 2 TEM images of (A) PtNPs, and (C) PtNPs@MIP, and EDS of (B) PtNPs, (D) PtNPs@MIP.

PtNPs in Fig. 2B reveals Pt elemental signals, which indicated the formation of PtNPs. While the EDS spectrum in Fig. 2D appears C, O, Si, and Pt chemical signals confirm the formation of PtNPs@MIP composite.

ATR FT-IR spectroscopy confirmed the formation of an MIP coating on the PtNPs core surface. Fig. S1A† shows the FTIR spectra of PQ (curve a) and MIP films, before (curve b) and after (curve c), template removal, and NIP film (curve d). There are significant differences between MIP films before and after template removal. Before template removal, MIP film (curve b) produced peaks at 1645, 1467, and 1444 cm^{-1}, which we assigned to stretching modes of C=N in the pyridine ring, and C=C in the PQ molecule. After template removal, the MIP (curve c) and NIP film (curve d) exhibit absorption bands at 1640, 1092, and 787 cm^{-1}, which we attributed to C=O, Si–O–Si, and Si–OH vibrations, respectively. These findings indicate the successful silane coating on PtNPs and the subsequent polymerization of MIP. The absence of any PQ absorption bands in curve c (MIP film after template removal) indicates successful removal of the PQ template.[35–37]

Electrochemical characteristics of the PtNPs@MIP/SPGrE and bare SPGrE were compared in Fig. S1B† in order to clarify the electrocatalytic and electron transfer's improvement of the synthesized PtNPs@MIP. We observed that well-defined redox peaks from $[Fe(CN)_6]^{3-/4-}$ appeared at both bare SPGrE and PtNPs@MIP/SPGrE (Fig. S1B†). Interestingly, PtNPs@MIP/SPGrE shows the greatest peak current and the smallest anodic-to-cathodic peak separation (ΔE_p). These results indicated that the enhanced electrochemical signal obtained from PtNPs@MIP/SPGrE occurred because the PtNPs@MIP increased the electron transfer between the electrode surface and electrochemical probes.

Fig. S2† displays the impedance spectra of bare SPGrE (inset), PtNPs/SPGrE, PtNPs-SiO_2/SPGrE, PtNPs@MIP/SPGrE and PtNPs@NIP/SPGrE. The Randle's equivalent circuit model was used to fit the experimental data. The lowest semicircular diameter was obtained from the PtNPs/SPGrE, (R_{ct} = 118 Ω)

(Fig. S2†), which indicates the fastest electron-transfer kinetics of $[Fe(CN)_6]^{3-/4-}$, compared to PtNPs-SiO_2/SPGrE (R_{ct} = 135 Ω), PtNPs@MIP/SPGrE (R_{ct} = 526 Ω), PtNPs@NIP/SPGrE (R_{ct} = 929 Ω), and bare SPGrE (R_{ct} = 1400 Ω). The impedances of PtNPs/SPGrE was significantly lower than bare SPGrE indicating the excellent conductivity enhancement of PtNPs. PtNPs@MIP/SPGrE and PtNPs@NIP/SPGrE were significantly higher than PtNPs/SPGrE, indicating the presence of poly-MAA films produced during polymerization. Moreover, the impedance of the MIP modified electrode was smaller than that of the NIP electrode, possibly because the large numbers of imprinted cavities in the MIP film allows for better diffusion of the $[Fe(CN)_6]^{3-/4-}$ redox probe, and so enhances electron transfer.

3.2 Electrochemical behaviors of PQ on the PtNPs@MIP/SPGrE

We used cyclic voltammetry (CV) to investigate the PQ recognition ability at bare SPGrE, PtNPs/SPGrE, PtNPs-SiO_2/SPGrE, PtNPs@NIP/SPGrE, and PtNPs@MIP/SPGrE (Fig. 3A). PtNPs/SPGrE exhibits higher oxidation current than bare SPGrE due to the excellent properties of PtNPs such as extraordinary catalytic, conductivity, biocompatibility, and electrochemical properties. After coating PtNP with SiO_2 (PtNPs SiO_2/SPGrE), the oxidation current slightly increased. This result indicated that coating of PtNPs with SiO_2 can accelerate the oxidation process. Interestingly, the current obtained from PtNPs@MIP/SPGrE was greater than that obtained from either PtNPs@NIP/SPGrE or bare SPGrE, indicating that the PtNPs@MIP nanocomposite exhibits a very high affinity for PQ. On the other hand, PtNPs@NIP has no significant PQ affinity and cannot adsorb PQ on the electrode surface to enhance the electrochemical signal. We assume that the ability of PtNPs@MIP to enhance the PQ signal, compared to the bare electrode and PtNPs@NIP, is because of selective cavities formed in the polymer structure. The created specific recognition cavities on the PtNPs@MIP enhance electrode properties in terms of sensitivity and selectivity:

1. PtNPs@MIP modified electrode enhances the current response by a factor of approximately 4.0 over that of the unmodified electrode. The oxidation current arises as PQ molecules diffuse from the solution *via* biding sites on the PtNPs@MIP to the electrode surface. The great affinity of PtNPs@MIP for PQ electrostatic interactions may originate the hydrogen bonds between specific recognition cavities and then produces the stronger signal than unmodified electrode. Hence, the greater electrochemical response seen for the PtNPs@MIP/SPGrE has two causes: (i) the PtNPs@MIP coating on SPGrE enhances electrical conductivity and electrocatalytic activity toward PQ redox activity and (ii) PtNPs@MIP provides molecular recognition sites, and so has a greater affinity toward PQ.

2. The selectivity will be enhanced because imprinted cavities are complementary in size, conformation and shape to PQ molecules. Other substances with different structures from the PQ target analyte cannot bind strongly to the polymer recognition sites and thus produce very weak responses. Therefore, PtNPs@MIP provides high selectivity for the determination of PQ.

We investigated the electrochemical behavior of PQ at the PtNPs@MIP/SPGrE. Fig. 3B clearly shows the two well-defined PQ redox couples. The PtNPs@MIP/SPGrE produces oxidation peaks at approximately −1.08 V (P1) and −0.71 V (P2) and reduction peaks at −0.85 V (P3) and −1.25 V (P4). The peak current increases with PQ concentration, and the response mechanism involves PQ molecules that complement the imprinted cavities, diffusing to the electrode. From these results, we conclude that the PtNPs@MIP/SPGrE is suitable for the quantification of PQ.

To investigate the number of electrons involved in the oxidation of PQ on PtNPs@MIP/SPGrE, we recorded the CV curves of 500 μM PQ at scan rates ranging from 50 to 300 mV s^{-1} (Fig. S3A†). Anodic and cathodic peak currents (μA) increase linearly with the scan rate's square root ($V^{1/2}$ $s^{-1/2}$). Linear regression analysis (Fig. S3B†) provides an r^2 value of 0.991 (P1) and 0.997 (P2) for oxidation, and 0.995 (P3) and

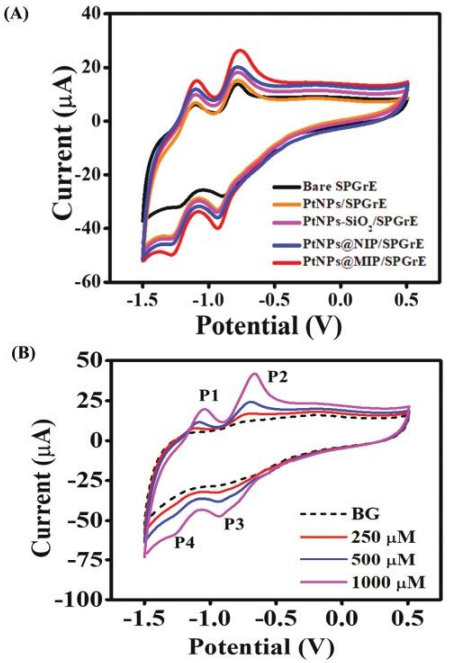

Fig. 3 Cyclic voltammograms of (A) 500 μM paraquat (PQ) on a bare SPGrE, PtNPs/SPGrE, PtNPs-SiO_2/SPGrE, PtNPs@NIP/SPGrE and PtNPs@MIP/SPGrE in 0.1 M K_2SO_4 supporting solution and (B) cyclic voltammograms of 250, 500, and 1000 μM PQ on PtNPs@MIP/SPGrE in 0.1 M K_2SO_4 supporting solution.

0.981 (P4) for reduction reactions, indicating a diffusion-controlled quasi-reversible electrochemical process. The relationship between the peak potential $E_{p,a}$ and ν is defined by Laviron as eqn (1).[38–40]

$$E_{p,a} = E^{\circ\prime} + \frac{RT}{(1-\alpha)nF}\ln \nu \quad (1)$$

Here, α is the transfer coefficient, n the number of electrons transferred, ν the scan rate, and $E^{\circ\prime}$ is the formal redox potential obtained from the intercept. The value of (α) can be easily calculated from the following equation.[39]

$$\frac{1.15RT}{\alpha F} = 2.303 \times \text{slope} \quad (2)$$

Taking T = 298 K, R = 8.314 J K^{-1} mol^{-1}, and F = 96 480 C mol^{-1}, and slope is obtained from Fig. S3C.† Therefore, the transfer coefficient (α) was calculated to be 0.33 and 0.22 for P1 and P2, respectively. The value of electron transfer number (n) calculated to be 0.98 and 0.57 (approximately equal to 1) for P1 and P2, respectively. These results indicate that the electrochemical oxidation reactions of PQ on PtNPs@MIP/SPGrE is one-electron transfer process. The reaction mechanism may be two successive one-electron transfers (eqn (3) and (4)).[41,42]

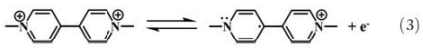
(3)

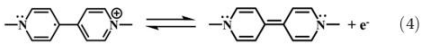
(4)

The Randles-Sevcik' equation (eqn (5)) was used to estimate the diffusion coefficient of the PtNPs@MIP/SPGrE.

$$I_{p,a} = 268600n^{3/2}AD^{1/2}C^{1/2} \quad (5)$$

Taking the peak current ($I_{p,a}$) = 10.31 × 10^{-6} A, the electron transfer number (n) of PQ = 1, the electroactive surface area of the sensor (A) = 0.126 cm^2, concentration (C) of PQ = 5 × 10^{-7} mol cm^{-3}, and scan rate (ν) = 0.05 V s^{-1}. The diffusion coefficient was calculated to be 7.424 × 10^{-6} cm^2 s^{-1}.

3.3 Optimization of the parameters

3.3.1 Effects of PtNPs@MIP loading. The loading of PtNPs@MIP on the graphene-screen printed electrode's surface is important for the characteristics of the modified SPGrE. We use linear sweep voltammetry to study the effect of PtNPs@MIP loading. In this work, LSV was used to evaluate concentrations of PtNPs@MIP in the range of 2–8 mg L^{-1}, with 500 μM PQ in 0.1 M K_2SO_2 solution (Fig. S4A†). Fig. S4B† shows the current responses from P1 and P2 oxidation reactions. Increasing the concentration of PtNPs@MIP from 2 to 6 mg L^{-1} increases the SPGrE response because of the increase in recognition sites on the electrode surface. However, raising the PtNPs@MIP concentration beyond a threshold level of 6 mg L^{-1} leads to decreased sensor response, probably due to reduced electrode surface conductivity. The optimal loading of PtNPs@MIP on SPGrE was therefore chosen as 6 mg L^{-1}.

3.3.2 ASV on the PtNPs@MIP/SPGrE. We applied ASV to determine PQ to improve the sensitivity of the method. The deposition potential and duration time used during the accumulation step are important parameters in stripping voltammetry. Fig. S5† illustrates the influence of deposition potential and deposition time on PQ's anodic stripping peak currents at PtNPs@MIP/SPGrE. As shown in Fig. S5A,† the PQ stripping peak increases rapidly as the deposition potential becomes more negative (from −0.8 to −1.4 V). However, the peak current levels off as the deposition potential approaches −1.4 V and drops at more negative values. Therefore, we chose an optimum deposition potential of −1.4 V.

For the deposition time, we investigated the dependence of peak currents over the range of 20–140 s on the PtNPs@MIP/SPGrE. PQ peak currents increased almost linearly with the deposition time (Fig. S5B†). However, to balance the sensitivity and analysis time, we selected a deposition time of 60 s as optimal for all analyses.

3.4 PtNPs@MIP/SPGrE analytical characteristics

Herein, MAA is selected as monomer due to its larger numbers of functional carboxylic groups, which makes it feasible to fine-tune interaction sites to optimally interact with PQ, *e.g.* by forming hydrogen bonds. The content of EGDMA cross-linker is also important in controlling the morphology of the polymer matrix and in stabilizing the imprinted binding site. Our preliminary results point out that MAA : EGDMA mole ratio of 1 : 1 is the optimum recipe to fabricate the PtNPs@MIP. For real sample application, vegetables were extracted with water (pH ~ 7), while the supporting electrolyte (K_2SO_4 solution, pH ~ 6). At the pH about 6 to 7, PQ exists in its cationic form (PQ^{2+}), whereas MAA (pK_a 4.66) in the MIP can be in the deprotonated form of the carboxylic group. Therefore, high affinity between the target analyte and the recognition sites resulted from the strong electrostatic interaction between PQ^{2+} and negatively charged of MIP.

Under optimum ASV conditions (deposition at −1.4 V for 60 s), the PQ stripping peak current occurs in the range of −1.5 V to +0.5 V at 50 mV s^{-1}. The proposed method provides well-defined peak profiles with PQ concentration dependency (Fig. 4A). Furthermore, we obtained a linear calibration curve over the range of 0.05–1000 μM. The linear regression equation for P1 is 0.036 ± 0.001x + 1.253 ± 0.031, with a determination coefficient (r^2) of 0.991 while the equation for P2 is 0.067 ± 0.001x + 2.061 ± 0.050, with a determination coefficient (r^2) of 0.999. The limit of detection (LOD) calculated from three times the standard deviation of the blank ($3S_b$, n = 7) according to ISO11843[43] is 0.02 μM. The limit of quantification (LOQ) is 0.05 μM, obtained from the lowest concentration in the calibration curve. We compared the analytical performance of the PtNPs@MIP/SPGrE to related modified electrodes for the determination of PQ (Table 1). Our proposed MIP sensor exhibits the widest linear range for PQ determination (0.05–1000 μM) among all related methods. Furthermore, the LOD for our sensor (0.02 μM) is comparable to the LOD for the sensor using mesoporous silica films (MSF)[1] or multiwalled

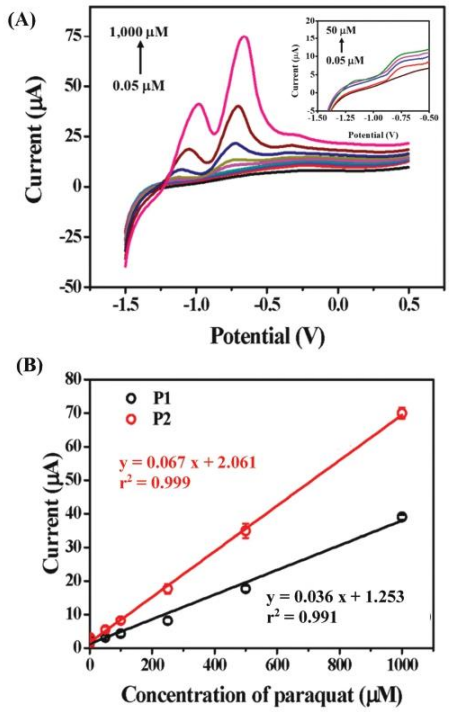

Fig. 4 (A) Anodic stripping voltammograms of PQ with difference concentration from 0.05 µM to 1000 µM on PtNPs@MIP/SPGrE and the inset show ASV of PQ at the lower concentrations. (B) Corresponding calibration curve of paraquat.

carbon nanotubes immobilized with a dihexadecyl hydrogenphosphate (MWCNTs-DHP),[20] or phospholipid[44] modified on glassy carbon electrodes, and graphene–zinc oxide nanocomposite (Gr–ZnO) modified on commercial screen-printed electrode,[4] and bismuth film modified on Cu plate electrode.[22] The LOD of our sensor is less than that of polypyrrole-grafted nitrogen-doped graphene (PPy-NGE) modified glassy carbon electrode,[21] CDtrodes (Au electrode prepared from recordable CD),[45] phthalocyanine modified pyrolitic graphite electrode,[46] and Nafion – a modified screen-printed graphene electrode (Nf/SPGrE) fabricated on a paper-based electrochemical device (ePAD).[47] All comparison electrodes presented (Table 1) have their own advantages/disadvantages in terms of synthesis and fabrication. CDtrode[45] fabricated by cutting and extracting polymeric film to exposure gold layer followed by constructing the electrical contact. Therefore, this method has a high potential to be disposable and portable device. On the other hand, commercial 3 mm-diameter BDD electrode[2] provided the LOD as low as 0.0015 µM. Although, the electrode[2] is easy to use but its application limited by the cost of electrode and non-flexible for modification as well as the fabrication as disposable electrode. In addition, most of the previously reports[1,2,44–46] were applied for samples containing low matrices *i.e.*, natural water[2,45,46] and river waters[1,44] and did not studied the tolerance for interferences of similar substances or other pesticides or herbicides. These literature comparisons highlight that our PtNPs@MIP/SPGrE offers an acceptable low detection limit and has a broader linearity range for PQ determination than previously reported sensors. Importantly, the LOQ for our PtNPs@MIP/SPGrE sensor is lower than the MRL, as established by Codex Alimentarius Commission for PQ residue on several fruit and vegetable samples, including tomato, cabbage, yardlong bean, and chili at 0.05 mg kg^{-1} (~0.2 µM), and cucumber at 0.02 mg kg^{-1} (~0.07 µM).[42,48] This point out that our sensor has high potential application for monitor the safety of food supplies, agricultural product and on-site analysis.

A survey of the literature show that this proposed PtNPs@MIP has been synthesized for the first time. Herein, MIP is straightforward synthesized on the functionalized PtNPs core followed by the removal of PQ template molecules. Thus, in this way, allowing to synthesize a low-cost artificial receptor with high selectivity towards PQ analyte. Our novel PtNPs@MIP is cost-effective with straightforward synthesis, and offers excellent mechanic stability. The highlight of this work is that the PtNPs@MIP was easily loaded on the electrode surface by drop casting and the analysis of PQ could be performed within a few minutes. We used the PtNPs@MIP nanocomposite to modify an SPGrE to create the new, highly sensitive, selective, compact, cost-effective and ready-to-use PQ sensor. We attribute these advantages to the highly conductive screen-printed graphene electrode's synergy with the good electrocatalytic characteristics of PtNPs@MIP, which significantly increases the electron transfer rate between PtNPs@MIP and SPGrE. Moreover, many Pt imprinted sites significantly enhance the selective surface area, leading to a modified electrode that performs with greater sensitivity and selectivity.

3.5 Selectivity reproducibility and stability

We investigated the imprinted sensor's selectivity to complex sample matrices analysis. We investigated the effects of foreign species to demonstrate the selectivity of the PtNPs@MIP/SPGrE toward the detection of PQ. Potential interferences might arise from similar substances, including other pesticides (chlorpyrifos, profenofos, carbofuran and glyphosate), herbicides (diuron and chlorotoluron and ions or compounds commonly found in extracted samples, *e.g.* phenol, caffeine, and ascorbic acid. We maintained PQ concentrations at 10 µM (control) and added potential interfering species to the test solution in the range of 5– to 20-fold greater concentration. As shown in Fig. 5A, there are no apparent effects on the PQ oxidation response (P2) when including up to a 5-fold excess concentration of profenofos, phenol, or caffeine, a 10-fold excess concentration of ascorbic acid, glyphosate, or

Table 1 Performance comparison of the presented electrode (PtNPs@MIP/SPGrE) with other related modified electrodes for PQ determination

Electrode	Modifier	Techniques	Linearity range (μM)	LOD (μM)	Ref.
GCE	MSF	SWV	0.01–0.05	0.012	1
	MWCNTs-DHP	SWV	0.05–1.5	0.01	20
	PPY-g-NGE	DPV	0.05–2.0	0.058	21
	AuNCs-CS-Ec-MIP	DPV	1.0×10^{-8}–1.0×10^{-4}	2.3×10^{-9}	29
	Gr–Au–ILs	SWV	0.02–0.1	0.007	42
	Phospholipid	ASV	0.05–0.6	0.022	44
BDDE	Bare	SWV	0.005–1.00	0.0015	2
Au	CDtrodes	SWV	0.14–2.8	0.08	45
PGE	Phthalocyanine	SWV	0.5–29.1	26.53	46
SPE	Gr–ZnO/Comm[a]	DPV	0.05–2.0	0.021	4
	Bi film/Cu plate[b]	SWV	0.12–4.20	0.012	22
	Nf/SPGrE/paper[c]	DPV	1–60	0.31	47
	PtNPs@MIP/SPGrE/PVC[d]	ASV	0.05–1000	0.02	This work

Electrode modifier. MSF = mesoporous silica films, MWCNTs-DHP = multiwalled carbon nanotubes immobilized with a dihexadecyl hydrogenphosphate (DHP) film, PPy-NGE = polypyrrole-grafted nitrogen-doped graphene, AuNPs-CS-MIP = Au nanocross–chitosan composited with electro-polymerization MIP, Gr-Au-ILs = graphene–gold–ionic liquid nanocomposite, CDtrodes = Au electrode prepared from recordable CD, Gr–ZnO = graphene-zinc oxide nanocomposite, Comm[a] = Commercial from Italsens Co., Bi film = bismuth film, Cu plate[b] = printed on copper plate, Nf = Nafion, SPGrE = screen printed graphene electrode, paper [c] = paper based electrochemical device (ePAD), PVC[d] = printed on PVC sheet. *Electrode*. GCE = glassy carbon electrode, BDDE = boron doped diamond electrode, Au = gold electrode, PGE = pyrolitic graphite electrode, SPE = screen printed electrode.

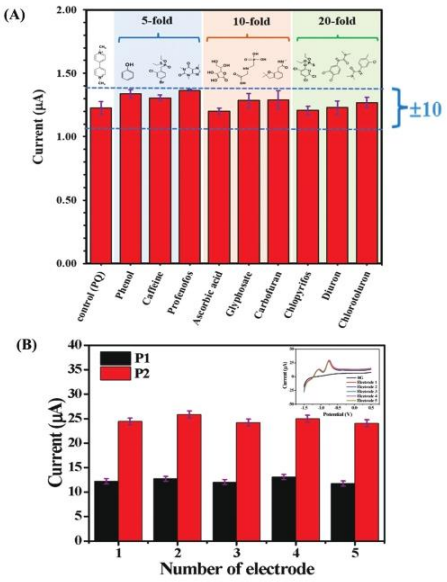

Fig. 5 (A) Selectivity of the proposed PtNPs@MIP/SPGrE for PQ detection; comparison between the current obtained from 10 μM PQ (control) and the current of 10 μM PQ with interfering substances. The dotted line shows the ±10% signal alteration range. (B) Reproducibility of the proposed MIP sensor; current responses of 100 μM PQ from five different MIP sensors. Inset; ASV signals response recorded in the presence of 100 μM PQ; supporting electrolyte; 0.1 M K_2SO_4 solution with five different PtNPs@MIP/SPGrE.

carbofuran, or a 20-fold excess of chlorpyrifos, or diuron, or chlorotoluron. These results confirm that the PtNPs@MIP/SPGrE provides high selectivity.

As a comparison, we also examine current response of various species only, 10 μM PQ (control) and the currents of phenol, caffeine and profenofos at the concentration of 50 μM (5-fold), ascorbic acid, glyphosate and carbofuran at the concentration 100 μM (10-fold), and chlorpyrifos, diuron and chlorotoluron at the concentration 200 μM (20-fold) at the PtNPs@MIP/SPGrE. It is obviously seen from Fig. S6† that high PQ current response observed at the MIP modified electrode. On the contrary, no significant current was observed from other species. The inset (Fig. S6†) clearly shown that the current response of the background has no apparent effects when adding carbofuran or glyphosate concentration up to 100 μM.

Selectivity pattern of the PtNPs@MIP/SPGrE toward PQ, phenol, glyphosate and carbofuran was investigated. Fig. S7† shows current responses of phenol and pesticides binding for MIP modified electrode and the NIP electrode. Imprinting factor (IF), which defined as the ratio of current response obtained from the MIP and NIP. As indicated in the back row of the graph, the calculated IF of the PQ target analyte were in the range of 0.123–2.503. Obviously, IF obtained from PtNPs@MIP higher than that obtained from competing compounds.

We ascribe the selectivity to the imprinted cavities' success in the polymer film, which has excellent binding and specific characteristics toward the target PQ molecule. These potential interference molecules are not cannot diffuse or bind strongly to recognition sites. Thus, these potential interferences did not produce an electrochemical-oxidation response and did not interfere with detection.

Sensitivity of the MIP sensor (Fig. 4B, 0.067 μA μM^{-1}) is approximately 2.5 times higher than that obtained from the

NIP modified electrode (0.028 μA μM^{-1}). The results thus clearly demonstrate appreciable selectivity and sensitivity of the developed PtNPs@MIP/SPGrE.

Fig. 5B shows that the PtNPs@MIP/SPGrE performs impressively with good precision. The relative standard deviation (RSD) <2.7%, calculated from three oxidation current values of 100 μM PQ. The electrode-to-electrode reproducibility, evaluated from RSD of five different freshly prepared sensors' responses, was 4.3%. For P1 and 2.9% for P2. Also, stability is an essential characteristic for the feasibility of real-life applications of the PQ sensor. We investigated the compact MIP sensor's stability by measuring the current signal for 100 μM at various intervals over 14 days. The MIP sensor retains 103% of its initial current response (P2) after repeated use for one week and 91% after two weeks when stored at ambient temperature (Fig. S8†). These results confirm that the developed compact MIP sensor provides high reproducibility and good stability.

Table 2 Determination of paraquat (PQ) in vegetable samples by the developed PtNPs@MIP sensor and recovery values for spiked PQ standard into real samples

Sample	Added (μM)	Found ± SD (μM)	%recovery	%RSD
Cabbage	—	0.081 ± 0.003	—	—
	5	4.948 ± 0.163	97.3	3.3
	10	9.914 ± 0.066	98.3	0.7
Cucumber	—	0.072 ± 0.001	—	—
	5	5.871 ± 0.149	116.0	2.5
	10	9.458 ± 0.079	93.9	0.8
Yardlong bean	—	0.095 ± 0.004	—	—
	5	5.236 ± 0.072	102.8	1.4
	10	9.755 ± 0.045	96.6	0.5
Kale	—	0.087 ± 0.001	—	—
	5	4.851 ± 0.109	95.3	2.3
	10	9.952 ± 0.056	98.7	0.6
Tomato	—	<LOQ	—	—
	5	5.243 ± 0.211	104.1	4.0
	10	9.828 ± 0.120	97.9	1.2
Onion	—	<LOQ	—	—
	5	5.480 ± 0.121	109.6	2.2
	10	9.698 ± 0.059	97.0	0.6
Lettuce	—	<LOQ	—	—
	5	5.263 ± 0.005	105.3	0.2
	10	9.831 ± 0.027	98.3	0.4

3.6 Real samples

We investigated the practical applicability and the performance of the fabricated PtNPs @MIP/SPGrE to analyze PQ in vegetable samples (yardlong bean, cabbage, lettuce, cucumber, kale, onion and tomato) and a certified reference material (CRM-QC 1435). The validity of the proposed PtNPs@MIP/SPGrE was tested by recovery determination. Paraquat in cabbage, cucumber, yardlong bean, and kale found 0.081 ± 0.003, 0.072 ± 0.001, 0.095 ± 0.004, and 0.087 ± 0.001 μM, respectively (Table 2).

Tomato, onion and lettuce were either contaminated with PQ below the LOQ or were free of PQ. The recoveries were determined by spiking 5 and 10 μM of PQ into actual samples. The results show the analytical recoveries for spiked paraquat standard (5 and 10 μM) to be in a range of 93.9% to 116.0%. The developed method provides good precision with %RSD values ranging from 0.2% to 4.0%.

We further evaluated the accuracy and precision of the proposed method in terms of intra-day and inter-day analysis. We determined the PQ content for two groups of tests: (i) spiked samples: blank tomato extracts and water samples, and (ii) certified reference material (CRM-QC1435, drinking water with certified PQ 66.7 ± 0.7 μg L^{-1}). As shown in Table 3, good intra-day and inter-day accuracy (%bias) in tomato extracts and water samples, *e.g.*, less than 2.6% for intraday and 2.4% for inter-day analysis. The acceptable %bias in CRM are −2.4% for intraday and −0.8% for inter-day analysis.[49,50] These results indicate that the PtNPs@MIP/SPGrE sensor is sufficiently accurate, precise, and suitable for quantifying PQ in these samples.

4. Conclusion

This study reports a compact electrochemical sensor for cost-effective and selective detection of paraquat based on a plati-

Table 3 Comparison of PQ determination in vegetables and CRM from intra-day and inter-day assay using the proposed PtNPs@MIP sensor

		Intraday assay		Inter-day assay	
Sample code	Expected (μM)	Found (μM)	Bias[a,b] (%)	Found (μM)	Bias[a,b] (%)
T#1	5	5.06 ± 0.17	1.2	4.89 ± 0.21	−2.2
T#2	10	9.88 ± 0.05	−1.2	9.85 ± 0.14	−1.5
W#1	5	5.13 ± 0.05	2.6	5.12 ± 0.05	2.4
W#2	10	9.89 ± 0.04	−1.1	9.91 ± 0.01	−0.9
	Certified (μg L^{-1})	Found (μg L^{-1})	Bias[c] (%)	Found (μg L^{-1})	Bias[c] (%)
CRM-QC 1435[c]	66.7 ± 0.7	65.07 ± 1.16	−2.4	66.17 ± 1.52	−0.8

T#1 and T#2 are tomato extracts (PQ free) spiked with PQ standards 5 and 10 μM, respectively. W#1 and W#2 are water solutions contained PQ 5 and 10 μM, respectively. [a] Bias calculated from the different between measurement results obtained from the developed method and a reference value from CRM. [b] Bias calculated from the different between measurement results obtained from the developed method and an expected value. [c] CRM of drinking water with the certified paraquat value of 66.7 ± 0.7 μg L^{-1}.

num nanoparticle coated with molecularly imprinted polymer-modified on a graphene-screen printed electrode (PtNPs@MIP/SPGrE). We fabricated the PtNPs@MIP by successively covering the surface of PtNPs with SiO_2 and vinyl end-groups and then terminated with an MIP shell. The resulting PQ-imprinted nanoparticles possess a large surface-to-volume ratio, enhancing accessibility of a large fraction of template sites on the polymer surface. Strategically, printing PQ onto the PtNPs surface not only significantly increases the specific surface area by providing large numbers of imprinted sites for improving selectivity and electron transfer between the target PQ molecule and the electrode surface, but also enhances the electrocatalytic activity for signal generating of the sensing platform. Our novel PtNPs@MIP is selective, easy to synthesize, and offers excellent catalytic activity. We used the PtNPs@MIP nanocomposite to modify an SPGrE to create the new, highly sensitive, selective, compact, and cost-effective sensor. Under the optimum condition, the proposed compact MIP sensor showed wide linearity ranged from 0.05 to 1000 μM, a low detection limit of 0.02 μM, high selectivity, good reproducibility, and stability. The imprinted sensor is highly sensitive and selective toward PQ. Used in the detection of PQ in vegetable extracts, the proposed ready-to-use MIP sensor could provide an alternative approach to determine paraquat residuals in vegetables and fruits and improving food safety.

Author contributions

Kanpitcha Somnet: Investigation, writing – original draft. Suphatsorn Thimoonnee: Investigation. Chanpen Karuwan: Screen-printed graphene paste electrode (SPGrE) investigation. Wichayaporn Kamsong: TEM investigation. Adisorn Tuantranont: Supervision. Maliwan Amatatongchai: Investigation, validation, conceptualization, writing – review & editing, supervision.

Conflicts of interest

The authors declare that they have no conflict of interest.

Acknowledgements

The authors acknowledge the support provided by the National Electronics and Computer Technology Center (NECTEC), the National Science and Technology Development Agency (NSTDA) *via* the Young Scientist and Technologist Program (YSTP grant no. SCA-CO-2562-9968-TH), and the Thailand Graduate Institute of Science and Technology (TGIST grant no. SCA-CO-2562-9842-TH). The authors wish to thank the support from the Center of Excellence for Innovation in Chemistry (PERCH-CIC), the Ministry of Higher Education, Science, Research, and Innovation.

References

1 T. Nasir, G. Herzog, M. Hebrant, C. Despas, L. Liu and A. Walcarius, *ACS Sens.*, 2018, **3**, 484–493, DOI: 10.1021/acssensors.7b00920.
2 K. Tyszczuk-Rotko, I. Bęczkowska and A. Nosal-Wiercińska, *Diamond Relat. Mater.*, 2014, **50**, 86–90, DOI: 10.1016/j.diamond.2014.09.011.
3 M. A. E. Mhammedi, M. Bakasse and A. Chtaini, *J. Hazard. Mater.*, 2007, **145**, 1–7, DOI: 10.1016/j.jhazmat.2007.02.054.
4 H. Liu, M. Chen, Y. Lin and Y. Liu, *Int. J. Electrochem. Sci.*, 2017, **12**, 8599–8608, DOI: 10.20964/2017.09.15.
5 M. K. Rai, J. V. Das and V. K. Gupta, *Talanta*, 1997, **45**, 343–348, DOI: 10.1016/S0039-9140(97)00136-7.
6 F. Maya, J. M. Estela and V. Cerdà, *Talanta*, 2011, **85**, 588–595, DOI: 10.1016/j.talanta.2011.04.022.
7 N. C. Posecion, E. M. Ostrea and D. M. Bielawski, *J. Chromatogr. B: Anal. Technol. Biomed. Life Sci.*, 2008, **862**, 93–99, DOI: 10.1016/j.jchromb.2007.11.002.
8 R. M. de Almeida and M. Yonamine, *J. Chromatogr. B: Anal. Technol. Biomed. Life Sci.*, 2007, **853**, 260–264, DOI: 10.1016/j.jchromb.2007.03.026.
9 C. Fukea, T. Araoa, Y. Morinagaa, H. Takaesua, K. Amenob and T. Miyazakia, *Leg. Med.*, 2002, **4**, 156–163, DOI: 10.1016/S1344-6223(02)00011-1.
10 M. R. Brunetto, A. R. Morales, M. Gallignani, J. L. Burguera and M. Burguera, *Talanta*, 2003, **59**, 913–921, DOI: 10.1016/S0039-9140(02)00645-8.
11 M. Ibáñez, Y. Picó and J. Mañes, *J. Chromatogr. A*, 1996, **728**, 325–331, DOI: 10.1016/0021-9673(95)00902-7.
12 X. Lee, T. Kumazawa, M. Fujishiro, C. Hasegawa, T. Arinobu, H. Seno, A. Ishii and K. Sato, *J. Mass Spectrom.*, 2004, **39**, 1147–1152, DOI: 10.1002/jms.695.
13 R. Garcia-Febrero, J. Salvador, F. Sanchez-Baeza and M. Marco, *Food Control*, 2014, **41**, 193–201, DOI: 10.1016/j.foodcont.2014.01.008.
14 Z. Niewola, J. P. Benner and H. Swaine, *Analyst*, 1986, **111**, 399–403, DOI: 10.1039/AN9861100399.
15 F. Yao, H. Liu, G. Wang, L. Du, X. Yin and Y. Fu, *Int. J. Environ. Sci.*, 2013, **25**, 1245–1251, DOI: 10.1016/S1001-0742(12)60124-7.
16 H. Fang, X. Zhang, S. J. Zhang, L. Liu, Y. M. Zhao and H. J. Xu, *Sens. Actuators, B*, 2015, **213**, 452–456, DOI: 10.1016/j.snb.2015.02.121.
17 P. Chuntib and J. Jakmunee, *Talanta*, 2015, **144**, 432–438, DOI: 10.1016/j.talanta.2015.06.066.
18 L. Ritter, K. Solomon, P. Sibley, K. Hall, P. Keen, G. Mattu and B. Linton, *J. Toxicol. Environ. Health*, 2002, **65**, 1–142, DOI: 10.1080/152873902753338572.
19 E. Mallat, C. Barzen, R. Abuknesha, G. Gauglitz and D. Barceló, *Anal. Chim. Acta*, 2001, **427**, 165–171, DOI: 10.1016/S0003-2670(00)01016-3.
20 L. L. C. Garcia, L. C. S. F.-Filho, G. G. Oliveira, O. F.-Filho and C. E. Banks, *Sens. Actuators, B*, 2013, **181**, 306–311, DOI: 10.1016/j.snb.2013.01.091.

21 J. Li, W. Lei, Y. Xu, Y. Zhang, M. Xia and F. Wang, *Electrochim. Acta*, 2015, **174**, 464–471, DOI: 10.1016/j.electacta.2015.06.028.
22 L. C. S. de Figueiredo-Filho, M. Baccarin, B. C. Janegitz and O. Fatibello-Filho, *Sens. Actuators, B*, 2017, **240**, 749–756, DOI: 10.1016/j.snb.2016.08.157.
23 B. Bräuer, C. Unger, M. Werner and P. A. Lieberzeit, *Sensors*, 2021, **21**, 5550, DOI: 10.3390/s21165550.
24 D. Refaat, M. G. Aggour, A. A. Farghali, R. Mahajan, J. G. Wiklander, I. A. Nicholls and S. A. Piletsky, *Int. J. Mol. Sci.*, 2019, **20**, 6304, DOI: 10.3390/ijms20246304.
25 X. Tang, D. Zhang, T. Zhou, D. Nie, Q. Yang, L. Jin and G. Shi, *Anal. Methods*, 2011, **3**, 2313–2321, DOI: 10.1039/C1AY05279A.
26 M. Amatatongchai, W. Sroysee, P. Jarujamrus, D. Nacapricha and P. A. Lieberzeit, *Talanta*, 2018, **179**, 700–709, DOI: 10.1016/j.talanta.2017.11.064.
27 M. Amatatongchai, S. Thimoonnee, P. Jarujamrus, D. Nacapricha and P. A. Lieberzeit, *Microchem. J.*, 2020, **158**, 105298, DOI: 10.1016/j.microc.2020.105298.
28 X. Tan, Q. Hu, J. Wu, X. Li, P. Li, H. Yu, X. Li and F. Lei, *Sens. Actuators, B*, 2015, **220**, 216–221, DOI: 10.1016/j.snb.2015.05.048.
29 X. Shan, J. de D. Habimana, J. Ji, J. Sun, F. Pi, Y. Zhang and X. Sun, *J. Solid State Electrochem.*, 2019, **23**, 1211–1220, DOI: 10.1007/s10008-018-04192-3.
30 C. Karuwan, A. Wisitsoraat, D. Phokharatkul, C. Sriprachuabwong, T. Lomas, D. Nacapricha and A. Tuantranont, *RSC Adv.*, 2013, **3**, 25792–25799, DOI: 10.1039/C3RA44187C.
31 P. Pasakon, J. P. Mensing, D. Phokaratkul, C. Karuwan, T. Lomas, A. Wisitsoraat and A. Tuantranont, *J. Appl. Electrochem.*, 2019, **49**, 214–227, DOI: 10.1007/s10800-018-1268-1.
32 M. Amatatongchai, W. Sroysee, S. Chairam and D. Nacapricha, *Talanta*, 2017, **166**, 420–427, DOI: 10.1016/j.talanta.2015.11.072.
33 M. Amatatongchai, W. Sroysee, P. Sodkrathok, N. Kesangam, S. Chairam and P. Jarujamrus, *Anal. Chim. Acta*, 2019, **1076**, 64–72, DOI: 10.1016/j.aca.2019.04.075.
34 T. Zou, P. He, J. Cao and Z. Li, *J. Chromatogr. Sci.*, 2015, **53**, 204–209, DOI: 10.1093/chromsci/bmu041.
35 D. A. Sidhoum, M. M. Socías-Viciana, M. D. Ureña-Amate, A. Derdour, E. González-Pradas and N. Debbagh-Boutarbouch, *Appl. Clay Sci.*, 2013, **83–84**, 441–448, DOI: 10.1016/j.clay.2013.07.007.
36 W. Insuwan and K. Rangsriwatananon, *Eng. J.*, 2017, **21**, 15–23, DOI: 10.4186/ej.2017.21.2.15.
37 W. Rongchapo, C. Keawkumay, N. Osakoo, K. Deekamwong, N. Chanlek, S. Prayoonpokarach and J. Wittayakun, *Adsorpt. Sci. Technol.*, 2017, **36**, 684–693, DOI: 10.1177/0263617417715394.
38 E. Laviron, *J. Electroanal. Chem.*, 1979, **101**, 19–28, DOI: 10.1016/S0022-0728(79)80075-3.
39 A. J. Bard and L. R. Faulkner, *Electrochemical Methods Fundamentals and Applications*, Wiley, Hoboken, 2nd edn 2004.
40 Y. Wang, L. Yao, X. Liu, J. Cheng, W. Liu, T. Liu, M. Sun, L. Zhao, F. Ding, Z. Lu, P. Zou, X. Wang, Q. Zhao and H. Rao, *Biosens. Bioelectron.*, 2019, **142**, 111483, DOI: 10.1016/j.bios.2019.111483.
41 J. Zhang, Z. Lin, Y. Qin, Y. Li, X. Liu, Q. Li and H. Huang, *ACS Omega*, 2019, **4**, 18398–18404, DOI: 10.1021/acsomega.9b02658.
42 F. Cui, L. Chu and X. Zhang, *Anal. Methods*, 2012, **4**, 3974–3980, DOI: 10.1039/C2AY25795E.
43 ISO 11843, Capability of Detection, Part I/II, Geneve, 19.
44 H. Tomková, R. Sokolová, T. Opletal, P. Kučerová, L. Kučera, J. Součková, J. Skopalová and P. Barták, *J. Electroanal. Chem.*, 2018, **821**, 33–39, DOI: 10.1016/j.jelechem.2017.12.048.
45 D. De Souza, L. Codognoto, S. A. S. Machado and L. A. Avaca, *Anal. Lett.*, 2005, **38**, 331–341, DOI: 10.1081/AL-200045163.
46 I. C. Lopes, D. De Souza, S. A. S. Machado and A. A. Tanaka, *Anal. Bioanal. Chem.*, 2007, **388**, 1907–1914, DOI: 10.1007/s00216-007-1397-6.
47 K. Charoenkitamorn, C. Chotsuwan, S. Chaiyo, W. Siangproh and O. Chailapakul, *Sens. Actuators, B*, 2020, **315**, 128089, DOI: 10.1016/j.snb.2020.128089.
48 Anonymous, List of Codex maximum residue limits, pesticides database search, available from: http://www.fao.org/fao-who-codexalimentarius/codex-texts/dbs/pestres/pesticide-detail/en/?p_id=57, 2021, accessed 27 January 2021.
49 A. G. González, M. Á. Herrador and A. G. Asuero, *Talanta*, 2010, **82**, 1995–1998, DOI: 10.1016/j.talanta.2010.07.071.
50 T. P. J. Linsinger, *TrAC, Trends Anal. Chem.*, 2008, **27**, 916–923, DOI: 10.1016/j.trac.2008.08.013.

Journal of Electroanalytical Chemistry 914 (2022) 116302

Contents lists available at ScienceDirect

Journal of Electroanalytical Chemistry

journal homepage: www.elsevier.com/locate/jelechem

A compact *N*-nitrosodiphenylamine imprinted sensor based on a Pd nanoparticles-MIP microsphere modified screen-printed graphene electrode

Kanpitcha Somnet [a], Pattawan Soravech [a], Chanpen Karuwan [b], Adisorn Tuantranont [b], Maliwan Amatatongchai [a,*]

[a] Department of Chemistry and Center of Excellence for Innovation in Chemistry, Faculty of Science, Ubon Ratchathani University, Ubon Ratchathani 34190, Thailand
[b] Graphene Sensor Laboratory (GPL), Graphene and Printed Electronics for Dual-Use Applications Research Division (GPERD), National Security and Dual-Use Technology Center (NSD), National Science and Technology Development Agency (NSTDA), Pathum Thani 12120, Thailand

ARTICLE INFO

Keywords:
Ready-to-use sensor
N-nitrosamines
Molecularly imprinted polymer
Core-shell microsphere
Food quality control

ABSTRACT

Herein, we report the fabrication of a compact voltammetric sensor for the sensitive and selective determination of *N*-nitrosodiphenylamine (NDPhA) based on a screen-printed graphene electrode modified with a molecularly imprinted polymer coating on a palladium nanoparticle core (PdNPs@MIP/SPGrE). In addition, a novel approach for 3D-imprinting of NDPhA on the PdNPs surface is presented. PdNPs were first synthesized by chemical reduction using sodium borohydride. Then, Core-shell polymerization was achieved by successively coating the surface of PdNPs with poly(vinylpyrrolidone) and terminating with an MIP consisting of poly(*N*-Isopropylacrylamide)-co-trimethylolpropane trimethacrylate.

Morphological, structural, and electrochemical characterization reveals that the as-prepared micro-sized spherical PdNPs@MIP has a uniform, high electro-catalytic activity and a specific surface area with many NDPhA imprinted sites. We constructed the compact NDPhA imprinted sensor by coating the SPGrE surface with PdNPs@MIP. Quantitative analysis was performed by linear sweep anodic stripping voltammetry (LSASV) using a deposition potential of +0.02 V for 60 s. The linear working ranges for NDPhA measurements were 0.01–0.1 μM (r^2 = 0.996) and 0.1–100 μM (r^2 = 0.992) with corresponding sensitivities of 51.935 and 0.821 (μA s) μM^{-1}, respectively. The system provides a good precision of %RSD 1.67% with an estimated detection limit ($3S_b$, n = 3) of 0.0013 μM. The intraday and inter-day accuracy (%bias) of the certified reference material (CRM) are −0.74% and −1.01%, respectively. We demonstrate the successful application of the fabricated compact sensor to determine NDPhA in beverage and synthetic samples. The compact NDPhA imprinted sensor can provide an alternative approach to food quality control.

1. Introduction

N-nitrosamines are a group of potential human carcinogens formed from nitrification or oxidation of amine precursors [1,2]. They exist widely in human life and consumer items such as processed food [3], beverages [2,4], cosmetics [5,6], and cigarettes [7,8]. Nitrosodiphenylamine (NDPhA), as a type of volatile *N*-nitrosamine, has been classified as one of the carcinogenic and mutagenic compounds [9] and listed as one of five contaminants potentially occurring in the public water system by the United-states environmental protection agency (US-EPA) [4,10]. Its high toxicity and potential contamination in the water system have resulted in public concern regarding food safety and human health. US-EPA set NDPhA maximum concentration at 7 μg L^{-1} (0.035 μM) in drinking water based on a lifetime cancer risk of 1 in 100,000 [11]. As a result, developing rapid, sensitive, and selective detection methods for NDPhA monitoring in drinking water, beverages, and food is critical for public health. Various analytical methods have been applied to NDPhA detection, including gas chromatography [12] and liquid chromatography [13], in tandem with mass-spectrometric and fluorometric detection [11]. It is always desirable to develop time-saving, cost-effective, ready-to-use methods for on-site analysis and household testing kits for monitoring and control. Due to the advantages of simplicity, low cost, and short time-to-results compared with other methods, electrochemical methods are considered a suitable complementary tool to meet this need.

In a previous report, various electrochemical methods for detecting NDPhA have been proposed using differently designed electrode materials, for example, the use of Hg [14], Au [15], and glassy carbon

* Corresponding author.
E-mail address: maliwan.a@ubu.ac.th (M. Amatatongchai).

https://doi.org/10.1016/j.jelechem.2022.116302
Received 21 February 2022; Received in revised form 11 March 2022; Accepted 8 April 2022
Available online 12 April 2022

[16–18] as working electrodes. Analysis based on amperometric detection of NDPhA in a flow injection system with ruthenium oxide stabilized by cyano cross-linked film in a modified glassy carbon electrode (GCE) [16]. The nanomaterial-based sensors with voltammetric detections of NDPhA use poly(diallyldimethylammonium chloride)-stabilized graphene/platinum nanoparticles (PDDA-Gr/PtNPs) [17], and graphite polyurethane composite (GPUE) [18] modified GCEs. However, all these electrodes have certain drawbacks, such as problems associated with electrode fouling and high positive potential for oxidation of NDPhA (0.75–1.56 V vs. Ag/AgCl). As a result, many substances could interfere with the measurements. To the best of our knowledge, there is no report of using a screen-printed electrode for creating compact NDPhA sensors. Sensors for ready-to-use, inexpensive, portable, and well suited for on-sited monitoring applications still need further improvement. Moreover, for practical application/actual commercialization, sensitivity and selectivity need to be improved to perform well in food samples.

Molecularly imprinted polymers (MIP) with tailor-made affinity and specificity to target analytes have been demonstrated in many applications, including electrochemical sensors to promote the performance and selectivity of sensors [19,20]. We can tune the polymerization by changing the ratio of the monomers and the template, the initiation method, or source the surface or place where it occurs [21,22]. Further, we can incorporate the polymer chains to several surfaces to form different architectures such as layers, core–shell, or beads. Core-shell polymerization or polymerization of the shell of the MIP around the core produces a higher surface-area-to-volume ratio, more easily accessible recognition sites leading to improvement of biding kinetics, binding capacity, and lower heterogeneities [23–26]. Among the alternative nano-cores, palladium nanoparticles (PdNPs) are one of the good choices due to their extraordinary catalytic, conductivity, electrochemical properties [27] and abundance and lower cost in comparison with Pt and Au nanoparticles [28,29]. Good electrical properties and the excellent conductivity of the PdNPs core combined with the specific recognition site of the MIP shell endows the sensor with powerful performance for the target analytes. Thus, this NDPhA imprinting on core–shell sensing platforms will offer selectivity and sensitivity and be accurate for food sample analysis.

Herein, we present a novel NDPhA compact electrochemical sensor based on a screen-printed graphene electrode modified with palladium nanoparticles covered with a molecularly imprinted polymer (PdNPs@MIP/SPGrE). This is the first report of NDPhA imprinted polymer being polymerized on a PdNPs surface. The 3D-imprinting on PdNPs surface was achieved by successively coating the surface of PdNPs with PVP, then terminating with poly(*N*-Isopropylacrylamide)-co-trimethylolpropane trimethacrylate imprinted polymer. Our novel PdNPs@MIP is cost-effective, simple to synthesize, contains many NDPhA imprinted sites, and has an excellent electro-catalytic activity towards the oxidation of NDPhA. We readily prepared the SPGrE by screen-printing, and the synthesized PdNPs@MIP was drop cast on the electrode surface to fabricate the NDPhA-recognition site imprinted sensor. Our compact sensor (PdNPs@MIP/SPGrE) provides excellent selectivity and sensitivity, quick analysis, uses a minute quantity of reagent, and is convenient for large-scale production. It is well suited to food-quality control and on-site monitoring applications.

2. Experimental

2.1. Chemicals and reagents

All chemicals were analytical grade. We used deionized-distilled water for standard and reagent preparation (water Pro-Ps, USA). Palladium chloride ($PdCl_2$, 59% Pd) was purchased from Acros Organics (Geel, Belgium). Tri-sodium citrate, sodium borohydride ($NaBH_4$), ethanol, methanol, poly(vinylpyrrolidone) with an average molecular mass of 10,000 g mol^{-1} (PVP-10), *N*-Isopropylacrylamide (NIPAM, 97%), 2,2′-azobis(2-methylpropionitrile) (AIBN), trimethylolpropane trimethacrylate (TRIM), Boric acid (H_3BO_3, 99.5%), Phosphoric acid (H_3PO_4, 85%), and acetic acid (CH_3COOH, 99.7%) were obtained from Sigma-Aldrich (St. Louis, USA). Nitrosodiphenylamine (NDPhA, 99.5%) was obtained from Chem Service (West Chester, PA). In addition, we purchased a certified reference material of NDPhA (CRM 31032/607, Nitrosamine calibration mix) from Restex Corporation (Bellefonte, PA, USA.).

2.2. Apparatus

2.2.1. Screen printed graphene electrode (SPGrE)

Disposable electrochemical analytical devices were fabricated in-house according to our previously described protocols [23,30]. The configuration of the devices comprised of a three-electrode cell construction (Scheme 1), a 4 mm-circular working electrode (graphene), a reference electrode (Ag/AgCl), and a counter electrode (graphene). The screen-printed graphene electrodes (SPGrE) were prepared using an MK-MINI screen printer (Minami, Japan). Commercial graphene ink (Serve Science Ltd, Thailand) was screen printed onto clear polyvinyl chloride (PVC) (Navanakornplastic Co. Ltd., Pathum Thani, Thailand) sheets through silk-screen printing mesh (mesh size 120 μm) for two cycles. Next, a reference area was screen-printed with Ag/AgCl ink (Gwent Electronic Materials Ltd., Pontypool, U.K.) on the PVC sheet for two cycles. Finally, we printed a detection area with insulating ink on the PVC sheet for two cycles and then baked the sheet at 60 °C for 1 h to remove any solvent. Next, we assembled a homemade electrode holder (5.0 × 5.0 × 1.0 cm) from an acrylic sheet and placed an assembled electrical connector inside the body. The center of the holder lid was drilled to make a 2.0 cm sample injection hole. The electrode holder was designed for efficient handling of sample/standard adding and for tight fixing of the SPGrE.

2.2.2. Electrochemical measurements

We performed all electrochemical measurements using a homemade reactor with an EmStat3 potentiostat (5.0 × 6.7 × 2.8 cm) (PalmSens BV, The Netherlands). Further, we used “PSTrace for windows” with multi-trace software. The measurement cell was formed by a working electrode (PdNPs@MIP/SPGrE), a reference electrode (Ag/AgCl), and a counter electrode (SPGrE). The circular modified graphene working electrode (4 mm diameter) had an active surface area of around 0.126 cm^2. Cyclic voltammograms (CV) were recorded using 0.04 M Britton–Robinson buffer (B-R buffer) electrolyte solution, at a scan rate of 50 mV s^{-1} and across a potential range of −0.3 to +0.6 V. We selected linear sweep anodic stripping voltammetry (LSASV) for quantitative analyses. After filling the detection area with the standard or sample solution, we applied a deposition potential of +0.02 V for 60 s. Then, the linear sweep scanned from −0.2 to +0.8 V at a scan rate of 50 mV s^{-1} to remove the deposited NDPhA, and the corresponding current signal was recorded.

2.2.3. Nanomaterial characterization

The details of the apparatus used to characterize the synthesized composite materials, and impedance spectroscopy (EIS) are all specified in supporting information (S.I.) section 1.

2.3. Preparation of NDPhA sensor (PdNPs@MIP/SPGrE)

2.3.1. Synthesis of PdNPs@MIP microsphere

Palladium nanoparticles (PdNPs) were selected as cores for the imprinted surface. We adopted the method described by Ullah and

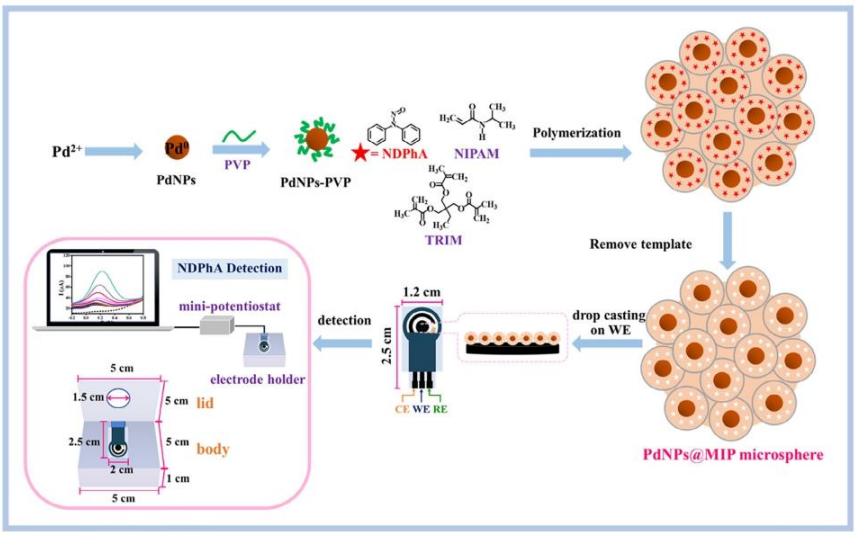

Scheme 1. Preparation of palladium nanoparticles coated with molecularly imprinted polymers (PdNPs@MIP) and the NDPhA imprinted sensor via drop coating on the SPGrE.

his co-workers [31] to synthesize PdNPs. Firstly, we mixed an aqueous solution of trisodium citrate (0.5 mL, 0.4 M) and a solution of $PdCl_2$ (5 mL, 0.10 M) into a flask containing DI water (30 mL). The mixture was stirred continuously at 60 °C for 30 min. Next, we added an aqueous solution of $NaBH_4$ (0.5 mL, 0.1 M) to the flask, and the reaction continued under constant stirring until the color turned to dark brown (~2 h), which indicated the successful synthesis of PdNPs (Scheme 1). Finally, the precipitate was centrifuged, washed thrice with DI water, and let dry at 80 °C for 2.5 h.

Scheme 1 illustrates the synthesis of palladium nanoparticles coated with molecularly imprinted polymers (PdNPs@MIP). PdNPs were coated with poly(vinylpyrrolidone) or PVP to create the polymerizable functional groups using a sol–gel method [32,33]. First, PVP (0.04 g) was dissolved in ethanol (3 mL) to make a PVP solution. The solution was mechanically stirred and maintained at 50 °C. Next, PdNPs (40 mg) were added to the PVP solution and vigorously stirred for 30 mins at room temperature. Finally, the precipitate was centrifuged, washed thrice with DI water, and let dry in a desiccator to yield the PdNPs-PVP nanocomposites.

We created nitrosodiphenylamine or NDPhA recognition sites on the surface of PdNPs cores via the precipitation polymerization method. Briefly, NDPhA template (0.12 mmol), NIPAM functional monomer (0.24 mmol), and PdNPs-PVP (20 mg) were mixed in 20 mL of methanol under ice for 1 h. This allowed the creation of complexes between the functional monomer and the template via facial hydrogen bonding. Next, TRIM cross-linker (0.9 mmol) and AIBN initiator (0.06 mmol) were added to the mixture. The solution was mixed at room temperature for a few minutes and then sonicated for 10 min. After purging with nitrogen for 5 min, the solution was sealed and placed in a water bath at 60 °C for 18 h. We collected the synthesized particles after centrifugation at 10,000 rpm for 5 min. The template molecule was extracted to generate recognition sites by washing eight times with ethanol (80 mL) and dried overnight at 100 °C. Similarly, a control non-imprinted polymer (NIP) was prepared following the same procedure but without NDPhA.

2.3.2. Fabrication of PdNPs@MIP/SPGrE

The PdNPs@MIP dispersion (2.5 μL, 5 mg mL^{-1} in dimethylformamide) was dropped onto the SPGrE surface and allowed to dry at room temperature to furnish the imprinted sensor (PdNPs@MIP/SPGrE).

2.4. Accuracy test and actual sample application

We analyzed the NDPhA content in beverage samples (beer, dark wine, red wine, green tea, orange juice, and apple juice), synthetic samples, and Certified Reference Materials (CRM) to evaluate the performance of the proposed dual-imprinted sensor (PdNPs@MIP/SPGrE). Samples were filtered through a 0.25-μm cellulose membrane, diluted appropriately with B-R buffer at pH 3, and then determined via an external calibration curve. To assess the accuracy of the NDPhA imprinted sensor, we investigated recoveries with 0.05 or 0.1 μM of spiked NDPhA added to the samples before filtration. We determined the samples for the analyte and calculated the recoveries. We compared NDPhA concentration results obtained from our compact sensor to those obtained from a standard HPLC method [34]. The HPLC method used for validation in this work is outlined in S.I., section 2.

The calibration mix (CRM 31032/607) of nitrosamines, with a certified concentration of NDPhA of 10,122.087 ± 94.340 μM was evaluated by applying the developed PdNPs@MIP sensor.

3. Results and discussion

3.1. Structure and morphological characterization

Fig. S1a shows the absorption spectrum of palladium nanoparticles after successfully reducing $NaBH_4$ compared with those of a $PdCl_2$ solution. $PdCl_2$ solution reveals a strong peak at 420 nm (blue line) related to the Pd^{2+} ion. After reducing Pd^{2+} to Pd^0, the peaks disappeared with a change in color from yellow to dark brown due to exci-

tation of surface plasmon vibration in the PdNPs, formed at a peak range of 370–440 nm [35–37].

Moreover, ATR FTIR spectroscopy confirms the formation of NDPhA recognition sites on the molecularly imprinted polymer coated on the PdNPs core. FTIR spectra (Fig. S1b) were recorded from NDPhA (curve a), PdNPs@MIP before (curve b), and after (curve c) removal of the NDPhA template molecules and PdNPs@NIP (curve d). The bands at 1318, 1292, and 1052 cm^{-1} for NDPhA (curve a) were due to the characteristic stretching vibration bands of N═O (1321–1292 cm^{-1}) and N—N (1052 cm^{-1}) [38], respectively. The PdNPs@MIP spectrum before template removal (curve b) shows the absorption bands of the characteristic peaks of NDPhA (star marked in curve b), illustrating the presence of NDPhA in the polymer matrix. After template removal, the spectrum (curve c) bands (at 1318, 1292, and 1052 cm^{-1}) disappear due to loss of NDPhA via ethanol extraction. These results suggest the successful removal of NDPhA from the PdNPs@MIP film. Meanwhile, the film spectra (curves b, c, and d) show absorption characteristic bands of NIPAM (triangle marked in curve d) at 2972, 1640, 1459, and 1387 cm^{-1} that assign to C—N of amide, C═O stretching of amide, C–$(CH_3)_2$ isopropyl groups, and C—H bending in –CH_2– groups and –$C(CH_3)_2$, respectively [39-42]. We attributed the peaks at 1730 and 1150 cm^{-1} (diamond marked in Fig. S1b, curve d) to symmetric and asymmetric C—O—C stretching of the ester group and C═O stretching of TRIM cross-linker [39]. All the results confirmed the successful fabrication of the PdNPs@MIP.

We used SEM and TEM to characterize the morphology of PdNPs, PdNPs-PVP, and PdNPs@MIP nanocomposites. EDS and XPS were used to investigate the Pd atom's composition, elemental fraction, and valence state in the as-prepared PdNPs@MIP. SEM image of bare SPGrE's surface (Fig. S2) exhibits smooth, thin, and appears nanosheets, which is the typical morphology for graphene. The synthesized PdNPs (Fig. 1a) appears approximately spherical with an average diameter of 22.0 ± 1.7 nm (count = 20), whereas PdNPs-PVP (Fig. 1b) is larger than the unmodified PdNPs due to the formation of a PVP layer on the surface of the PdNPs as revealed by SEM. The SEM image (Fig. 1d) of the PdNPs@MIP exhibits a spherical shape and uniform microsphere with a mean diameter of approximately 2.3 ± 0.8 μm (count = 10). A close-up view of PdNPs@MIP (TEM image, Fig. 1c) indicated a shell consisting of PdNPs with an average diameter of around 22 nm covered on the sphere surface of MIP particles. The EDS spectrum (Fig. 1d) reveals the presence of C (66.58 wt %), N (8.54 wt%), O (22.24 wt%), and Pd (2.63 wt%) atoms. This provides evidence for attachment between the PdNPs core and the organic part corresponding to the polymer matrix synthesized from NIPAM and TRIM. Further, the elemental mapping in Fig. 1(e and f) indicates an equal distribution on the PdNPs@MIP microsphere (containing C,

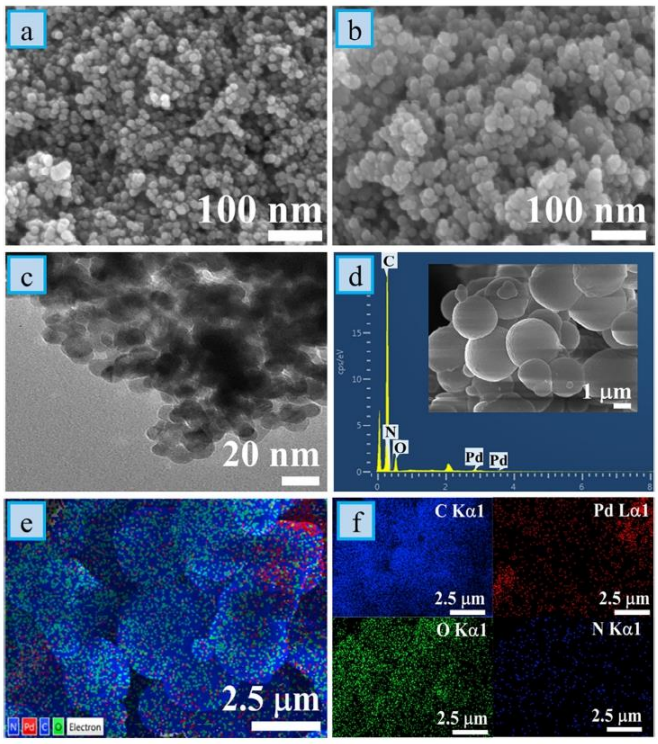

Fig. 1. SEM images of (a) PdNPs and (b) PdNPs-PVP. TEM images of (c) PdNPs@MIP, (d) EDS of PdNPs@MIP, and (e) mixture of mapping analysis of (f) C, Pd, O, and N elements in the PdNPs@MIP microspheres.

N, O, and Pd elements). These results revealed that PdNPs are indeed entirely covered on the MIP microsphere.

XPS revealed the chemical state of Pd in the as-prepared PdNPs@MIP microsphere. The full spectrum of PdNPs@MIP (Fig. S3a) illustrates three pre-dominant peaks. In the C 1s spectrum (Fig. S3b), we attributed the peaks at 284.5, 285.1, 286.2, 287.1, and 288.6 eV to C—C/C—H, C—N, *N*-C=O, C—O, and O–C=O, respectively. Fig. S3c shows that the O 1 s spectrum of PdNPs@MIP could be deconvoluted into three peaks at 531.8, 533.2, and 534.6 eV, related to the chemical binding energies of *N*-C=O, C—O, and O–C=O, respectively [43–45]. Furthermore, we ascribed the 399.3 eV, N 1s peak (Fig. S3d) to the NH_2 in amide functionalities from poly(*N*-Isopropylacrylamide) [43–45]. The spectrum of Pd contains two peaks with binding energies of 336.0 and 341.3 eV for Pd $3d_{5/2}$ and Pd $3d_{3/2}$, respectively (Fig. S3e), which result from the reduction of Pt^{2+} to Pd^0 [46]. This observation confirms the successful formation of NDPhA imprinted polymer covering the PdNPs.

3.2. Electrochemical characterization

3.2.1. Electrochemical impedance spectroscopy

We examined the electron transfer kinetics of the bare and modified electrodes using EIS. Fig. 2a shows the EIS data obtained for a bare SPGrE, PdNPs/SPGrE, PdNPs-PVP/SPGrE, PdNPs@MIP/SPGrE, and PdNPs@MIP/SPGrE. The lowest semicircular diameter was obtained from the PdNPs/SPGrE (R_{ct} = 34.1 Ω), which indicates the fastest electron-transfer kinetics of $[Fe(C.N.)_6]^{3-/4-}$, compared to bare SPGrE (R_{ct} = 1930 Ω), PdNPs-PVP (R_{ct} = 151 Ω,) PdNPs@MIP (R_{ct} = 175 Ω) and PdNPs@NIP modified electrode (R_{ct} = 360 Ω). The lowest impedance of PdNPs/SPGrE indicates the excellent conductivity enhancement of PdNPs. The highest impedances from the NIP modified electrode indicate the presence of poly(*N*-Isopropylacrylamide) film. This film blocks the electrochemical reaction of $[Fe(CN)_6]^{3-/4-}$ on the electrode surface. The MIP has a lower impedance than the NIP-modified electrode because of NDPhA recognition sites in the MIP films. This permit diffusion of the $[Fe(CN)_6]^{3-/4-}$ redox probe, enhancing the electron transfer.

Cyclic voltammetry serves to analyze the electrochemical behavior of NDPhA on the bare SPGrE, PdNPs/SPGrE, PdNPs@MIP/SPGrE, and PdNPs@NIP/SPGrE. As shown in Fig. 2b, the characteristic oxidation peak of NDPhA appears at about +0.15 V at all the electrodes. Bare SPGrE shows only weak current response, while modified electrodes lead to higher current response. After modifying SPGrE with PdNPs, the anodic peak current of NDPhA increased 3.68 times that at the bare SPGrE due to PdNP's good electrocatalytic activity, high conductivity, and large surface area [29,47,48]. Moreover, the peak current at the PdNPs@MIP/SPGrE is 9.20 times higher than the bare SPGrE. Enhancement of anodic peak current is because of the high electrocatalytic activity and conductivity of PdNPs and the formation of hydrogen bonds between specific recognition cavities in the MIP microsphere and NDPhA that improve the accumulation of NDPhA on the electrode surface. However, the PdNPs@NIP/SPGrE exhibits an anodic current peak less than PdNPs@MIP/SPGrE. The absence of NDPhA recognition sites on NIP-modified electrodes generates an obstruction effect from the polymer that blocks the binding of NDPhA target analyte on the electrode surface. In other words, the higher NDPhA oxidation peak at PdNPs@MIP/SPGrE results from the formation of specific binding sites offered by the successful imprinting process, resulting in a higher electron transfer rate. As a result, the MIP sensor has a greater affinity for the analyte molecules, which is in accord with previous reports [19,49].

The role of PdNPs for electro-catalytic the oxidation of NDPhA was also demonstrated as in Fig. S4. It is clearly seen that anodic peak current at PdNPs@MIP/SPGrE is higher than the MIP/SPGrE. Enhancement of peak current is because of the high electrocatalytic activity, specific surface area and the formation of many specific NDPhA recognition cavities in the MIP microsphere that improve the current signal of NDPhA on the electrode surface.

3.3. Optimization of the sensor preparation and detection conditions

3.3.1. Polymerization

MIPs were synthesized with different template-to-monomer molar ratios and monomer-to-crosslinker molar ratios to optimize the imprinting conditions. The template molecule (NDPhA): monomer (NIPAM) ratio is crucial. It influences the number of imprinted cavities and the binding affinity between NDPhA and recognition sites. We chose NIPAM as a monomer because it has more amide functional groups, making it possible to obtain a good interaction with NDPhA through hydrogen bonds, to form a non-covalent interaction. Fig. 3a reveals that the NDPhA oxidation peak current increases with the NDPhA: NIPAM molar ratio increased from 1:0 to 1:2 but slightly decreased at larger ratio.

Polymerization is incomplete at low NDPhA: NIPAM ratios, so there are fewer imprinted cavities. A ratio of 1:2 provides the maximum current response and imprinting ability from NIPAM, indicating that the

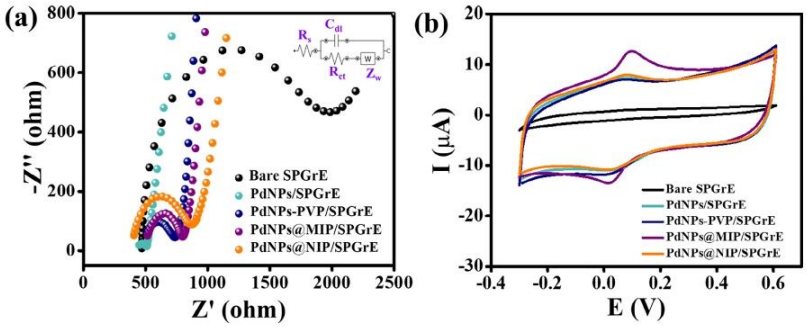

Fig. 2. (a) Nyquist plot observed for bare SPGrE, PdNPs/SPGrE, PdNPs-PVP/SPGrE, PdNPs@MIP/SPGrE and PdNPs@MIP/SPGrE in 0.1 M KCl containing 5 mM $[Fe(CN)_6]^{3-/4-}$ over the frequency range 0.1 Hz to 100 kHz; amplitude = 10 mV. Inset; Randles equivalent circuit model; here R_s, C_{dl}, R_{ct}, and Z_w stand for the ohmic resistance of electrolyte (R_s), double layer capacitance (C_{dl}), electron transfer resistance (R_{ct}), and Warberg impedance (Z_w). (b) CV curve of 250 μM NDPhA on bare SPGrE, PdNPs/SPGrE, PdNPs-PVP/SPGrE, PdNPs@MIP/SPGrE, and PdNPs@NIP/SPGrE in 0.04 M B-R buffer (pH 3.0) supporting solution.

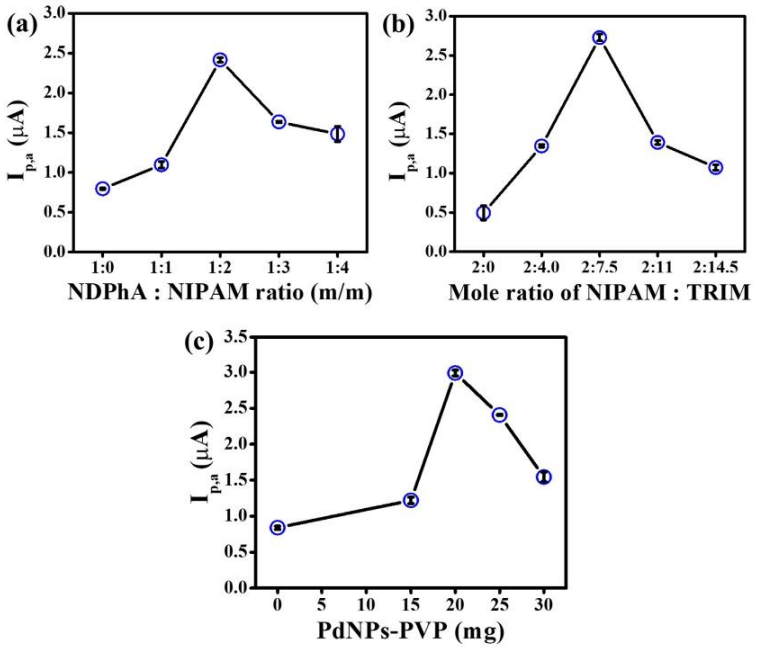

Fig. 3. Optimization conditions affect the determination of NDPhA. Variation of electrode response for NDPhA (250 μM) with changing of (a) NDPhA: NIPAM mole ratio and (b) NIPAM: TRIM mole ratio and (c) PdNPs-PVP loading (mg), using 0.04 M B-R buffer pH 3.0 as supporting solution.

most significant number of imprinting cavities in the polymer network had formed. Above this ratio, the current response decreases. Excess NIPAM monomer produces thicker polymer films and blocks NDPhA molecules from accessing binding sites, thereby reducing the number of specific binding sites. This circumstance is consistent with previous reports [49,50]. Therefore, we selected the ratio of 1:2 as the optimal template-to-monomer ratio.

Cross-linker content is also significant in modulating the shape of the polymer matrix and maintaining the imprinted binding site. The effect of the monomer: cross-linker (NIPAM: TRIM) molar ratio on the PdNPs@MIP current response was investigated at 2.0, 2.40, 2:7.5, 2:11, and 2:14.5 (Fig. 3b). Peak current increases from a ratio of 2:0 up to 2:7.5. Further increases in the mole ratio to 2:14.5 result in a significant decrease in signal. It is also possible that excess TRIM forms hydrogen bonds with NIPAM and with the NDPhA template molecule. This competition can reduce the number of interactions between template molecule and monomer, resulting in fewer recognition cavities in the polymer and decreasing the number of binding sites. In addition, excess TRIM cross-linker forms a rigid polymer that prevents NDPhA from entering cavities in the proper position and orientation, reducing retention efficiency. Therefore, we chose a molar ratio of 2:7.5 for the monomer and cross-linker to maximize sensitivity.

PdNPs play an important role in electro-catalytic of the NDPhA oxidation and influence the number of NDPhA imprinting sites in the MIP microsphere. Thus, the amount of PdNPs-PVP core on the imprinting conditions was studied. The NDPhA anodic peak current increases with the PdNPs-PVP core from 0 to 20 mg but decreased at higher loading (Fig. 3c). The increased current response on increasing PdNPs-PVP core may result from an increase in the density of NDPhA imprinting sites per unit surface area on the MIP matrix. Therefore, we selected PdNPs-PVP amount of 20 mg to provide the largest NDPhA anodic peak current as optimal condition for the MIP microsphere synthesized.

3.3.2. Mechanism of NDPhA detection on the PdNPs@MIP sensor

We investigated the electrochemical behaviors of NDPhA on the proposed PdNPs@MIP/SPGrE by studying the effects of scan rate (ν) and pH of the electrolyte solution to determine the detection mechanism. We set the scan rate dependency to between 50 and 150 mV s^{-1} to investigate the number of electrons involved in the oxidation of NDPhA (Fig. S5a). Fig. S5b shows a plot of the NDPhA anodic and cathodic peak currents (μA) increasing linearly with the scan rate's square root ($V^{1/2}$ $s^{-1/2}$). Linear regression analysis provides a correlation coefficient (r^2) of 0.9980 ($I_{p,a}$) for oxidation, and 0.9975 ($I_{p,c}$) for reduction reactions. There is a diffusion-controlled reversible electrochemical process at the surface of the PdNPs@MIP/SPGrE. The relationship between the peak potential $E_{p,a}$ and ν is defined by Laviron as Eq. (1) [51,52].

$$E_{p,a} = E_0 + \frac{RT}{(1-\alpha)nF} ln \frac{(1-\alpha)nF}{RTk_s} + \frac{RT}{(1-\alpha)nF} ln\nu \quad (1)$$

where E_0 represents the formal potential, k_s is the standard rate constant of the reaction, R is the gas constant, T is the temperature, F is the Faraday constant, ν is the scanning rate, α is the transfer coefficient, and n is the electron transfer number. We can use the slope to calculate

the (1 − α) n term. The slope is 0.0527 (Fig. S5c), taking T = 298 K, F = 96,485 C mol^{-1} and R = 8.314 J mol^{-1} K^{-1}, so, (1 − α) n is 0.4873. We calculate α according to Bard and Faulkner, in Eq. (2) [53].

$$\alpha = \frac{47.7}{E_{p,a} - E_{p,a/2}} \quad (2)$$

Here, $E_{p,a/2}$ is the oxidation peak potential where the current is half the oxidation peak value. Therefore, the transfer coefficient (α) is 0.53 and the electron transfer number (n) 1.03 ≈ 1. One-electron transfer in the oxidation of NDPhA is in accord with a previous report [17].

Moreover, we can determine the k_s value from the intercept of the straight line between $E_{p,a,}$ and ln ν (Fig. S5c). The value of E_0 is obtained from the intercept of $E_{p,a}$ vs. ν plot [54,55]. In our PdNPs@MIP/SPGrE, the intercept is −0.1559 V (Fig. S5c), and E_0 is 0.0262 V (Fig. S5d); hence the k_s value calculated according to the Laviron equation is 593.69 s^{-1}. Using this method, the k_s value obtained from bare SPGrE is 128.63 s^{-1}. The k_s value for PdNPs@MIP/SPGrE is ~5 times higher than that of the bare electrode. This circumstance reveals the higher efficacy of the proposed MIP sensor for significantly promoting the oxidation reaction of NDPhA.

The electrolyte's pH significantly impacts the binding of NDPhA target molecules to the recognition cavities on the polymer. To investigate the influence of pH, we recorded signals of NDPhA using the PdNPs@MIP/SPGrE with B-R buffer electrolyte in the pH range of 2.0–8.0 (Fig. S6a). Fig. S6b shows the effects of pH on the NDPhA oxidation peak potential ($E_{p,a}$) and peak current ($I_{p,a}$). The NDPhA peak potential shifts toward a less positive value with increasing electrolyte pH, whereas the anodic peak current decreases. The binding strength of NDPhA to the MIP recognition site varies depending on the pH environment. This is because a binding interaction exists between the functional groups in the template molecules and MIP. At different pH levels, the functional groups dissociate to varying degrees, causing the interaction between the functional groups to shift. This leads to a change in the binding strength of template molecules to MIP. The maximum peak current was at pH 3.0. Thus, an electrolyte pH of 3.0 gives the best performance for NDPhA binding and catalytic activity in the oxidation process.

The linear equation of the plot between oxidation peak potential against pH (Fig. S6b) is as follows: $E_{p,a}$ (V) = −0.0568 pH + 0.2354 (r^2 = 0.9934). According to Nernst theory, we determined the m/n ratio from Eq. (3) [56].

$$E_{p,a} = -\left(\frac{0.0570m}{n}\right)pH + b \quad (3)$$

where n and m represent the total number of electrons (e^-) and protons (H^+), respectively.

The slope of our developed sensor (−0.0568) is close to the Nernstian slope (−0.0570), indicating that m/n is estimated to be 1. As a result, Scheme 2a shows a possible electrochemical mechanism of NDPhA on PdNPs@MIP/SPGrE.

This proposed mechanism is consistent with the previous works reported for a solid graphited polyurethane composite electrode (GPUE) [18] and boron-doped diamond electrode [57].

3.3.3. Enhancement of the NDPhA detection

To achieve good sensitivity, we optimized the effect of PdNPs@MIP on the surface of SPGrE and the deposition time used in linear sweep anodic stripping (LSASV) for enhancing electrochemical responsiveness. Fig. S7a shows that the response increases with increasing PdNPs@MIP loading, from 3 to 5 mg L^{-1}. However, greater loading generally results in a decreased signal response. The reduced signal might result from the thickness of the modified layer reducing the adsorption efficiency and hindering electron transfer from the binding NDPhA and electrode surface. Thus, the optimal concentration of PdNPs@MIP for modifying the SPGrE is 5 mg L^{-1}.

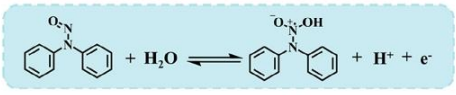

Scheme 2. The proposed electrochemical oxidation mechanism of NDPhA on the PdNPs@MIP/SPGrE.

LSASV is a powerful technique for pre-concentrating the analyte by electro-depositing on the working electrode before stripping for the determination. The deposition potential and time are important parameters to optimize the accumulation process to achieve high sensitivity and precision. In this work, we investigated the influence of deposition potential and time on NDPhA oxidation current signals. We have optimized deposition potential (−0.02, 0.00 and +0.02 V) and the results (data not shown) indicated that NDPhA gave the highest signal at the deposited potential at +0.02 V. For deposition time, the signals ranged from 0 to 300 s for PdNPs@MIP/SPGrE, using a deposition potential of +0.02 V. Fig. S7b revealed that anodic stripping peak current increases rapidly with increasing deposition time from 0 to 60 s and then decreases after 60 s. As a result, we fixed the optimal deposition time at 60 s to determine NDPhA.

3.4. Analytical features

We analyzed the analytical performance of the LSASV detection method with the developed PdNPs@MIP/SPGrE. As demonstrated in Fig. 4A, the peak current increases with increasing NDPhA concentrations ranging from 0.01 to 100 μM. The calibration plot has its greatest slope at a concentration of less than 0.1 μM. The linear regression equation is given by: $I_{p,a}$ (μA) = 51.935 ± 5.636 (μM) + 5.505 ± 0.294, r^2 = 0.996 (Fig. 4b). At high NDPhA concentration, over the range of 0.1–100 μM, the slope of the plot indicates reduced linear sensitivity of 0.821 ± 0.013 (μA s) μ M^{-1} with a linear correlation of 0.992 (Fig. 4c). The detection limit (LOD) determined using three times the standard deviation of the blank ($3S_b$, n = 3) is 0.0013 μM. Table 1 compares the analytical characteristics of our NDPhA imprinted sensor to those of previously modified electrodes from the literature. The performance of our PdNPs@MIP/SPGrE was comparable to or better than those reported for other NDPhA sensor designs.

Additionally, our sensor detects NDPhA at the lowest potential ($E_{p,a}$ = 0.20 V), reducing the risk of interference from sample constituents. Moreover, the use of PdNPs@MIP/SPGrE offers the lowest LOD. These results suggested that the PdNPs@MIP microsphere played an essential role in enhancing electrochemical activity. Our PdNPs@MIP/SPGrE sensor provides excellent selectivity and sensitivity, quick analysis, cost-effectiveness, and minute reagent usage. These advantages result from the excellent electrocatalytic activity of the PdNPs core and many NDPhA imprinted sites in the shell. The imprinted sites increase the selective surface area and offer faster electron transfer rates between PdNPs@MIP and the SPGrE surface. We readily prepared the SPGrE by screen-printing and loaded PdNPs@MIP on the electrode surface by drop-casting. Hence the NDPhA imprinted sensor is convenient for large-scale and cost-effective production. Moreover, our method offers comparable or superior sensing performance with additional advantages of being ready-to-use with straightforward synthesis, flexibility, and mechanical stability. Further, this is the first report of using an NDPhA-recognition imprinted sensor for the selective and sensitive determination of NDPhA using voltammetric measurements in a compact sensor.

3.5. Enhancing anti-interference ability, reproducibility, and stability

We examined the selective detection of NDPhA on the proposed sensor in the presence of possible interfering species found in beverage

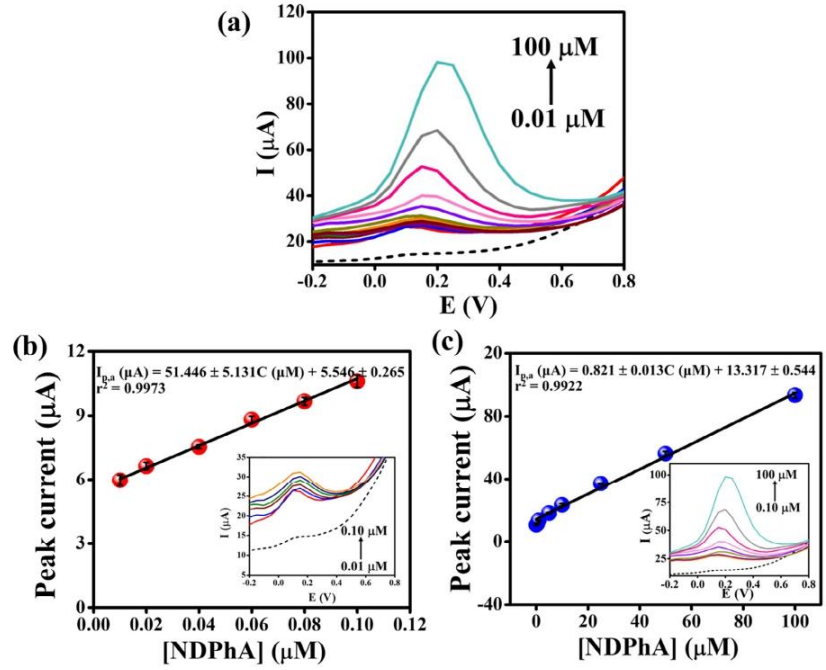

Fig. 4. (a) LSASV curves of NDPhA on PdNPs@MIP/SPGrE in 0.04 M B-R buffer at different concentrations (0.01, 0.04, 0.06, 0.08, 0.10, 0.50, 1, 5, 10, 25, 50, and 100 µM). Linear calibration curve between the oxidation peaks current ($I_{p,a}$) and the concentration of NDPhA in the ranges of (b) 0.01–0.10 µM, and (c) 0.1–100 µM.

Table 1
Comparison of the developed MIP sensor with other methods.

Electrode	Modifier	Technique	$E_{p,a}$ (V)	Linearity range (µM)	LOD (µM)	Sample	Reference
DME	–	DPP	–	0.10–2.4	0.032	–	[14]
Au	Porous Au	CV	+1.56	10,000–100,000	–	–	[15]
GCE	RuO-CN	AMP, in FIA	+1.06	0.20–1.0	0.10	Water	[16]
	PDDA-Gr/PtNPs	DPV	+1.34	0.10–50	0.033	Tap water	[17]
	GPUE	SWV	+0.75	2.5–18	0.27	Synthetic urine	[18]
SPGrE	PdNPs@MIP	LSASV	+0.20	0.01–0.1 0.1–100	0.0013	Beverages	This work

Electrode.
DME = Dropping Mercury Electrode, Au = gold disk electrode, GCE = Glassy carbon electrode, SPGrE = Screen-printed graphene electrode.
Modifier.
Porous Au = porous gold electrode running in the medium of liquid ionic [$BMIM^+$] [BF_4^-], RuO-CN = a film of mixed valent ruthenium oxides stabilized by cyano cross-links, PDDA-Gr/PtNPs = graphene and platinum nanoparticles stabilized by poly(diallyldimethylammonium chloride), GPUE = graphite-polyurethane composite, PdNPs@MIP = palladium nanoparticles coated with a molecularly imprinted polymer.
Technique.
DPP = Differential pulse polarography, CV = Cyclic voltammetry, AMP = Amperometry in flow injection analysis, DPV = Differential pulse voltammetry, SWV = Square wave voltammetry, LSASV = Linear sweep anodic stripping voltammetry.

samples. The interfering species included ascorbic acid, glucose, fructose, citric acid, caffeine, ethanol, $NaNO_3$, NaCl, and substances with similar structures such as diphenylamine and uric acid. We used two different methods in these experiments. In the first method, both MIP and NIP electrodes were operated under a rebinding process in a solution of NDPhA or other substances. We calculated the value of the imprinting factor (IF) from Eq. (4) [58].

$$IF = \frac{i_p currentMIP}{i_p currentNIP} \quad (4)$$

The largest IF values confirm good imprinting of MIP. On the other hand, IF values close to 1 infer that the imprinting effect is almost insignificant, which means that the interaction between the MIP and the template is somewhat unspecific, more involved to surface interactions than to any generated recognition cavities [21].

Fig. 5a shows responses for PdNPs@MIP/SPGrE (front row, purple bar) and PdNPs@NIP/SPGrE (middle row, orange bar) when exposed to solutions containing the respective NDPhA or other substances at a concentration of 1 μM. The IF values of this work (Fig. 5a, back row, blue bar) for NDPhA is 10.15. For other compounds, it is in the range of 0.41–1.05, so the IF value for the target NDPhA is much higher than that obtained from competing compounds. These results thus clearly demonstrate appreciable selectivity of the developed sensor. The electrode selectivity was enhanced because PdNPs@MIP has imprinted cavities complementary in size conformation and shape to NDPhA molecules. Therefore, specific polymer recognition sites will allow only NDPhA molecules to bind. Other compounds with different structures from the NDPhA target cannot diffuse or bind strongly to the recognition sites.

In the second method, a current signal of 1.0 μM NDPhA in the presence of varying concentrations of the interferents, as mentioned above, was investigated with the MIP electrode. As shown in Fig. 5b, the $I_{p\ a}$ changed less than 10% in the presence of a 50-fold excess of diphenylamine, a 250-fold excess of ascorbic acid and uric acid, and a 1000-fold excess of glucose, fructose, citric acid, caffeine, ethanol, $NaNO_3$, and NaCl. Only NDPhA provides a strong current response at the PdNPs@NIP/SPGrE electrode (Fig. 5a). Other species did not produce any substantial current. These findings suggested that the NDPhA molecules effectively transferred to the polymeric network, and the PdNPs@MIP can detect the NDPhA molecules preferentially among other substances.

We analyzed the reproducibility of the fabricated NDPhA imprinted sensor by comparing the current response of 1 μM NDPhA for five different PdNPs@MIP/SPGrE electrodes (Fig. S8a). All NDPhA imprinted

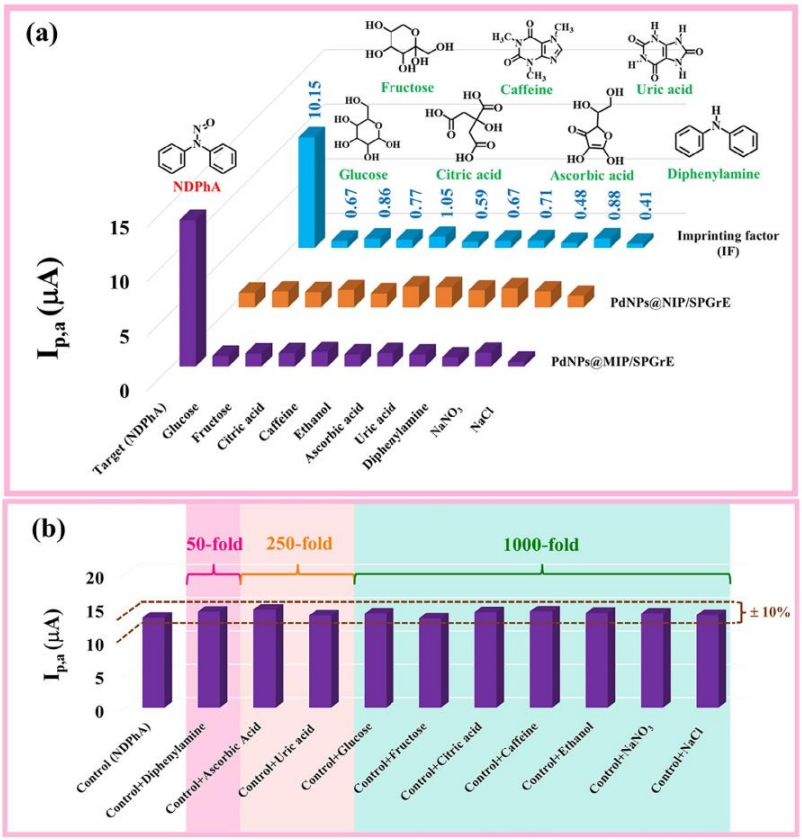

Fig. 5. (a) The selectivity of the imprinted (PdNPs@MIP/SPGrE) and non-imprinted (PdNPs@NIP/SPGrE) sensors for NDPhA and foreign interferences. (b) Selectivity evaluation of the proposed MIP sensor for NDPhA at 1 μM, diphenylamine at 50 μM, ascorbic acid and uric acid at 250 μM, glucose, fructose, citric acid, caffeine, ethanol, $NaNO_3$, and NaCl at 1000 μM.

Table 2
Comparison of NDPhA determination in beer, wines (dark and red wines), green tea, and juices (orange and apple juices) using the proposed MIP sensor and the reference values obtained from HPLC.

Sample	Added (μM)	Proposed MIP sensor			HPLC			Relative error (%)
		Found (μM)	% Recovery	%RSD	Found (μM)	% Recovery	%RSD	
Beer	–	<LOD	–	–	<LOD	–	–	–
	0.05	0.047	94.00	1.39	0.048	96.00	1.19	− 2.08
	0.10	0.097	97.00	1.13	0.096	96.00	2.41	+1.04
Dark wine	–	<LOD	–	–	<LOD	–	–	–
	0.05	0.049	98.00	2.06	0.049	98.00	2.49	0.00
	0.10	0.094	94.00	4.22	0.093	93.00	4.43	+1.08
Red wine	–	<LOD	–	–	<LOD	–	–	–
	0.05	0.047	94.00	2.01	0.047	94.00	1.83	0.00
	0.10	0.092	92.00	3.89	0.095	95.00	2.45	−3.15
Green tea	–	<LOD	–	–	<LOD	–	–	–
	0.05	0.049	98.00	1.16	0.048	96.00	1.29	+2.04
	0.10	0.098	98.00	2.53	0.099	99.00	2.78	− 1.01
Orange juice	–	<LOD	–	–	<LOD	–	–	–
	0.05	0.048	96.00	3.98	0.047	94.00	1.37	+2.13
	0.10	0.089	89.00	0.51	0.090	90.00	2.23	− 1.11
Apple juice	–	<LOD	–	–	<LOD	–	–	–
	0.05	0.048	96.00	3.21	0.049	98.00	4.94	− 2.04
	0.10	0.098	98.00	4.91	0.094	94.00	2.74	+4.26
Synthetic sample	–	0.050	–	–	0.049	–	–	+2.04
	0.05	0.099	98.00	1.80	0.098	98.00	1.71	+1.02
	0.10	0.145	95.00	1.62	0.144	95.00	1.10	+0.69

% Relative error = $([NDPhA]_{MIP\ sensor} - [NDPhA]_{HPLC})/([NDPhA]_{HPLC}) \times 100$.

sensors responded with similar currents, with an RSD of 1.67%. Additionally, we investigated the stability of the NDPhA imprinted sensor by measuring the current signal of 1 μM NDPhA at various intervals over four weeks. The results (Fig. S8b) showed that after 28 days, the signal of the NDPhA imprinted sensor retains 81 % of its initial current. These results demonstrate that the imprinted sensor possesses good reproducibility and stability for detecting NDPhA.

3.6. Real sample analysis

We further tested the accuracy and application of the PdNPs@MIP sensor in the quantitative analysis of NDPhA in six beverage samples, including beer, wines (dark and red wines), green tea, orange juice, apple juice, and a synthetic sample. We used HPLC coupled with a photodiode array detector set at 280 nm (details in ESI Section 2 and Fig. S9) as a comparison method to quantify the set of samples. In addition, we investigated sample recoveries (spiked levels of 0.05 and 0.10 μM) to validate the analysis. Table 2 compares the results of NDPhA concentrations in beverages and calculated recovery values as analyzed by the MIP sensor and HPLC. The measurements obtained from the two methods are in good agreement. The recoveries of our developed MIP sensor are in the acceptable range (92.00–98.00%) with sustainable repeatability (%RSD less than 4.91%). Relative differences are in the range of −3.15% to 4.26%. These results indicate no significant matrix interference in the analyzed samples. Therefore, we conclude that the proposed MIP sensor is sufficiently accurate, precise, and suitable for the NDPhA determination in beverage samples.

Table 3
Intra-day and Inter-day assay precision and accuracy for determination of NDPhA in certified reference materials (CRM) using the proposed MIP sensor.

CRM	Proposed MIP sensor		Bias (%)
	Found (μM)	RSD (%)	
Intra-day	10,046.667 ± 75.719	0.75	−0.74
Inter-day	10,019.998 ± 84.855	0.85	−1.01

CRM31032/607, with the certified value of NDPhA at 10,122.087 ± 94.340 μM.

We further evaluated the accuracy and precision of the proposed MIP sensor in terms of intra-day and inter-day analysis. The NDPhA content of certified reference materials (CRM31032/607) was determined using our MIP sensor. As shown in Table 3, good intra-day and inter-day accuracy (%bias) in CRM, *e.g.*, −0.74% for intra-day and −1.01% for inter-day analysis, are obtained. These results reflect that the proposed PdNPs@MIP/SPGrE sensor is accurate, precise, and appropriate for the determination of NDPhA in real samples.

4. Conclusions

We successfully fabricated a novel NDPhA compact electrochemical sensor based on palladium nanoparticles coated with a molecularly imprinted polymer (PdNPs@MIP) and applied for NDPhA determination in beverages. The graphene electrode (SPGrE) was readily prepared by screen-printing, and the synthesized PdNPs@MIP was dropped cast on the electrode surface to fabricate the NDPhA-recognition site imprinted sensor. The 3D-imprinting on PdNPs' surface was successfully carried out by successively coating the surface of PdNPs with PVP, then terminating with MIP. The as-prepared micro-size spherical PdNPs@MIP is uniform, with high electro-catalytic activity and specific surface area with many NDPhA imprinted sites. As far as we know, this is the first report of using an NDPhA-recognition imprinted sensor to selectively and sensitively determine NDPhA using voltammetric measurements on a compact sensor. Our method offers superior sensing performance with additional advantages of being ready-to-use, cost-effective, straightforward synthesis, good flexibility, mechanical stability, and suited to large-scale production. The PdNPs@MIP/SPGrE exhibited excellent performance, including a low detection limit (0.0013 μM), wide linearity, good repeatability, and stability. These excellent properties result from the electrocatalytic properties of the PdNPs core and the large number of NDPhA imprinted sites in the shell, which increase the selective surface area

and offer fast electron transfer rates. Additionally, our developed sensor detects NDPhA at the very low potential of 0.20 V, which minimizes the risk of interference from sample constituents and enhances the anti-interference ability of the sensor for the determination of NDPhA in a complex matrix. Our proposed MIP sensor exhibits high accuracy, high precision, and excellent performance when applied to the determination of NDPhA in beverages.

CRediT authorship contribution statement

Kanpitcha Somnet: Investigation, Validation, Writing – original draft. **Pattawan Soravech:** Investigation. **Chanpen Karuwan:** Investigation. **Adisorn Tuantranont:** Supervision. **Maliwan Amatatongchai:** Conceptualization, Investigation, Supervision, Writing – review & editing.

Declaration of Competing Interest

The authors declare that they have no known competing financial interests or personal relationships that could have appeared to influence the work reported in this paper.

Acknowledgments

The authors acknowledge the support provided by the National Electronics and Computer Technology Center (NECTEC), the National Science and Technology Development Agency (NSTDA) via the Thailand Graduate Institute of Science and Technology (TGIST grants No. SCA-CO-2563-12226-TH for K.S.). In addition, the authors wish to thank the Center of Excellence for Innovation in Chemistry (PERCH-CIC) and the Ministry of Higher Education, Science, Research, and Innovation.

Appendix A. Supplementary data

Supplementary data to this article can be found online at https://doi.org/10.1016/j.jelechem.2022.116302.

References

[1] C.C. Fan, T.F. Lin, N-nitrosamines in drinking water and beer: Detection and risk assessment, Chemosphere 200 (2018) 48–56, https://doi.org/10.1016/j.chemosphere.2018.02.025.
[2] D.W. Lachenmeier, D. Fügel, Reduction of nitrosamines in beer—review of a success story, Brew Sci 60 (2007) 84–89.
[3] W. Li, N. Chen, Y. Zhao, W. Guo, N. Muhammd, Y. Zhu, Z. Huang, Online coupling of tandem liquid-phase extraction with HPLC-UV for the determination of trace N-nitrosamines in food products, Anal. Methods 10 (2018) 1733–1739, https://doi.org/10.1039/C8AY00014J.
[4] S. Lu, D. Wu, G. Li, Z. Lv, P. Gong, L. Xia, Z. Sun, G. Chen, X. Chen, J. You, Y. Wu, Facile and sensitive determination of N-nitrosamines in food samples by high-performance liquid chromatography via combining fluorescent labeling with dispersive liquid-liquid microextraction, Food Chem. 234 (2017) 408–415, https://doi.org/10.1016/j.foodchem.2017.05.032.
[5] P. Miralles, I. van Gemert, A. Chisvert, A. Salvador, Stir bar sorptive-dispersive microextraction mediated by magnetic nanoparticles-metal organic framework composite: determination of N-nitrosamines in cosmetic products, J. Chromatogr. A 1604 (2019), https://doi.org/10.1016/j.aca.2016.04.042 460465.
[6] P. Miralles, A. Chisvert, A. Salvador, Determination of N-nitrosamines in cosmetic products by vortex-assisted reversed-phase dispersive liquid-liquid microextraction and liquid chromatography with mass spectrometry, J. Sep. Sci. 41 (2018) 3143–3151, https://doi.org/10.1002/jssc.201800388.
[7] A. Ishizaki, H. Kataoka, A sensitive method for the determination of tobacco-specific nitrosamines in mainstream and side stream smokes of combustion cigarettes and heated tobacco products by online in-tube solid-phase microextraction coupled with liquid chromatography-tandem mass spectrometry, Anal. Chim. Acta 1075 (2019) 98–105, https://doi.org/10.1016/j.aca.2019.04.073.
[8] Y. Zhou, H. Zhang, X. Wang, D. Qi, W. Gu, D. Wu, B. Liu, Development of a heart-cutting supercritical fluid chromatography-high-performance liquid chromatography coupled to tandem mass spectrometry for the determination of four tobacco-specific nitrosamines in mainstream smoke, Anal. Bioanal. Chem. 411 (2019) 2961–2969, https://doi.org/10.1007/s00216-019-01746-w.
[9] C. Giménez-Campillo, M. Pastor-Belda, N. Campillo, J. de D. Hernández, I. Guillén, P. Vizcaíno, I. López-García, M. Hernández-Córdoba, N. Arroyo-Manzanares, P. Viñas, Ultrasound Assisted Extraction Approach to Test the Effect of Elastic Rubber Nettings on the N-Nitrosamines Content of Ham Meat Samples, Foods 10 (2021) 2564. 10.3390/foods10112564
[10] H. Ramezani, H. Hosseini, M. Kamankesh, V. Ghasemzadeh-Mohammadi, A. Mohammadi, Rapid determination of nitrosamines in sausage and salami using microwave-assisted extraction and dispersive liquid–liquid microextraction followed by gas chromatography–mass spectrometry, Eur. Food Res. Technol. 240 (2014) 441–450, https://doi.org/10.1007/s00217-014-2343-4.
[11] Y. Hu, J. Liu, J. Li, T. Chen, M. Wu, Dual-functional imprinted magnetic nanoprobes for fluorescence detection of N-nitrosodiphenylamine, Anal. Methods 10 (2018) 2384–2389, https://doi.org/10.1039/C8AY00584B.
[12] Z. Li, Z. Qian, S. Hu, T. Gong, Q. Xian, Molecularly imprinted solid phase extraction coupled with gas chromatography-mass spectrometry for determination of N-Nitrosodiphenylamine in water samples, Chemosphere 212 (2018) 872–880, https://doi.org/10.1016/j.chemosphere.2018.08.159.
[13] Z. Li, J. Wang, X. Chen, S. Hu, T. Gong, Q. Xian, A novel molecularly imprinted polymer-solid phase extraction method coupled with high performance liquid chromatography tandem mass spectrometry for the determination of nitrosamines in water and beverage samples, Food Chem. 292 (2019) 267–274, https://doi.org/10.1016/j.foodchem.2019.04.036.
[14] R. Samuelsson, Pulse polarographic determination of nitrosamines: part 2. Methods for the determination of N-Nitrosodiphenylamine and N-Nitrosodibutylamine, Anal. Chim. Acta 108 (1979) 213–219, https://doi.org/10.1016/S0003-2670(01)93057-0.
[15] H.L. Yang, G.H. Chu, Q. Zhang, G.J. Zhou, J.H. Li, X.H. Xia, Electrochemical determination of NDPhA via its electrocatalysis at porous au electrode in room temperature ionic liquid, Electroanalysis 20 (2008) 2003–2008, https://doi.org/10.1002/elan.200804254.
[16] W. Gorski, J.A. Cox, Amperometric determination of N-Nitrosamines in aqueous solution at an electrode coated with a ruthenium-based inorganic polymer, Anal. Chem. 66 (1994) 2771–2774, https://doi.org/10.1021/ac00089a027.
[17] X. Peng, J. Zou, Z. Liu, Y. Guo, Electrochemical sensor for facile detection of trace N-nitrosodiphenylamine based on poly (diallyldimethylammonium chloride)-stabilized graphene/platinum nanoparticles, New J. Chem. 43 (2019) 820–826, https://doi.org/10.1039/C8NJ04892D.
[18] L.V. Martoni, M. Baccarin, É.T. Cavalheiro, R.M. Buoro, Electrochemical behavior of N-Nitrosodiphenylamine and its determination in synthetic urine samples using a graphite-polyurethane composite electrode, J. Electroanal. Chem. 857 (2020), https://doi.org/10.1016/j.jelechem.2019.113747 113747.
[19] Y. Wang, L. Yao, X. Liu, J. Cheng, W. Liu, T. Liu, M. Sun, L. Zhao, F. Ding, Z. Lu, P. Zou, X. Wang, Q. Zhao, H. Rao, $CuCo_2O_4$/N-Doped CNTs loaded with molecularly imprinted polymer for electrochemical sensor: Preparation, characterization and detection of metronidazole, Biosens. Bioelectron. 142 (2019), https://doi.org/10.1016/j.bios.2019.111483 111483.
[20] X. Yue, X. Luo, Z. Zhou, Y. Bai, Selective electrochemical determination of tertiary butylhydroquinone in edible oils based on an in-situ assembly molecularly imprinted polymer sensor, Food Chem. 289 (2019) 84–94, https://doi.org/10.1016/j.foodchem.2019.03.044.
[21] A. Herrera-Chacón, X. Cetó, M. del Valle, Molecularly imprinted polymers – towards electrochemical sensors and electronic tongues, Anal. Bioanal 413 (2021) 6117–6140, https://doi.org/10.1007/s00216-021-03313-8.
[22] J. Wang, W. Du, X. Huang, J. Hu, W. Xia, D. Jin, Y. Shu, Q. Xu, X. Hu, A novel metronidazole electrochemical sensor based on surface imprinted vertically cross-linked two-dimensional Sn_3O_4 nanoplates, Anal. Methods 10 (2018) 4985–4994, https://doi.org/10.1039/C8AY01824C.
[23] K. Somnet, S. Thimoonnee, C. Karuwan, W. Kamsong, A. Tuantranont, M. Amatatongchai, Ready-to-use paraquat sensor using a graphene-screen printed electrode modified with a molecularly imprinted polymer coating on a platinum core, Analyst 146 (2021) 6270–6280, https://doi.org/10.1039/D1AN01278A.
[24] B. Fresco-Cala, A.D. Batista, S. Cárdenas, Molecularly imprinted polymer micro- and nano-particles: A review, Molecules 25 (2020) 4740, https://doi.org/10.3390/molecules25204740.
[25] Z. Mamipour, A. Nematollahzadeh, M. Kompany-Zareh, Molecularly imprinted polymer grafted on paper and flat sheet for selective sensing and diagnosis: a review, Microchim. Acta 188 (2021) 1–21, https://doi.org/10.1007/s00604-021-04930-x.
[26] A.A. Lahcen, A. Amine, Recent advances in electrochemical sensors based on molecularly imprinted polymers and nanomaterials, Electroanalysis 31 (2019) 188–201, https://doi.org/10.1002/elan.201800623.
[27] J. Chen, H. Huang, Y. Zeng, H. Tang, L. Li, A novel composite of molecularly imprinted polymer-coated PdNPs for electrochemical sensing norepinephrine, Biosens. Bioelectron. 65 (2015) 366–374, https://doi.org/10.1016/j.bios.2014.10.011.
[28] P.M. Uberman, L.A. Pérez, S.E. Martín, G.I. Lacconi, Electrochemical synthesis of palladium nanoparticles in PVP solutions and their catalytic activity in Suzuki and Heck reactions in aqueous medium, RSC Adv. 4 (24) (2014) 12330.
[29] J. Li, J. Liu, G. Tan, J. Jiang, S. Peng, M. Deng, D. Qian, Y. Feng, Y. Liu, High-sensitivity paracetamol sensor based on Pd/graphene oxide nanocomposite as an enhanced electrochemical sensing platform, Biosensors Bioelectronics 54 (2014) 468–475.
[30] W. Kamsong, V. Primpray, P. Pasakon, C. Sriprachuabwong, S. Pakapongpan, J.P. Mensing, A. Wisitsoraat, A. Tuantranont, C. Karuwan, Highly sensitive and disposable screen-printed ionic liquid/graphene based electrochemical sensors,

Electrochem. Commun. 135 (2022), https://doi.org/10.1016/j.elecom.2022.107209 107209.
[31] I. Ullah, K. Khan, M. Sohail, K. Ullah, A. Ullah, S. Shaheen, Synthesis, structural characterization and catalytic application of citrate-stabilized monometallic and bimetallic palladium@copper nanoparticles in microbial anti-activities, Int. J. Nanomed. 12(2017) 8735–8747. 10.2147%2FIJN.S145085.
[32] M. Savotha, N. R. Dhineshbabu, G. Sriram, Iron-Polyvinylpyrrolidone (Fe-PVP) nanocomposite coated Inductive Proximity Sensor, Appl. Sci. Lett. 1 (2015) 62–67. 10.17571/appslett.2015.01015.
[33] N. Nontawong, M. Amatatongchai, S. Thimoonnee, S. Laosing, P. Jarujamrus, C. Karuwan, S. Chairam, Novel amperometric flow-injection analysis of creatinine using a molecularly-imprinted polymer coated copper oxide nanoparticle-modified carbon-paste-electrode, J. Pharm. Biomed. Anal., 175 (2019) 112770. 10.1016/j.jpba.2019.07.018.
[34] United States, Occupational Safety & Health Administration, OSHA Analytical Methods Manual; method No. 23, OSHA Analytical Laboratory 1 (1990).
[35] K.S. Siddiqi, A. Husen, Green synthesis, characterization and uses of palladium/platinum nanoparticles, Nanoscale Res. Lett. 11 (2016) 1, https://doi.org/10.1186/s11671-016-1695-z.
[36] F. Arsiya, M.H. Sayadi, S. Sobhani, Green synthesis of palladium nanoparticles using Chlorella vulgaris, Mater. Lett. 186 (2017) 113–115, https://doi.org/10.1016/j.matlet.2016.09.101.
[37] D.S. Sheny, D. Philip, J. Mathew, Rapid green synthesis of palladium nanoparticles using the dried leaf of Anacardium occidentale, Spectrochim. Acta A Mol. Biomol. Spectrosc. 91 (2012) 35–38, https://doi.org/10.1016/j.saa.2012.01.063.
[38] M. Piskorz, T. Urbanski, Ultraviolet and infrared spectra of some nitrosamines, Bull. Acad. Pol. Sci., Ser. Sci. Chim. 11 (1963) 607–613.
[39] S. Bucatariu, G. Fundueanu, I. Prisacaru, M. Balan, I. Stoica, V. Harabagiu, M. Constantin, Synthesis and characterization of thermosensitive poly(N-isopropylacrylamide-co-hydroxyethylacrylamide) microgels as potential carriers for drug delivery, J. Polym. Res. 21 (11) (2014), https://doi.org/10.1007/s10965-014-0580-7.
[40] H. Xu, X.D. Yuan, B.D. Shen, J. Han, Q.Y. Lv, L. Dai, M.G. Lin, C. Yu, J.X. Bai, H.L. Yuan, Development of poly(N-isopropylacrylamide)/alginate copolymer hydrogel-grafted fabrics embedding of berberine nanosuspension for the infected wound treatment, J. Biomater. Appl. 28 (2013) 1376–1385, https://doi.org/10.1177/0885328213509503.
[41] Y.K. Kim, E.-J. Kim, J.H. Lim, H.K. Cho, W.J. Hong, H.H. Jeon, B.G. Chung, Dual stimuli-triggered nanogels in response to temperature and ph changes for controlled drug release, Nanoscale Res. Lett. 14 (2019) 1–9, https://doi.org/10.1186/s11671-019-2909-y.
[42] G. Zou, J. Shen, P. Duan, X. Xia, R. Chen, B. Jin, Temperature-Sensitive poly(N-isopropylacrylamide)/Konjac Glucomannan/graphene oxide composite membranes with improved mechanical property, swelling capability, and degradability, Int. J. Polym. Sci. 2018 (2018) 1–10, https://doi.org/10.1155/2018/7906747.
[43] X. Yang, Z. Sun, J. Gao, C. Yang, D. Tang, Plasma-initiated polymerization of N-isopropylacrylamide and functionalized with dopamine for the adhesion to Hela cells, Polym. Bull. 77 (2019) 963–974, https://doi.org/10.1007/s00289-019-02784-1.
[44] X. Meng, Y. Ji, G. Yu, Y. Zhai, Preparation and Properties of Polyvinylidene Fluoride Nanocomposites Membranes based on *Poly(N-Isopropylacrylamide)* modified graphene oxide Nanosheets, Polymers 11 (2019) 473, https://doi.org/10.3390/polym11030473.
[45] H.R. Thomas, D.J. Phillips, N.R. Wilson, M.I. Gibson, J.P. Rourke, One-step grafting of polymers to graphene oxide, Polym. Chem. 6 (2015) 8270–8274, https://doi.org/10.1039/C5PY01358E.
[46] M. Gholinejad, M. Bahrami, C. Nájera, A fluorescence active catalyst support comprising carbon quantum dots and magnesium oxide doping for stabilization of palladium nanoparticles: Application as a recoverable catalyst for Suzuki reaction in water, Mol. Catal. 433 (2017) 12–19, https://doi.org/10.1016/j.mcat.2016.12.010.
[47] L. Gao, W. Yue, S. Tao, L. Fan, Novel Strategy for Preparation of Graphene-Pd, Pt Composite, and Its Enhanced Electrocatalytic Activity for Alcohol Oxidation, Langmuir 29 (2013) 957–964. 10.1021/la303663x
[48] P.M. Uberman, L.A. Pérez, S.E. Martín, G.I. Lacconi, Electrochemical synthesis of palladium nanoparticles in PVP solutions and their catalytic activity in Suzuki and Heck reactions in aqueous medium, RSC Adv. 4 (2014) 12330–12341, https://doi.org/10.1039/C3RA47854H.
[49] N. Nontawong, P. Ngaosri, S. Chunta, P. Jarujamrus, D. Nacapricha, P.A. Lieberzeit, M. Amatatongchai, Smart sensor for assessment of oxidative/nitrative stress biomarkers using a dual-imprinted electrochemical paper-based analytical device, Anal. Chim. Acta 1191 (2022), https://doi.org/10.1016/j.aca.2021.339363 339363.
[50] A.T. Gökçeören, B.F. Şenkal, C. Erbil, Effect of crosslinker structure and crosslinker/monomer ratio on network parameters and thermodynamic properties of Poly (N-isopropylacrylamide) hydrogels, J. Polym. Res. 21 (2014) 1–12, https://doi.org/10.1007/s10965-014-0370-2.
[51] Y. Liu, L. Zhang, N. Zhao, Y. Han, F. Zhao, Z. Peng, Y. Li, Preparation of molecularly imprinted polymeric microspheres based on distillation–precipitation polymerization for an ultrasensitive electrochemical sensor, Anal. The 142 (2017) 1091–1098, https://doi.org/10.1039/C7AN00059F.
[52] A. Fatahi, R. Malakooti, M. Shahlaei, Electrocatalytic oxidation and determination of dexamethasone at an Fe_3O_4/PANI–CuII microsphere modified carbon ionic liquid electrode, RSC Adv. 7 (2017) 11322–11330, https://doi.org/10.1039/C6RA26125F.
[53] A.J. Bard, L.R. Faulkner, Fundamentals and applications, Electrochem. Methods 2 (2001) 580–632.
[54] Y. Wu, X. Ji, S. Hu, Studies on electrochemical oxidation of azithromycin and its interaction with bovine serum albumin, Bioelectrochemistry 64 (2004) 91–97, https://doi.org/10.1016/j.bioelechem.2004.03.005.
[55] M.H. Parvin, E. Azizi, J. Arjomandi, J.Y. Lee, Highly sensitive and selective electrochemical sensor for detection of vitamin B12 using an Au/PPy/FMNPs@TD-modified electrode, Sens. Actuators B Chem. 261 (2018) 335–344, https://doi.org/10.1016/j.snb.2018.01.168.
[56] A.A. Ensafi, P. Nasr-Esfahani, B. Rezaei, Metronidazole determination with an extremely sensitive and selective electrochemical sensor based on graphene nanoplatelets and molecularly imprinted polymers on graphene quantum dots, Sens. Actuators B Chem. 270 (2018) 192–199, https://doi.org/10.1016/j.snb.2018.05.024.
[57] R.T.S. de Oliveira, G.R. Salazar-Banda, S.A.S. Machado, L.A. Avaca, Electroanalytical determination of N-nitrosamines in aqueous solution using a boron-doped diamond electrode, Electroanalysis 20 (2008) 396–401, https://doi.org/10.1002/elan.200704055.
[58] B. Hatamluyi, M. Rezayi, H.R. Beheshti, M.T. Boroushaki, Ultra-sensitive molecularly imprinted electrochemical sensor for patulin detection based on a novel assembling strategy using Au@ Cu-MOF/N-GQDs, Sens. Actuators B Chem. 318 (2020), https://doi.org/10.1016/j.snb.2020.128219 128219.

CURRICURUM VITAE

NAME	Kanpitcha Somnet
INSTITUTIONS ATTENDED	Ubon Ratchathani University, 2016 Bachelor of Science (Chemistry)
GRANTS	Thailand Graduate Institute of Science and Technology (TGIST) from National Science and Technology Development Agency (NSTDA) in the Academic Years of 2020-2022 (TGIST grants No.SCA-CO-2563-12226-TH)